NASA CR- 159668



# ADVANCED TURBO-PROP AIRPLANE INTERIOR NOISE REDUCTION-SOURCE DEFINITION

B. Magliozzi and Bennett M. Brooks

Hamilton Standard
United Technologies Corporation
Windsor Locks, Conn. 06096

Final Report
Contract NAS3-20614
October, 1979



National Aeronautics and
Space Administration

Washington, D.C. 20546

| 1. Report No. | 2. Government Accession No. | 3. Recipient's Catalog No. |
|---|---|---|
| NASA CR 159668 | | |

| 4. Title and Subtitle | 5. Report Date |
|---|---|
| Advanced Turboprop Airplane Interior Noise Reduction-Source Definition | October, 1979 |
| | 6. Performing Organization Code |
| 7. Author(s) | 8. Performing Organization Report No. |
| B. Magliozzi, Bennett M. Brooks | |
| 9. Performing Organization Name and Address | 10. Work Unit No. (TRAIS) |
| Hamilton Standard<br>United Technologies Corporation<br>Windsor Locks, Conn. 06096 | 11. Contract or Grant No.<br>NAS3-20614 |
| | 13. Type of Report and Period Covered |
| 12. Sponsoring Agency Name and Address | Final Report |
| National Aeronautics and Space Administration<br>Washington, D.C. 20546 | 14. Sponsoring Agency Code |

15. Supplementary Notes

Technical Monitors: J.H. Dittmar, NASA Lewis Research Center, Cleveland, Ohio
J. Mixson, NASA Langley Research Center, Hampton, Virginia

16. Abstract

Acoustic pressure amplitudes and phases were measured in model scale on the surface of a rigid semi-cylinder mounted in an accoustically treated wind tunnel near a prop-fan (an advanced turboprop with many swept blades) model. Operating conditions during the test simulated those of a prop-fan at 0.8 Mach number cruise. Acoustic pressure amplitude and phase contours were defined on the semi-cylinder surface. Measurements obtained without the semi-cylinder in place were used to establish the magnitude of pressure doubling for an aircraft fuselage located near a prop-fan. Pressure doubling effects were found to be 6 dB at 90° incidence decreasing to no effect at grazing incidence. Comparisons of measurements with predictions made using a recently developed prop-fan noise prediction theory which includes linear and non-linear source terms showed good agreement in phase and in peak noise amplitude. Predictions of noise amplitude and phase contours, including pressure doubling effects derived from test, are included in the report for a full scale prop-fan installation.

| 17. Key Words | 18. Distribution Statement |
|---|---|
| Turboprop Noise<br>Prop-Fan Noise<br>Fuselage Noise<br>Noise Level Contours<br>Phase Angle Contours | Unlimited |

| 19. Security Classif. (of this report) | 20. Security Classif. (of this page) | 21. No. of Pages | 22. Price |
|---|---|---|---|
| Unclassified | Unclassified | 89 | |

N80-13882 #

CONTENTS

# FOREWORD

All of the testing reported herein was conducted in the Acoustic Research Tunnel at the United Technologies Research Center.

The authors wish to express their thanks for the support provided by the personnel of the United Technologies Research Center, especially that of Dr. W. P. Patrick.

## SUMMARY

Hamilton Standard, under contract to NASA, has completed an experimental evaluation of the acoustic noise levels on the surface of a simulated fuselage located in the near-field of a model prop-fan.

Condenser microphones were used at 21 locations on the surface of a 76.2 cm (30 in) diameter semi-cylinder to define the noise intensity and relative phase distribution on the simulated fuselage. For this program, the simulated fuselage was attached to a special nozzle in the United Technologies Research Center Acoustic Research Tunnel so that the surface on which noise was measured was immersed in the flow, simulating a fuselage surface in cruise. The source of noise was a 4-bladed 62.2 cm (24.5 in) diameter SR-3 model prop-fan which was operated at subsonic, transonic, and supersonic tip speeds to simulate a high altitude cruise condition. Since the tunnel was operated at a Mach number of 0.267, below the current full-scale cruise Mach number of 0.8, the prop-fan model was oversped to achieve the full-scale relative tip speed.

The simulated fuselage was first located at a nominal tip clearance of 0.4 prop-fan diameters. Subsequently, the simulated fuselage was relocated to a tip clearance of 0.8 prop-fan diameters. Finally, noise was measured at an 0.8 diameter tip clearance without the simulated fuselage (free-field condition) at equivalent fuselage locations. Measurements for the two latter configurations were used to determine the effect of the fuselage on source noise and on the noise measured on the fuselage surface (pressure doubling effects).

The data were analyzed to show the amplitudes and relative phases of the prop-fan noise harmonics at each of the 21 microphone locations. Comparisons of the measurements made on the simulated fuselage at 0.8 diameter clearance with those made at equivalent free-field locations were used to derive pressure doubling effects. As the wavelength of the sound at the lowest frequency of interest is small compared to the model fuselage diameter, geometric acoustics apply. Thus, pressure doubling effects were found to be essentially independent of frequency. A dependence on incidence angle was found, however. The angle of incidence (including convection effects) dependence indicated that for angles greater than 60 degrees (with 90 degrees being normal incidence) the pressure doubling effects resulted in an increase of 6 dB for the noise on the fuselage surface compared to that under free-field conditions. Below 60 degrees incidence, the pressure doubling effects decreased to 0 dB for grazing incidence. The simulated fuselage was found to have no effect on the relative phase distribution of the noise.

The presence of the fuselage was found to have a negligible effect on the source noise. This was an expected result, as the air-flow into the prop-fan was not disturbed by the fuselage. This was determined from hot-wire anemometer measurements and flow visualization.

Comparison of calculated sound pressure level and phase angle contours (including the empirically derived pressure doubling effects) with measured contours showed fairly good agreement for the supersonic tip speed condition. Based on this comparison, it was concluded that the current prop-fan noise prediction procedure is adequate for the estimation of amplitude and phase distribution on a fuselage surface when empirically-derived pressure doubling effects are included.

Using the prop-fan noise prediction procedure and the empirically-derived pressure doubling effects, sound pressure level and phase angle contours were estimated on the surface of a full-size fuselage. For this estimate, a 3.83 m (12.55 ft) diameter eight-bladed prop-fan, incorporating the SR-3 blade design, operating at 243.8 m/sec (800 ft/sec) tip speed at 0.8 Mach number cruise at 10 688 m (35 000 ft) altitude was assumed. A peak level of 150 dB at blade passage frequency was estimated, occurring slightly behind the plane of rotation. The 10 dB-down points are about 1.5 m (5 ft) behind the peak noise level location and 2.6 m (8.5 ft) ahead of the peak noise level location. The phase angle contours show a gradual phase change from 0 to 180 degrees, then an increase in the rate of change. The initial phase change rate is about 90 degrees in 0.3 m (1 ft) at 0.9 m (3 ft) behind the plane of rotation, increasing to a phase change rate of 360 degrees in 0.3 m (1 ft) at 2.7 m (9 ft) ahead of the plane of rotation.

# INTRODUCTION

Advanced turboprop propulsion is currently being investigated as a means of improving fuel efficiency of future transport aircraft. Initial studies have confirmed that the advanced turboprop (prop-fan) is more fuel efficient than advanced high-bypass-ratio turbofans. The objectives for a prop-fan airplane are to provide high performance at 0.7 to 0.8 Mach number cruise and have cabin noise levels consistent with those of current turbofan transports.

In initial prop-fan studies, it was concluded that interior noise levels for prop-fan airplanes would exceed the current interior noise targets for passenger-carrying airplanes, if the same transmission loss values are provided as in contemporary fuselage-structure construction. Limited studies applying current technology in noise control show that the interior noise can be controlled, but at the expense of some reduction in fuel savings due to increase fuselage weight. Recent investigations (references 1 and 2) have demonstrated that by incorporating the noise reduction goal into the fuselage structural design process, the effectiveness of the structure in reducing noise can be greatly improved over that of a conventional structure of the same weight.

The current turbofan aircraft interior noise reduction programs address broadband boundary layer and jet noise and have not addressed the discrete low frequency noise spectrum of the prop-fan propulsion concept. Thus, there is a need for a new direction in airframe design where the goal of noise reduction becomes an integral part of the design process. Achieving a quiet prop-fan or turboprop aircraft interior without compromising the fuel savings potential can best be accomplished with such an approach.

In order to design an advanced fuselage, the noise reduction requirements must first be established. This is dependent on the exterior noise field (due to the prop-fan) and the desired interior noise levels. Although the exterior noise field can be predicted, measured prop-fan noise levels incident on a fuselage surface under cruise conditions are not available for verification of the predictions.

In the test and analysis work reported in this document, the source noise characteristics of the SR-3 prop-fan design were established. This was accomplished in a two-phase program. In Phase I, the noise from a model prop-fan was measured using microphones flush-mounted in a rigid fuselage surface in model scale in the United Technologies Research Center Acoustic Research Tunnel under simulated cruise conditions. In Phase II, the measured data was adjusted to full-scale for high-altitude cruise conditions.

## TEST PROGRAM

### Model Description

Prop-Fan Model.- The prop-fan SR-3 model was used for all testing in this program. The SR-3 model blade has significant sweep and narrow tips to improve efficiency and reduce near-field noise during high speed cruise. The SR-3 blade model was designed to operate at 0.8 Mach number, 10 668 m (35 000 ft) altitude, 244 m/s (800 ft/sec) tip speed and a power loading of 302 kW/$m^2$ (37.5 SHP/$D^2$, where D is diameter in feet). Design characteristics include: 8 blades, 235 activity factor per blade (a parameter which is a function of blade area), 0.214 integrated design lift coefficient, 34.5 degrees blade sweep (measured on the helix formed by the advancing blade), NACA series 16 airfoils at the blade tip, and NACA series 65/circular arc airfoils at the blade root.

The aeroacoustic design of SR-3 is described in greater detail in reference 3. The aerodynamic test results for SR-3 are discussed in reference 4.

The small scale model used for this test has a nominal diameter of 62.2 cm (24.5 in). However, since the blade has sweep and offset, the actual diameter varies with blade angle. In addition, the diameter is a function of tip speed due to elastic deflection under centrifugal load. For the blade angles and tip speeds tested in this program, the actual model diameter was 64.8 cm (25.5 in). The nominal diameter of 62.2 cm (24.5 in) was used as a normalizing reference for all set-ups in the test program, such as simulated fuselage tip clearance, i.e. tip clearances for the fuselage of 0.4 nominal diameter and 0.8 nominal diameter were tested.

The current prop-fan model was designed to operate in an eight-blade configuration. The cruise design power loading of 302 kW/$m^2$ (37.5 SHP/$D^2$) requires a power input of 354 kW (475 SHP) for the 62.2 cm (24.5 in) diameter model when operated at sea level density. It was determined that simulation of the prop-fan cruise condition in the UTRC tunnel required 22 to 45 kW (30 to 60 SHP) per blade depending on tip helical Mach number. The UTRC propeller drive rig (PDR) has an available power input of 112 kW (150 SHP) at 12 000 RPM, which is not enough to simulate the eight blade full scale loading. Thus, the test model was run in a four-blade configuration, which allowed simulation of full scale power loading per blade. Further discussion of prop-fan model configurations in acoustic test can be found in reference 5.

Fuselage Model. - The simulated fuselage model was constructed from 6.4 mm (1/4 in) steel boiler plate. It is a half cylinder 76.2 cm (30 in) in diameter and 152.4 cm (60 in) long. This model diameter provides a prop-fan-to-fuselage diameter ratio similar to that for a full scale aircraft. The fuselage model was used for testing at two tip clearances which have been proposed for full-scale aircraft. For 0.4 D tip clearance testing, the fuselage model was attached to the inlet nozzle so that the surface was immersed in boundary layer flow simulating a fuselage in flight. For 0.8 D tip clearance testing the fuselage was detached from the nozzle and located outside the tunnel flow stream.

## Facility Description

All testing for this program was conducted in the Acoustic Research Tunnel at the United Technologies Research Center (UTRC) in East Hartford, Connecticut. A detailed description of this facility is given in reference 6. The tunnel is an open-circuit, open jet design (Eiffel configuration). The test chamber is lined with fiberglass wedges to provide an acoustic environment that is anechoic over a frequency range of 200 Hz to 20 kHz. A detailed discussion of the tunnel set-up for prop-fan model acoustic testing is given in reference 5.

Inlet Nozzle. - An inlet nozzle of 1.168 m (46 in) diameter was designed and fabricated for this program. This nozzle allows a maximum flow velocity of about 0.29 Mach number. Tunnel speed is determined from total pressure measurements at the inlet contraction upstream of the anechoic test section and static pressure measurements within the anechoic chamber. Since losses are confined to the boundary layer, total pressure upstream and downstream of the contraction are predicted as well as verified to be equal. This test section velocity has been shown to be temporally steady. Due to the inlet honeycomb and turbulence screen the test section velocity is spatially uniform to within 0.3 percent with a controlled turbulence level of less than 0.15 percent.

Fuselage-Nozzle Interface. - A schematic drawing of the nozzle-fuselage model at 0.4 D tip clearance is shown in Figure 1. The prop-fan plane of rotation was located 45.7 cm (18 in) downstream of the nozzle exit. The nozzle has two sections, a 121.9 cm (48 in) long diverging section faired to a 30.5 cm (12 in) long straight exit section. A three-dimensional nozzle insert was installed to fair the flow from the concave nozzle to the convex fuselage. A cross-sectional view of this test configuration looking upstream is shown in Figure 2. The prop-fan on the right was immersed in the potential core of the tunnel jet. Analytical studies showed that the nozzle insert introduced negligible inflow distortion. The test section of the fuselage model was immersed in the boundary layer flow which began upstream in the nozzle. Photographs of the model are shown in Figures 3 and 4. The numbered locations indicate acoustic test microphone positions. The location marked R.F. is the reference microphone position. In the photographs, the reference position is occupied by a pitot tube pressure probe used for a flow survey of the model. Note that all surface interfaces were faired to insure smooth flow.

Propeller Drive Rig. - The propeller drive rig was powered by a constant torque, water cooled, variable frequency A.C. motor rated at 112 kW (150 SHP) at 12 000 RPM. The rig included a low-noise slipring assembly for transmission of blade dynamic strain and rotor shaft torque meter signals. A once-per-revolution pulse generator (1 P pipper) was used to provide a rotational speed and rotor position reference.

Flow Survey. - A survey was made with the prop-fan and fuselage model installed to verify that the test would simulate the cruise flight flow field. This consisted of three parts: 1) A hot wire anemometry study to determine the

location of the open jet tunnel shear layer relative to the prop-fan blade tips, 2) A pitot tube pressure probe study of the boundary layer on the fuselage surface, 3) A visualization of flow along the fuselage surface using tufts.

A hot-wire anemometer flow study was made to determine the extent of penetration of the open jet turbulent shear layer into the potential core of the tunnel test section and to confirm that there was no interaction between the shear layer and the prop-fan blade tips. This study was similar to that described in reference 5. The four-blade SR-3 model was operated at 1.016 tip helical Mach number at a loading of 21.4 kW (28.7 SHP) per blade. Tunnel flow velocity was 0.269 Mach number.

A 0.0051 mm (0.0002 in) diameter tungsten hot-wire with measured frequency response of 17 kHz was installed so that it could be traversed radially in the prop-fan plane of rotation (see Figure 5). The how-wire traverse covered the range 1.9 cm (0.75 in) to 36.2 cm (14.25 in) from the blade tip. Both turbulence intensity and mean flow velocity were measured. These, shown in Figure 6, give an indication of the shear-layer location. The mean velocity falls to 99 percent of its free-stream value at about 7 cm (2.8 in) tip clearance. This distance can be considered one measure of the clearance between the blade tip and the shear layer. Another measure of the shear layer boundary is the change in r.m.s. percent turbulence level as the probe is traversed from within the potential core into the shear layer. Applying the criterion that an increase of 0.5% in turbulence intensity defines the shear layer boundary, the tip clearance would be estimated at 5 cm (2 in). The high levels very near the blade tip are due to acoustic excitation by the prop-fan.

A more sensitive measure of the shear-layer potential core interface is the onset of intermittency. Intermittency is defined as the occurrence of alternating periods of laminar and turbulent flow in the instantaneous velocity signal at a fixed location. It is caused by large eddies at the interface of turbulent and non-turbulent regions, and is readily detected by observing the oscilloscope trace of hot wire signal. The most inboard location at which intermittency was observed was at 3.2 cm (1.3 in) blade tip clearance. Thus, by the most severe criterion the prop-fan placement in the tunnel jet for this test was such that the blade tips remained free of shear layer turbulence ingestion.

A pitot-tube pressure probe study was made to determine the nature of the boundary layer on the fuselage surface. The probe was installed on the fuselage such that it could be traversed radially from the surface outward to 6.4 cm (2.5 in). It could also be rotated. The probe can be seen in Figures 3 and 4. The probe traverse test was conducted at three of the microphone locations just behind the prop-fan plane of rotation. The first probe position was at the microphone location at the same height as the fuselage centerline. The second probe position was at the outermost microphone location (i.e., the one furthest from the centerline location toward the top of the fuselage). The third probe position was between the first two. A tunnel speed of 0.20 Mach number was tested with the prop-fan operating at 0.90 tip helical Mach number and 14.7 kW (19.7 SHP) per blade. A tunnel speed of 0.265 Mach number was tested with the prop-fan operating at both 1.02 tip helical Mach number and 12.4 kW (16.7 SHP) per blade and

1.14 tip helical Mach number and 23.7 kW (31.8 SHP) per blade. Pressure at the pitot-tube in each radial traverse position was compared with pressure at a surface flush-mounted static tap located at the most downstream microphone location. From the square-root of the pressure differential, the flow velocity can be determined. The results of these tests indicate that all but the four outermost microphone locations are within the region of boundary layer flow. Turbulent boundary layer thickness on the centerline agrees well with classical calculations using a 1/7 velocity profile. Off-center, the flow is skewed slightly (~17°) but still well defined. The outer location is clearly outside the shear layer in a non-structured flow region.

The flow visualization study using tufts glued to the fuselage surface confirm the result seen from the pitot-tube testing. Photographs were taken and closed circuit TV observations were made. A photograph of the fuselage with a tunnel speed of 0.267 Mach number and the prop-fan operating at 1.115 tip helical Mach number and 25.4 kW (34.1 SHP) per blade is shown in Figure 7. The small round dots on the surface are plugged microphone locations. The black tufts are all of the same length. Most of the tufts are reasonably straight, indicating a smooth flow. The tufts near the outermost microphone are fluttering visibly, indicating a flow less well defined.

In summary, the flow survey results show that the prop-fan operated immersed in the clean low turbulence flow of the tunnel jet potential core. The simulated fuselage was under a well-defined turbulent boundary layer at all but the outermost microphone locations. The region of boundary layer flow is shown in Figure 8. It was asymmetrical due to prop-fan rotation.

## Instrumentation

The instrumentation systems used for acoustic data acquisition and measurement of tunnel and rotor operating conditions are described in detail in reference 5. Acoustic data was recorded on a magnetic tape recorder set up for F.M. intermediate band width recording under the IRIG-B standard.

Six channels of acoustic data were recorded during each test run. In order to minimize channel-to-channel phase distortion, the acoustic data signals were recorded using a single seven-channel record head. For correlation of acoustic data with rotor position and to obtain harmonic order analyses, a reference signal from the once-per-revolution (1P) photoelectric pulse generator (pipper) located on the propeller drive rig was recorded on the remaining channel.

Microphones with very low phase distortion (B&K type 4138 3mm (1/8 in) diameter) were used for the simulated fuselage surface flush mount test and all near field acoustic testing. This was necessary to achieve accurate measurement of the spatial distribution of phase on the fuselage surface and of near field acoustic pulse shape. The nominal values for the phase lag of the output voltage of these microphones are 3° at 10 kHz increasing to 10° at 20 kHz. This is sufficiently low for accurate determination of relative phase.

Prior to the start of testing the acoustic data acquisition system was calibrated for phase response. The six microphone channels were calibrated in pairs. For each calibration an identical 500 mV sine wave was injected into the two microphone preamplifiers. Eight signals with frequencies in the range of 100 Hz to 20 kHz were recorded.

The microphones were flush-mounted to the fuselage surface using vibration isolation mounting plugs. Reference free-field acoustic measurements were made with a 6 mm (1/4 in) diameter microphone (B&K 4136). The uncertainty of sound pressure level at an arbitrary frequency between 300 Hz and 20 kHz recorded by the acoustic data acquisition system was ±1.1 dB.

Tunnel flow speed was derived from measurements of atmospheric pressure and tunnel static and total pressure to obtain the tunnel pressure ratio ($P_t/P_s$). Tunnel Mach number follows from isentropic flow equations. The uncertainty in tunnel Mach number was 0.6 percent or less depending on tunnel speed. Test section total temperature was obtained from a thermocouple located in the tunnel inlet calibrated to an accuracy of 1/10 degree Kelvin. Rotor RPM was obtained from the once-per revolution pulse generator (1P pipper) and a calibrated frequency counter. The uncertainty in rotor RPM was ±6 RPM. Rotor power was obtained from a measurement of shaft torque and rotor RPM. The strain gage system mounted on the rig shaft was calibrated prior to the start of testing. The estimated accuracy of this static torque calibration was 2 percent.

## Test Procedure

The acoustic test configuration for the simulated fuselage at 0.4 prop-fan diameter tip clearance is shown schematically in Figure 8. A maximum of six acoustic data channels could be recorded in a single pass, since it was necessary to record using one tape head to retain phase information. Thus, for each test condition, acoustic data from the 21 microphone locations were recorded in four groups of six microphones as indicated on the figure. The number 1 microphone was kept fixed and was recorded with each group as a reference. The remaining five microphones were moved to different locations for each test pass. Therefore, each test condition for the simulated fuselage test was fun four times. The once-per-revolution pulse was also recorded for each test pass. Thus, there is an absolute phase reference for data at each location and each field location is directly comparable to the reference location. In addition to surface measurements, data was taken with a free field microphone in the plane of rotation at 1.6 diameter tip clearance.

A summary of the test operating conditions is given in Table I. A test condition map is shown in Figure 9. Acoustic data was obtained as described above for the boiler plate simulated fuselage at 0.4 prop-fan diameter tip clearance. Three rotational speeds of 9000, 10 000, and 11 300 PRM were tested. The 9000 RPM testing was done with a tunnel Mach number of 0.20, while a nominal tunnel Mach number of 0.265 was used for the remaining testing. Since the tunnel was operated below the full-scale prop-fan cruise Mach number, the model was oversped

to achieve full-scale design relative tip speeds. Exact operating conditions tested during each run were dependent upon atmospheric conditions. They were approximately 1.15 tip helical Mach number at 25.0 kW (33.6 SHP) per blade, 1.02 tip helical Mach number at 13.9 kW (18.6 SHP) per blade, and 0.91 tip helical Mach number at 14.6 kW (19.6 SHP) per blade. Similar test conditions were run for the fuselage in the 0.8 D tip clearance position. In addition, limited data was taken for slow continuous sweeps of both prop-fan RPM and tunnel Mach number. The rotational speed was swept from 8500 RPM (low power) to 11 300 RPM at a constant tunnel axial Mach number of about 0.266. The tunnel Mach number was swept from 0.188 to 0.289 for constant 10 000 RPM prop-fan speed.

Acoustic data were also taken at thirteen free-field locations which corresponded to selected fuselage locations at the 0.8 diameter tip clearance position, using two microphone arrays. This was done in order to determine the effects of the fuselage on measured noise (pressure doubling effects). Equivalent test operating conditions to the fuselage test were run. One of the microphone arrays is shown in Figure 10.

Limited acoustic measurements were made at three fixed microphone locations within the tunnel stream potential core, as shown in Figures 11 and 12. The prop-fan and microphones were located within the inner boundary of shear layer turbulence as defined by the intermittancy criterion. The three 3 mm (1/8 in) microphones were mounted such that they did not mutually interact in the flow. Their common radial location was 5.1 cm (2.0 in) outboard of the blade tips and they were axially located in the prop-fan plane of rotation at the prop-fan tip, 0.5 D upstream and 0.5 D downstream respectively. Also, measurements were made in the plane of rotation at 1.6 D clearance. Data were taken for three transonic operating conditions at moderate to high blade loading as shown in Table I and Figure 9.

## Data Reduction

Narrow-Band Frequency Analysis. - All the acoustic data acquired in this program were analyzed using a Spectral Dynamics model SD301C narrow-band frequency analyzer. The analysis range used was 0 to 20 kHz, which gave an effective filter bandwith of 60 Hz. From these analyses, the harmonic sound pressure levels were determined at each of the microphone locations.

The data acquired during the RPM and tunnel Mach number sweeps were reduced by performing narrow-band analyses at discrete intervals during the sweeps. For the RPM sweep, narrow band spectra were made at 200 RPM intervals from 8500 to 11 300 RPM. For the tunnel Mach number sweep, 15 narrow band spectra were made at the time intervals corresponding to constant increments of tunnel $\Delta p$. The sound pressure levels for the first six harmonics of blade passing frequency for an 8-bladed prop-fan (since the model was tested in a 4-bladed configuration, every other harmonic was used) and the overall level based on the sum of these six harmonics for the fuselage reference microphone

at a tip clearance of 0.4 diameter are presented in Appendix A. The levels have not been adjusted to reflect the addition of 4 more blades as only the relative levels and spectral characteristics as functions of relative tip Mach number are of interest here.

Since the data from the 21 microphone locations on the fuselage were acquired in four passes, the data from three of the passes were adjusted to conditions equivalent to those of the fourth pass. This was necessary, as ambient conditions had changed slightly during the acquisition of the data, thus power inputs to the propfan varied slightly. The data adjustment was made on the basis of the measurements made using the semi-cylinder reference microphone and the free-field reference microphone, which were both common to the four passes. The average change seen between each data set and the reference data set for these two microphones was applied to each of the harmonic levels. This resulted in a consistent set of measurements for all 21 microphone locations.

The normalized sound pressure levels of the first 10 harmonics of blade passing frequency for each of the three operating conditions and three test configurations are presented in Appendix A.

Relative Amplitude and Phase. - As the absolute phase of the acoustic signal is of no importance and only the relative phase distributions on the semi-cyliner surface are desired, the relative phases of the acoustic signal were determined by doing a transfer function analysis on the data using the semi-cylinder reference microphone signal as the input signal and each of the microphone signals as the output signals. The transfer function was determined using a Time Data Signal Analysis System using standard routines for calculating the transfer function and Hamilton Standard routines for tabulating the desired information. The transfer function H(f), was determined from the cross-power spectrum using the following relations:

$$H(f) = \frac{S_y(f)}{S_x(f)} = \frac{S_y(f) \cdot S^*_x(f)}{S_y(f) \cdot S^*_x(f)} = \frac{G_{xy}(f)}{G_{xx}(f)}$$

Where $S_x(f)$ and $S_y(f)$ are the Fourier transforms of inputs x and y, respectively, $G_{xy}(f)$ is the cross-power spectrum of x and y, $G_{xx}(f)$ is the power spectral density (PSD) of x, and * denotes complex conjugate. In this analysis, x was always the semi-cylinder reference microphone and y was each of the other microphones.

Since H(f) is a complex quantity, it can be represented by a magnitude and a phase. The magnitude of H(f) represents the amplitude of the signal relative to that of the reference signal ($P_y/P_{ref}$) while the phase of H(f) represents the phase difference ($\theta_y - \theta_{ref}$). Only the phase information was used and since $\theta_{ref}$ is common to all the data the quantity $\theta_y - \theta_{ref}$ defines the relative phase distribution on the semi-cylinder.

In order to avoid smearing and aliasing problems, the data was digitized synchronously using the once-per revolution (1P) pipper as a clock input. The 1P pipper was multiplied by 102.4 using a Spectral Dynamics SD134 Tracking Ratio Tuner to drive the digitizer so that each time frame of 1024 points would contain exactly 10 cycles of the acoustic signal. A 512-point Fourier transform was then done on each time frame, with 120 transforms averaged for each analysis. Since the data was highly periodic, only those points in the transforms corresponding exactly to blade passing frequency harmonics had any significance--the rest was random noise. Thus, only every 40th point in the transform was used. Because of the synchronous sampling and integral time frames used, these corresponded exactly to the blade passage frequency harmonics.

Phase calibration was accomplished by playing back the phase calibration data through the same playback/data reduction system. This provided relative phases between the reference microphone channel and each of the other data channels as functions of frequency. The microphone phase distortion was assumed negligible so that the only phase distortion correction applied to the data was that of the record/playback system determined as described above.

Appendix A contains the relative-phase data corrected for system response. It should be noted that the phases determined by the transfer function method yields the output phase lag relative to that of the input. In wave propagation theory, the convention is to use a negative phase (phase lead), so that the arithmetic sign of the phase values given in Appendix A have been reversed.

## DATA ANALYSIS

### RPM and Tunnel Mach Numbers Sweeps

The sound pressure level variation with prop-fan helical tip Mach number is summarized in Figure 13. The RPM sweep data shows a fairly smooth noise level increase from a helical tip Mach number of 0.878 (8500 RPM) to a helical tip Mach number of 1.143 (11 300 RPM). The 8P harmonic overall level increases at a more rapid rate than that of the 8P harmonic because the rise in the levels of the higher harmonics is greater than that in the lower harmonics. It should be noted, however, that the rapid increase in both overall and 8P harmonic levels is caused by an increase in power input, from 3.75 kW (5.0 SHP) per blade at 8500 RPM to 24.75 kW (33.2 SHP) per blade at 11 300 RPM.

The tunnel Mach number sweep at 10 000 RPM on Figure 13 also shows a smooth noise level variation with helical tip Mach number. In this case, however, the increasing inflow velocity results in decreasing blade section angles-of-attack and thus decreasing power input to the prop-fan, from 25.14 kW (33.7 SHP) per blade at the low tunnel Mach number to 8.43 kW (11.3 SHP) per blade at the high tunnel Mach number. Thus, as the helical tip Mach number is increasing, the blade loading is decreasing. Apparently, the blade loading effect on noise is stronger than that of tip Mach number.

It can thus be concluded that the variation in prop-fan noise level with tip Mach number is a smooth function. At constant through flow velocity the overall noise shows a monotonically increasing function of helical tip Mach number whose slope decreases slightly with increasing Mach number. The variation in prop-fan noise level with tip Mach number by varying tunnel Mach number at constant RPM shows a negative slope caused by the unloading of the blades.

### Harmonic Amplitude Contour Plots

The harmonic levels, determined from the narrow-band frequency analyses and included in Appendix A, were used to define constant sound pressure amplitude contours on the semi-cylinder surface. As the microphones were limited in number, a certain amount of subjective interpretation is required to define the contours. The contours shown in Figures 14 through 16 are for the 11 300 RPM condition with the simulated fuselage at 0.4 prop-fan diameter clearance. These were derived from the measurements at the 21 microphone locations. Plots were made of the levels along several lines defined by the microphones; for example microphone numbers 2, 5, 8, 11, 1, 18 and 21, microphone numbers 9, 10, 11, 12, and 13, microphone numbers 14, 15, 16, and 17, microphone numbers 10, 15, and 19, microphone numbers 12, 16, and 20, microphone numbers 7, 11, and 15, microphone numbers 6, 11, and 16, etc. From these plots, the locations on the semi-cylinder surface where the sound was a specific level were determined. These points were then joined by a smooth curve.

Figure 14 shows the measured sound pressure amplitude contours for the 4P (fundamental blade passing frequency) harmonic. As can be seen, the maximum noise level is about 148 dB and occurs slightly ahead of the plane of rotation. A second local peak occurs at a level of about 145 dB behind the plane of rotation. The pattern is not symmetrical about the centerline, partly because of pressure doubling effects due to the semi-cylinder. Figure 15 shows the sound pressure amplitude contours for the 8P harmonic. For this harmonic, the peak also occurs just ahead of the plane of rotation. Although the pattern for this harmonic appears more symmetrical than for the 4P harmonic, the contours are more closely spaced below the centerline than above the centerline. This occurs because the acoustic wave incidence is more normal on the top surface. On the lower surface, the sound approaches grazing incidence so that pressure doubling effects are less and the contours are more closely spaced (the effects of incidence angle in the pressure doubling effects will be discussed in a following section). In Figure 16, the 12P harmonic contours appear similar to those for the 8P harmonic.

## Harmonic Phase Angle Contour Plots

Phase angle contours were determined in a manner similar to that used for the sound pressure amplitude contours. The contours are shown in Figure 17 for the 4P harmonic and in Figure 18 for the 8P harmonic. Part of the interpolation involved determining when the phase passed beyond the tabulated range of ± 180 degrees. Although multiples of 360 degrees result in the same phase angles (i.e. 400 degrees is the same phase angle as 40 degrees), the angles were extended beyond ± 180 degrees to show continuity.

In Figure 17 the 4P harmonic phase angle contours appear as ellipse-like shapes centered at a point slightly ahead of the plane of rotation and above the semi-cylinder centerline. The 8P harmonic phase contours, in Figure 18, show more rapid changes in phase (as would be expected, since the wavelength is shorter). The shapes of these contours are generally similar to those for the 4P harmonic.

## Pressure Doubling Effects

The effect of the simulated fuselage surface on the harmonic sound pressure levels was determined by comparison of the measurements made with the microphones installed in the semi-cylinder at the 0.4 D location with calculated free-field levels using the prop-fan noise calculation procedure (reference 5). Pressure doubling effects were also calculated by comparing the levels measured with the fuselage at the 0.8 D location and those measured at equivalent free-field locations.

The pressure doubling effects for the fuselage located at 0.4 D clearance were estimated by first calculating the prop-fan noise levels and comparing them to those measured using the three near-field microphones. This comparison is summarized

in Table II for the first two harmonics of the 11 300 RPM prop-fan operating condition. As may be seen, the calculated levels are reasonably close to the measured levels except for the in-plane location at the fundamental and the aft location at the second harmonic. Next, the free-field noise levels were calculated at each of the 21 fuselage locations. The calculated levels were adjusted using the factors derived from the comparison of calculated and measured near-field levels. The adjustment factors were plotted as functions of prop-fan radiation angles (as calculated using the procedure described in Appendix B for a 2 inch tip clearance) with a smooth curve joining the three points for each harmonic, as shown in Figure 19. Based on the prop-fan radiation angles to each of the 21 microphone locations, adjustment factors were determined from Figure 19 and added to the calculated levels. Finally, the adjusted calculated levels were compared to the measured levels. The differences between measured and adjusted calculated levels are then the pressure doubling effects. The estimated pressure doubling effects using this approach are summarized in Table III. As may be seen, the estimated pressure doubling effects vary from 4.1 dB to 18.8 dB, with the average level being 14.6 dB for the 4P harmonic and 11.2 dB for the 8P harmonic. As the fuselage causes only one reflection, the anticipated result is in the range 0 to 6 dB. The higher-than-anticipated levels are believed to be the result of the large negative corrections in the 50 to 110 degree radiation angle region resulting from the comparison of measured and calculated levels for the in-plane near-field microphone. Discussion in reference 5 indicates that calculations for field points less than about one blade chord from the blade tips using the prop-fan noise calculation procedure may be in error due to non-linear propagation effects not accounted for in the theory. Thus, the derivation of pressure doubling effects summarized in Table III are probably in error due to the influence of non-linear propagation effects on the in-plane data.

Reference 5 presents comparisons of calculations and measurements made under free-field conditions at a tip clearance of 0.8 diameters, well beyond the non-linear propagation effects range. The comparisons between measured and calculated levels for the 8P harmonic are also summarized in Figure 19 as a function of radiation angle. As may be seen, these result in an S-shaped curve spanning the range -2.2 dB to 8.8 dB which is substantially different from that derived from the very-near-field measurements. This curve was also used to derive pressure doubling effects as previously described. These are summarized in Table IV, where the same adjustment curve was used for both 4P and 8P harmonics. As this table shows, the values of pressure doubling effects are in a more reasonable range.

The pressure doubling effects do not show any dependence on frequency, as both the fundamental and second harmonic show generally the same values at each microphone location. This is not unexpected, as the wavelengths are short enough relative to the fuselage diameter to be in the realm of geometric acoustics. Thus, the values for the two harmonics at each microphone location were averaged to reduce the scatter in the measurements. The averaged values are summarized in Table V. Also shown in Table V are the calculated incidence angles using the derivation from Appendix B without the shear layer effects, as the fuselage was immersed in the flow.

Figure 20 shows the two sets of pressure doubling effects plotted against incidence angle (where 90 degrees is normal incidence). It is apparent that there is some scatter in the data and no clear trend with incidence angle can be seen. However, both sets of data show predominantly high values for incidence angles above 45 degrees, lower values below 45 degrees, and lower values still for the points at 0.7 degrees incidence. A linear regression shows positive slopes for both sets of data which indicates that the pressure doubling effect increases with increasing incidence angle. Although a well defined, smooth curve fitting the data in Figure 20 cannot be established due to the scatter, full pressure doubling (6 dB) for near-normal incidence decreasing to no effect at grazing angles is suggested.

The measured prop-fan noise levels with the fuselage at 0.8 D clearance and at equivalent free-field locations were also used to estimate the pressure doubling effects. The data used in this analysis are presented in Appendix A. As with the previous data, there does not appear to be a dependence on frequency. Thus, the data for the ten harmonics and the three RPMs were averaged (30 points averaged for each microphone location). Table VI summarizes the averaged pressure doubling effects and the calculated sound incidence angles. The sound incidence angle was calculated as described in Appendix B, including shear-layer transmission effects. The shear-layer effects described in Appendix B have been simplified, as the refraction effects in the plane perpendicular to the tunnel axis are ignored (however, these are typically only a few degrees). The actual shear-layer effects were calculated using the computer program described in reference 5. Comparison of these with those calculated using the simplified derivation of Appendix B show differences of typically two to three degrees, well within the range of measurement accuracy.

Figure 21 shows the data plotted against incidence angle. There is much scatter in this data, although not as much as that shown in Figure 20, probably because of the averaging used and this being a comparison between measured values rather than measured vs. calculated. Although no clear trend is shown by the data, the cluster of data points beyond 60 degrees suggests that the full pressure doubling effect of 6 dB was attained. The data between 30 and 60 degrees show three points less than 6 dB and only two points above 6 dB, suggesting that the pressure doubling effects are decreasing with decreasing incidence angle. This is supported by the point at 10.3 degrees.

Neither the data from Figure 20 nor that from Figure 21 show clear trends in pressure doubling effects with incidence angle. This is due to the great amount of scatter, which is not really surprising since the total anticipated effect is only 0 to 6 dB. However, the data does suggest that the full effect of 6 dB is attained at normal incidence and decreases with decreasing incidence angle. The curve shown in Figure 21 was derived by an exponential curve fit passing through 0 dB at 0 degrees and through 6 dB at 60 degrees. The values from this curve were used for the pressure doubling corrections as functions of incidence angle.

## Effect of Simulated Fuselage on Source Noise Level

One of the areas investigated in this program was the influence of the presence of the semi-cylinder on the prop-fan noise source level. In this investigation, a microphone was located in the free-field (see test description section) at a constant position relative to the prop-fan during the entire test sequence. Thus, by comparing the spectra from this microphone for the configurations with the simulated fuselage located at 0.4 diameter clearance, the simulated fuselage located at 0.8 diameter clearance, and without the simulated fuselage in the test area the impact of the simulated fuselage on the source noise can be assessed.

Figure 22 summarizes the levels of the first 10 harmonics of blade passing frequency measured by the free-field reference microphone. At 9000 RPM,the data shows similar harmonic sound pressure levels for all three configurations. At 10 000 RPM, the data shows a weak trend which indicates that the presence of the simulated fuselage increases the measured levels slightly. Generally, the levels are slightly higher for the configuration with the semi-cylinder at 0.8 diameter clearance than for the configuration with no simulated fuselage, and they are slightly higher for the configurations with the semi-cylinder at 0.4 diameter clearance than for the configuration with the semi-cylinder at 0.8 diameter clearance. At 11 300 RPM, the no-fuselage and the 0.8 diameter clearance configurations show similar levels which are about 2 dB lower than those for the configuration with the fuselage at 0.4 diameter clearance.

On the basis of this data, it appears that the presence of the simulated fuselage causes an increase of about 2 dB in the source noise. As this increase is independent of frequency, being relatively constant for the 10 harmonics analysed, it is not believed that this is due to distortion of the tunnel airflow by the semi-cylinder. A more plausible explanation is that the increase is due to reflections from the semi-cylinder. Since the accoustic signal is highly periodic, the phase relationship between the direct signal and the reflected signal is related to the path length difference and remains constant in time. Two special cases can easily be visualized. Assuming that the direct and reflected signals have equal amplitudes at the microphone, in one case the path length difference is such that the two signals arrive at the same time. This is exactly equivalent to a pressure doubling at each harmonic, as the reflected and direct signal are in phase at the microphone. In the other case, the path length difference is such that the reflected wave pulse train arrives exactly mid-way between the direct wave pulse trains. The odd harmonics are cancelled and the even harmonics are doubled in amplitude (this is an analogous result to that of adding four more blades to the prop-fan). In actual practice, the reflected wave is weaker than the direct wave, due to the much longer distance traveled by the reflection, and these two special cases are probably never realized, so that the actual result will be something in-between. It is interesting to note that comparing the harmonic levels for the no-fuselage and 0.4 diameter clearance configurations at 11 300 RPM shows the constant increase in level anticipated for the first special case discussed above,while the comparison at 9000 RPM shows the alternating pattern anticipated for the second special case described above. (Note that the wavelength at the fundamental is small enough that geometric acoustics apply.)

It is thus concluded that the presence of the simulated fuselage does not have any appreciable effect on the level of noise generated by prop-fan per se, but that the variations in noise levels noted in the free-field reference microphone data are the result of reflections from the simulated fuselage.

## Comparison of Measured and Calculated Prop-Fan Noise

Harmonic Levels. - 4P and 8P harmonic noise levels on the simulated fuselage surface located at 0.4 prop-fan diameter clearance for the prop-fan operating at the 11 300 RPM condition were calculated using the current Hamilton Standard noise prediction methodology. As this procedure calculates noise under free-field conditions, the empirically derived pressure doubling effects were added to the estimates for comparison with the levels measured in the simulated fuselage.

Figure 23 shows the calculated sound pressure level contours for the 4P harmonic. As may be seen, the pressure doubling effects cause the patterns to be compressed below centerline and to be expanded above centerline due to the incidence angle effect (see previous discussion on pressure doubling effects). Compared to the measured sound pressure level contours, Figure 14, several discrepancies are apparent. Although the peak level of 148 dB is well predicted, the secondary peak seen in Figure 14 is not predicted. This secondary peak has been identified as a peak in the loading noise, which is not well calculated by the prop-fan noise predicted methodology for the low throughflow velocities for the Acoustic Research Tunnel conditions (see reference 5 for a more detailed discussion of comparisons of measured and calculated model prop-fan noise). The location of the peak noise level is fairly well calculated.

Figure 24 shows the calculated sound pressure level contours for the 8P harmonic. These are to be compared to the measured 8P harmonic sound pressure level contours shown in Figure 15. There, the agreement is better than for the 4P harmonic. Both the peak value of 148 dB and the location of the 148 dB "island" are well predicted. The calculated contours appear more closely spaced along the centerline than those measured. As for the 4P harmonic, the reason for this is the inaccuracy in the calculation of loading noise for the Acoustic Research Tunnel conditions. The contour below the centerline are in generally good agreement, except for the distortion apparent in the measurements. However, considering that the contours are only 1 dB apart and that the measurement accuracy is about ± 2 dB, it must be concluded that the agreement is fairly good.

It is thus concluded that based on the comparison of measured and calculated harmonic noise level distribution on the model fuselage, the estimates of harmonic noise levels of a full-size prop-fan in cruise will be acceptable. This comparison showed good agreement at the peak noise level location for the first three harmonics. The higher harmonics showed good agreement at all locations (recall that the fundamental

of the full scale SR-3 prop-fan will be 8P and not 4P as tested on model scale). Also, the prop-fan noise prediction methodology will provide better estimates of noise for the actual cruise condition than for the simulated cruise condition tested in the wind tunnel, as the loading noise can be more accurately calculated for the actual cruise condition (see reference 5).

Harmonic Phases. - Figure 25 shows the calculated phase angle contours for the 4P harmonic. These are seen to appear as ovoids roughly centered on a point near microphone location 10. The corresponding phase angle contour plot derived from the measurements is shown in Figure 17. Comparison of Figures 17 and 25 shows that both the measurements and the calculations show the centers of the "islands" to be above the centerline and ahead of the plane of rotation. Although the two plots do not exactly superimpose, it should be noted that absolute phase is not of importance. Thus, if the calculated phase angle contours are shifted forward about 10 cm (4 in), the two sets of contours line up fairly well. The rate of change of the phase for the calculations along the plane of rotation and behind the plane of rotation is in close agreement with that measured. Forward of the plane of rotation, the calculations show a less rapid change than that shown by the measurements.

Figure 26 shows the calculated phase angle contours for the 8P harmonic of the 11 300 RPM condition. Comparison with the measured phase angle contours, Figure 18, shows generally the same trends as those observed for the 4P harmonic. Again, the calculated contours have to be shifted for best agreement. Shifting the calculations forward about 7.5 cm (3 in) and down about 6 cm (2.5 in) provides very good agreement for phase contours from 90 to 540 degrees, although the 0 degree phase "center" misses by about 15 cm (6 in).

Thus, although the unimportant absolute phase is not particularly well calculated, the agreement between calculated and measured phase rate change is good over most of the simulated fuselage surface. As it is believed that the prop-fan noise under 0.8 Mach number cruise condition can be better calculated than that in the Acoustic Research Tunnel (see reference 5), these encouraging results indicate that the calculations of phase contours for the full scale prop-fan at cruise conditions will be highly representative of the true phase contours.

## Applicability to Other Prop-Fan Designs

Sound pressure level and phase angle contours have been defined for the SR-3 model prop-fan tested in the wind tunnel with low through-flow velocity. It should be noted that these contours are not directly applicable to the SR-3 prop-fan operating in cruise or to other prop-fan designs operating either in the tunnel or in cruise.

The reader is thus cautioned against using the data reported herein as universal noise distributions. The amplitude and phase contours will change significantly depending on prop-fan design (SR-3, SR-5, etc.), operating condition (tip speed,

flight speed), and installation (clockwise or counter clockwise rotation, fuselage tip clearance). To properly define the amplitude and phase distributions in general, the prop-fan noise prediction methodology must be used with the defined empirically-derived pressure doubling effects.

# FULL SCALE PREDICTIONS

## Introduction

Sound pressure level and phase angle contours were estimated for a full scale prop-fan operating at cruise conditions. For these estimates, a 3.83 m (12.55 ft) diameter prop-fan with eight SR-3 type blades operating at a tip speed of 243.8 m/sec (800 ft/sec), with a power input of 4400 kW (5900 SHP) was assumed for a 10 668 m (35 000 ft) altitude cruise at 0.8 Mach number. The geometry for the installation is summarized in Figure 27.

The sound pressure level contours were estimated on the basis of free-field noise estimates at the fuselage locations. These were adjusted for fuselage pressure doubling effects, using the corrections based on angle of incidence from Figure 21. The angle of incidence was calculated from the geometry shown in Figure 27 (assuming a cylindrical fuselage) and apparent source location due to convection effects as defined in Appendix B. Note that the direction of rotation of the full-scale prop-fan has been reversed relative to that of the model test, so that grazing incidence occurs at the top of the fuselage rather than at the bottom as was the case for the model test. This was done to take advantage of several potential benefits such as having the higher noise levels (at more normal incidence) below the cabin floor and shielding by the wing. The phase angle contours are based on the calculated acoustic phase angles.

## Estimated Full Scale Sound Pressure Level Contours

Figure 28 shows the predicted sound pressure level contours for the fundamental blade passing frequency. A peak noise level of 150 dB is estimated. Due to convection effects, the peak noise level appears behind the plane of rotation. At the peak noise level location, the pressure doubling effect is +6 dB. The 10 dB down points are about 1.5 m (5 ft) behind the peak noise level location and 2.6 m (8.5 ft) ahead of the peak noise level location. It may also be seen that the sound pressure level contours closely follow the fuselage circumference behind the peak noise location. Ahead of the peak noise level location, the contours are expanded, primarily due to reduced pressure doubling effects caused by shallower incidence angles. The contours are also contracted near the top of the fuselage due to reduced pressure doubling effects as the incidence angles are near grazing in this area.

## Estimated Full Scale Phase Angle Contours

Figure 29 shows the phase angle contours for the fundamental blade passing frequency tone. As this figure shows, the phase changes slowly from the zero-phase point to the 180 degree phase contour. Beyond the 180 degree phase contour, the phase changes very rapidly, increasing from a 180 degree change in 0.6 m (2 ft) at 0.9 m (3 ft) behind the plane of rotation to a change of 360 degrees in 0.3 m (1 ft) at 2.7 m (9 ft) ahead of the plane of rotation.

## CONCLUSIONS

Based on the analysis of the acoustic data acquired on a simulated fuselage in the near-field of a model SR-3 prop-fan, the following conclusions have been reached:

1. The effect of the fuselage is to cause pressure doubling of the amplitude and no effect on the phase. The pressure doubling effect is dependent on incidence angle and varies from no effect at grazing incidence to an increase of 6 dB for incidence angles greater than 60 degrees.

2. Amplitude and phase contours can be adequately predicted using the prop-fan noise prediction procedure described in reference 5, which was used in this study.

3. A full scale, 3.83 m (12.55 ft) diameter version of the prop-fan tested in this program located at 0.8 diameter clearance is estimated to produce a peak noise level of 150 dB, including pressure doubling effects, at the blade passing frequency harmonic. The 10 dB down points are estimated to occur 1.5 m (5 ft) behind the peak noise location and 2.6 m (8.5 ft) ahead of the peak noise location. The phase is calculated to change slowly behind the plane of rotation and very rapidly ahead of the plane of rotation.

## REFERENCES


1. Bhat, R.B., Sobieszczinski, J., and Mixson, J.S.: "Reduction of Aircraft Cabin Noise by Fuselage Structural Optimization," Proceedings of the National Noise and Vibration Control Conference and Exhibition, NOISEXPO '77, March, 1977.

2. SenGupta, G.: Low Frequency Cabin Noise Reduction Based on the Intrinsic Structural Tuning Concept, NASA CR-145262, March 1978.

3. Metzger, F. B.; Rohrbach, C.: "Aeroacoustic Design of the Prop-Fan." AIAA Paper No. 79-0610, 1979.

4. Jeracki, R.J.; et al: Wind Tunnel Performance of Four Energy Efficient Propellers Designed for Mach 0.8 Cruise, NASA TM 79124, 1979.

5. Brooks, B. M.; Metzger, F. B. : Acoustic Test and Analysis of Three Advance Turboprop Models. NASA CR159667, Oct. 1979.

6. Paterson, R.W.; Vogt, P. G. ; and Foley, W. M. : "Design and Development of the United Aircraft Research Laboratories Acoustic Research Tunnel." J. of Aircraft, Vol. 10, No. 7, 1973 pp 427-433.

TABLE I SUMMARY OF BOILERPLATE FUSELAGE TEST OPERATING CONDITIONS

| Run Number | Blade Angle | Temperature °K | Temperature °F | Tunnel Mach No. | RPM | Power kW | Power SHP | Tip Helical Mach No. | Comments |
|---|---|---|---|---|---|---|---|---|---|
| 263 | 21.5° | 304 | 88 | 0.267 | 11 300 | 94.3 | 126.4 | 1.143 | Boilerplate at |
| 264 | | 305 | 89 | 0.267 | 10 000 | 48.2 | 64.6 | 1.016 | 0.4 D Tip |
| 265 | | 304 | 88 | 0.201 | 9 000 | 52.3 | 70.1 | 0.901 | Clearance |
| 266 | | 298 | 76 | 0.267 | 11 300 | 100.2 | 134.3 | 1.155 | |
| 267 | | 297 | 75 | 0.267 | 10 000 | 55.5 | 74.4 | 1.028 | |
| 268 | | 297 | 75 | 0.200 | 9 000 | 58.3 | 78.2 | 0.911 | |
| 269 | | 299 | 79 | 0.265 | 11 300 | 101.4 | 135.9 | 1.151 | |
| 270 | | 299 | 78 | 0.265 | 10 000 | 51.8 | 69.5 | 1.025 | |
| 271 | | 299 | 78 | 0.200 | 9 000 | 56.9 | 76.3 | 0.909 | |
| 272 | | 299 | 79 | 0.267 | 11 300 | 100.2 | 134.3 | 1.152 | |
| 273 | | 299 | 79 | 0.265 | 10 000 | 50.8 | 68.1 | 1.024 | |
| 274 | | 299 | 78 | 0.200 | 9 000 | 57.9 | 77.6 | 0.909 | |
| 277 | 21.5° | 295 | 71 | 0.268 | 11 300 | 104.9 | 140.6 | 1.160 | 3 Microphones in |
| 278 | | 294 | 69 | 0.270 | 10 000 | 53.9 | 72.3 | 1.035 | Potential Core |
| 279 | | 293 | 68 | 0.201 | 9 000 | 61.1 | 81.9 | 0.917 | |
| 280 | 21.5° | 291 | 64 | 0.267 | 11 300 | 120.1 | 161.0 | 1.167 | Boilerplate at |
| 281 | | 291 | 64 | 0.266 | 10 000 | 58.1 | 77.8 | 1.038 | 0.8 D Tip |
| 282 | | 292 | 65 | 0.201 | 9 000 | 62.1 | 83.2 | 0.920 | Clearance |
| 285 | | 297 | 75 | 0.266 | 11 300 | 109.5 | 146.8 | 1.156 | |
| 286 | | 297 | 75 | 0.266 | 10 000 | 58.6 | 78.5 | 1.028 | |
| 287 | | 297 | 75 | 0.200 | 9 000 | 62.1 | 83.2 | 0.911 | |
| 288 | | 299 | 78 | 0.266 | 11 300 | 105.5 | 141.4 | 1.153 | |
| 289 | | 301 | 82 | 0.266 | 10 000 | 54.5 | 73.0 | 1.022 | |
| 290 | | 301 | 81 | 0.199 | 9 000 | 62.5 | 83.8 | 0.906 | |
| 291 | | 301 | 81 | 0.269 | 11 300 | 105.5 | 141.4 | 1.151 | |
| 292 | | 301 | 81 | 0.269 | 10 000 | 51.8 | 69.5 | 1.023 | |
| 293 | | 302 | 84 | 0.204 | 9 000 | 55.1 | 73.8 | 0.905 | |
| 294 | 21.5° | 301 | 82 | 0.268 | 11 300 | 108.4 | 145.3 | 1.149 | No Boilerplate. |
| 295 | | 302 | 83 | 0.269 | 10 000 | 52.9 | 70.9 | 1.022 | Equivalent Free- |
| 296 | | 301 | 82 | 0.202 | 9 000 | 57.9 | 77.6 | 0.906 | Field Locations |
| 297 | | 300 | 80 | 0.269 | 11 300 | 107.8 | 144.5 | 1.152 | At 0.8 D Tip |
| 298 | | 299 | 79 | 0.269 | 10 000 | 50.3 | 67.4 | 1.025 | Clearance |
| 299 | | 299 | 79 | 0.200 | 9 000 | 56.9 | 76.3 | 0.908 | |

TABLE II COMPARISON OF MEASURED AND CALCULATED NEAR-FIELD FREE-FIELD PROP-FAN HARMONIC NOISE LEVELS AT 11 300 RPM

| Location | Harmonic | Calc.,dB | Meas.,dB | Adj. Factor,dB |
|---|---|---|---|---|
| Forward | 4P | 138.0 | 142.0 | 4.0 |
| In-Plane | 4P | 148.0 | 136.5 | -11.5 |
| Aft | 4P | 130.8 | 130.5 | -0.3 |
| Forward | 8P | 128.5 | 133.0 | 4.5 |
| In-Plane | 8P | 149.5 | 143.5 | -6.0 |
| Aft | 8P | 116.2 | 127.5 | 11.3 |

TABLE III DERIVATION OF PRESSURE DOUBLING EFFECTS BASED ON MEASURED AND CALCULATED PROP-FAN NOISE LEVELS USING THE VERY-NEAR-FIELD MICROPHONE DATA

| Mic. Number | Radiation Angle, Deg | Adjust-ment, dB | Calc Level, dB | Adjusted Calc., dB | Measured Level, dB | Press. Doubling, dB |
|---|---|---|---|---|---|---|
| a. 4P Harmonic | | | | | | |
| 1 | 87.9 | -10.8 | 137.0 | 126.2 | 144.0 | 17.8 |
| 2 | 40.5 | -5.4 | 137.4 | 132.0 | 143.5 | 11.5 |
| 3 | 46.6 | -7.9 | 139.1 | 131.2 | 147.0 | 15.8 |
| 4 | 46.6 | -7.9 | 139.1 | 131.2 | 145.0 | 13.8 |
| 5 | 51.5 | -9.2 | 140.9 | 131.7 | 146.5 | 14.8 |
| 6 | 59.0 | -10.6 | 141.5 | 130.9 | 148.0 | 17.1 |
| 7 | 59.0 | -10.6 | 141.5 | 130.9 | 147.0 | 16.1 |
| 8 | 66.1 | -11.2 | 142.1 | 130.9 | 147.0 | 16.1 |
| 9 | 74.5 | -11.7 | 138.2 | 126.5 | 141.0 | 14.5 |
| 10 | 74.5 | -11.7 | 140.6 | 128.9 | 142.5 | 13.6 |
| 11 | 74.5 | -11.7 | 141.1 | 129.4 | 144.5 | 15.1 |
| 12 | 74.5 | -11.7 | 140.6 | 128.9 | 142.5 | 13.6 |
| 13 | 74.5 | -11.7 | 138.2 | 126.5 | 139.5 | 13.0 |
| 14 | 93.7 | -10.1 | 134.6 | 124.5 | 141.0 | 16.5 |
| 15 | 98.0 | -9.4 | 135.1 | 125.7 | 144.5 | 18.8 |
| 16 | 98.0 | -9.4 | 135.1 | 125.7 | 141.5 | 15.8 |
| 17 | 93.7 | -10.1 | 134.6 | 124.5 | 138.0 | 13.5 |
| 18 | 108.1 | -7.0 | 133.6 | 126.6 | 142.0 | 15.4 |
| 19 | 117.5 | -4.4 | 130.6 | 126.2 | 140.0 | 13.8 |
| 20 | 117.5 | -4.4 | 130.6 | 126.2 | 138.0 | 11.8 |
| 21 | 130.7 | -0.3 | 126.1 | 125.8 | 134.0 | 8.2 |
| b. 8P Harmonic | | | | | | |
| 1 | 87.9 | -5.4 | 137.3 | 131.9 | 146.0 | 14.1 |
| 2 | 40.5 | -0.8 | 131.2 | 130.4 | 134.5 | 4.1 |
| 3 | 46.6 | -2.7 | 135.2 | 132.5 | 144.0 | 11.5 |
| 4 | 46.6 | -2.7 | 135.2 | 132.5 | 143.5 | 11.0 |
| 5 | 51.5 | -3.8 | 138.2 | 134.4 | 146.0 | 11.6 |
| 6 | 59.0 | -5.0 | 140.5 | 135.5 | 147.0 | 11.5 |
| 7 | 59.0 | -5.0 | 140.5 | 135.5 | 147.5 | 12.0 |
| 8 | 66.1 | -5.4 | 142.1 | 136.7 | 147.5 | 10.8 |
| 9 | 74.5 | -6.0 | 139.0 | 133.0 | 142.0 | 9.0 |
| 10 | 74.5 | -6.0 | 141.5 | 135.5 | 145.5 | 10.0 |
| 11 | 74.5 | -6.0 | 142.0 | 136.0 | 148.0 | 12.0 |
| 12 | 74.5 | -6.0 | 141.5 | 135.5 | 145.5 | 10.0 |
| 13 | 74.5 | -6.0 | 139.0 | 133.0 | 138.0 | 5.0 |
| 14 | 93.7 | -4.9 | 134.1 | 129.2 | 142.0 | 12.8 |
| 15 | 98.0 | -4.0 | 133.6 | 129.6 | 144.5 | 14.9 |
| 16 | 98.0 | -4.0 | 133.6 | 129.6 | 143.0 | 13.4 |
| 17 | 93.7 | -4.7 | 134.1 | 129.4 | 141.5 | 12.1 |
| 18 | 108.1 | -1.3 | 129.2 | 127.9 | 143.5 | 15.6 |
| 19 | 117.5 | 2.4 | 122.7 | 125.3 | 138.0 | 12.7 |
| 20 | 117.5 | 2.4 | 122.7 | 125.3 | 136.0 | 10.7 |
| 21 | 130.7 | 11.1 | 113.4 | 122.3 | 133.0 | 10.7 |

TABLE IV DERIVATION OF PRESSURE DOUBLING EFFECTS BASED ON MEASURED AND CALCULATED PROP-FAN NOISE LEVELS USING EMPIRICAL ADJUSTMENTS FROM REFERENCE 5

| Mic No. | Radiation Angle, Deg | Adjust-ment, dB | 4P Calc. Level, dB | 4P Adj. Level, dB | 4P Meas. Level, dB | 4P Press Doub.Eff. dB | 8P Calc. Level, dB | 8P Adj. Level, dB | 8P Meas. Level, dB | 8P Press Doub.Eff., dB |
|---|---|---|---|---|---|---|---|---|---|---|
| 1 | 87.9 | 3.6 | 137.0 | 140.6 | 144.0 | 3.4 | 137.3 | 140.9 | 146.0 | 5.1 |
| 2 | 40.5 | - | 137.4 | - | 143.5 | - | 131.2 | - | 134.5 | - |
| 3 | 46.6 | - | 139.1 | - | 147.0 | - | 135.2 | - | 144.0 | - |
| 4 | 46.6 | - | 139.1 | - | 145.0 | - | 135.2 | - | 143.5 | - |
| 5 | 51.5 | 0.7 | 140.9 | 141.6 | 146.5 | 4.9 | 138.2 | 138.9 | 146.0 | 7.1 |
| 6 | 59.0 | -1.9 | 141.5 | 139.6 | 148.0 | 8.4 | 140.5 | 138.6 | 147.0 | 8.4 |
| 7 | 59.0 | -1.9 | 141.5 | 139.6 | 147.0 | 7.4 | 140.5 | 138.6 | 147.5 | 8.9 |
| 8 | 66.1 | -2.2 | 142.1 | 139.9 | 147.0 | 7.1 | 142.1 | 139.9 | 147.5 | 7.6 |
| 9 | 74.5 | -1.6 | 138.2 | 136.6 | 141.0 | 4.4 | 139.0 | 137.4 | 142.0 | 4.6 |
| 10 | 74.5 | -1.6 | 140.6 | 139.0 | 142.5 | 3.5 | 141.5 | 139.9 | 145.5 | 5.6 |
| 11 | 74.5 | -1.6 | 141.1 | 139.5 | 144.5 | 5.0 | 142.0 | 140.4 | 148.0 | 7.6 |
| 12 | 74.5 | -1.6 | 140.6 | 139.0 | 142.5 | 3.5 | 141.5 | 139.9 | 145.5 | 5.6 |
| 13 | 74.5 | -1.6 | 138.2 | 136.6 | 139.5 | 2.9 | 139.0 | 137.4 | 138.0 | 0.6 |
| 14 | 93.7 | 6.9 | 134.6 | 141.5 | 141.0 | -0.5 | 134.1 | 141.0 | 142.0 | 1.0 |
| 15 | 98.0 | 8.6 | 135.1 | 143.7 | 144.5 | 0.8 | 133.6 | 142.2 | 144.5 | 2.3 |
| 16 | 98.0 | 8.6 | 135.1 | 143.7 | 141.5 | -2.2 | 133.6 | 142.2 | 143.0 | 0.8 |
| 17 | 93.7 | 6.9 | 134.6 | 141.5 | 138.0 | -3.5 | 134.1 | 141.0 | 141.5 | 0.5 |
| 18 | 108.1 | 7.8 | 133.6 | 141.4 | 142.0 | -0.6 | 129.2 | 137.0 | 143.5 | 6.5 |
| 19 | 117.5 | 4.7 | 130.6 | 135.3 | 140.0 | 4.7 | 122.7 | 127.4 | 138.0 | 10.6 |
| 20 | 117.5 | 4.7 | 130.6 | 135.3 | 138.0 | 2.7 | 122.7 | 127.4 | 136.0 | 8.6 |
| 21 | 130.7 | - | 126.1 | - | 134.0 | - | 113.4 | - | 133.0 | - |

TABLE V AVERAGE PRESSURE DOUBLING EFFECTS BASED ON MEASURED AND CALCULATED PROP-FAN NOISE LEVELS (FUSELAGE AT 0.4 D CLEARANCE)

| Mic No. | Incidence Angle, Deg | Near-Field Ave., dB | Ref. 5 Corrections Ave., dB |
|---|---|---|---|
| 1 | 61.2 | 16.0 | 4.3 |
| 2 | 37.8 | 7.8 | - |
| 3 | 46.6 | 13.7 | - |
| 4 | 31.8 | 12.4 | - |
| 5 | 46.0 | 13.2 | 6.0 |
| 6 | 58.9 | 14.3 | 8.4 |
| 7 | 34.8 | 14.1 | 8.2 |
| 8 | 54.8 | 13.5 | 7.4 |
| 9 | 43.3 | 11.8 | 4.5 |
| 10 | 71.6 | 11.8 | 4.6 |
| 11 | 58.4 | 13.6 | 6.3 |
| 12 | 26.7 | 11.8 | 4.6 |
| 13 | 0.7 | 9.0 | 1.8 |
| 14 | 44.3 | 14.7 | 0.3 |
| 15 | 77.0 | 16.9 | 3.2 |
| 16 | 26.9 | 14.6 | -0.7 |
| 17 | 0.7 | 12.8 | -1.5 |
| 18 | 57.5 | 15.5 | 3.6 |
| 19 | 61.1 | 13.3 | 7.7 |
| 20 | 26.2 | 11.3 | 5.7 |
| 21 | 44.4 | 9.5 | - |

TABLE VI DERIVED PRESSURE DOUBLING EFFECTS BASED ON MEASURED FUSELAGE AND FREE-FIELD PROP-FAN NOISE LEVELS (FUSELAGE AT 0.8 D CLEARANCE)

| Mic No. | 9 000 RPM Average, dB | 10 000 RPM Average, dB | 11 300 RPM Average, dB | Total Average, dB | Incidence Angle, Deg. |
|---|---|---|---|---|---|
| 1 | 5.05 | 7.65 | 5.00 | 5.9 | 70.6 |
| 2 | -1.80 | 6.60 | 3.50 | 2.8 | 46.3 |
| 3 | | | | | 57.3 |
| 4 | | | | | 38.3 |
| 5 | -5.35 | -0.75 | -9.20 | -5.1 | 54.9 |
| 6 | | | | | 68.2 |
| 7 | | | | | 43.1 |
| 8 | 5.80 | 8.70 | 6.00 | 6.8 | 63.3 |
| 9 | 10.00 | 7.95 | 5.90 | 8.0 | 45.2 |
| 10 | 4.05 | 8.00 | 7.40 | 6.5 | 74.0 |
| 11 | 7.30 | 6.90 | 4.50 | 6.2 | 66.8 |
| 12 | 5.60 | 7.85 | 5.45 | 6.3 | 36.9 |
| 13 | 1.05 | 2.40 | 2.10 | 1.9 | 10.3 |
| 14 | | | | | 43.4 |
| 15 | 5.40 | 8.15 | 7.85 | 7.1 | 73.8 |
| 16 | 4.85 | 5.80 | 2.70 | 4.5 | 39.4 |
| 17 | | | | | 12.3 |
| 18 | 8.20 | 6.00 | 6.40 | 6.9 | 69.1 |
| 19 | | | | | 64.8 |
| 20 | | | | | 40.3 |
| 21 | -2.90 | 2.25 | 5.05 | 1.5 | 59.8 |

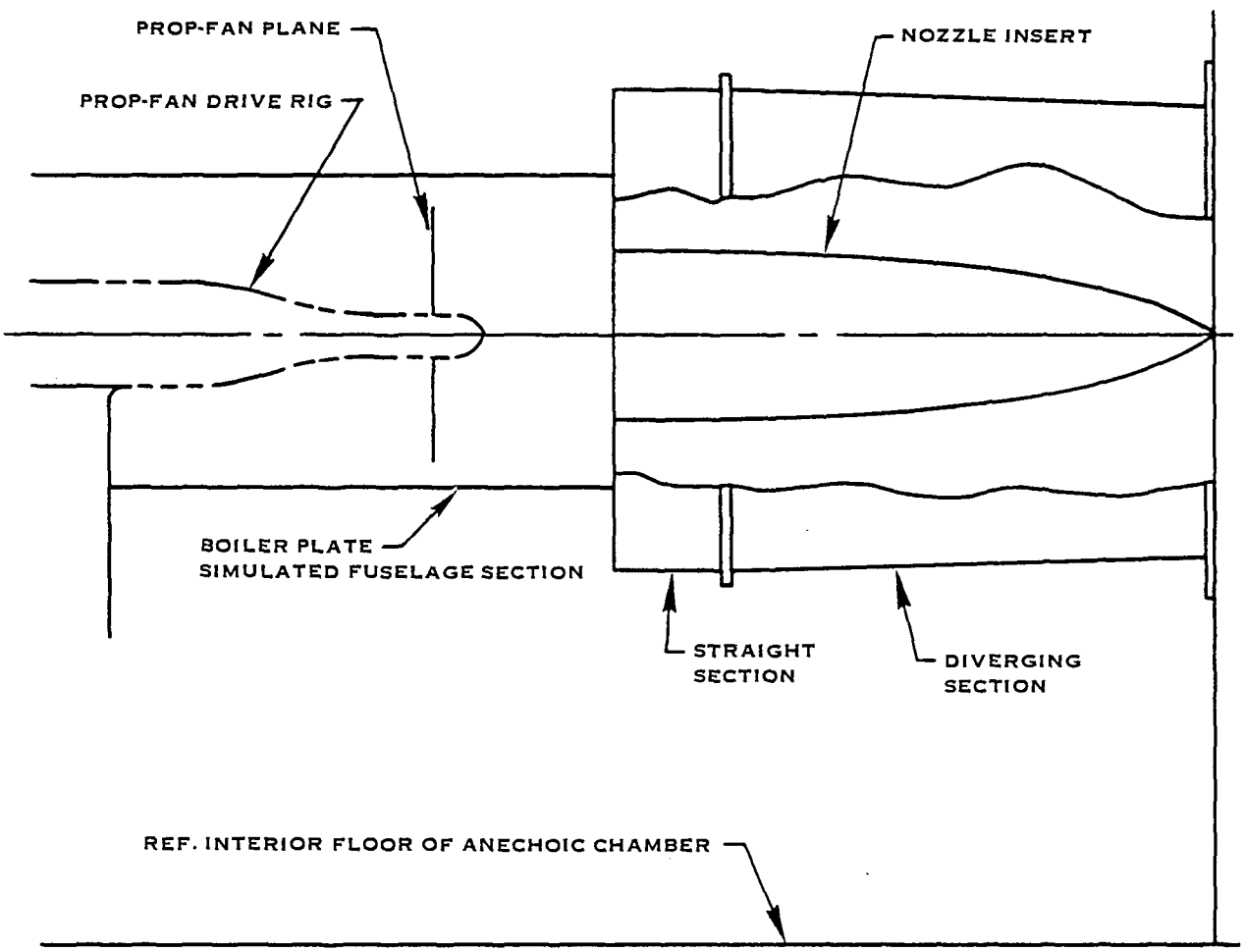


FIGURE 1. NOZZLE-FUSELAGE MODEL ASSEMBLY - SIDE VIEW

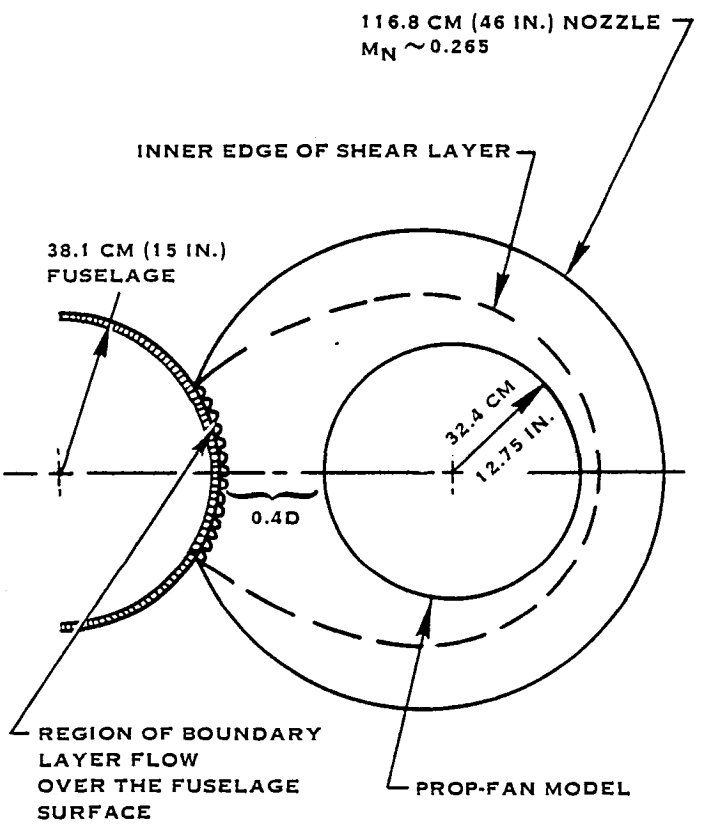


FIGURE 2. NOZZLE-FUSELAGE MODEL ASSEMBLY - END VIEW LOOKING UPSTREAM

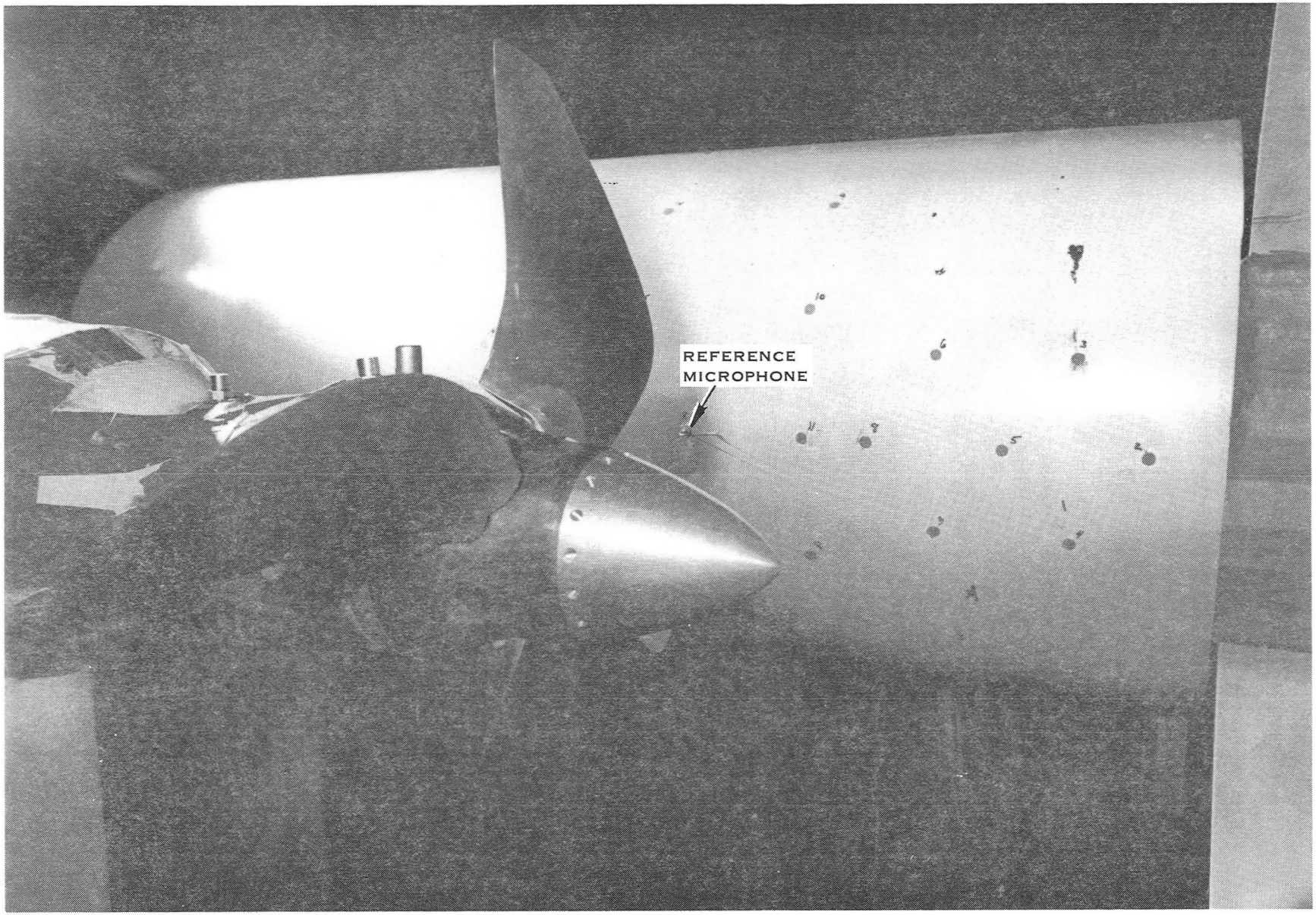


FIGURE 3. SIMULATED FUSELAGE ACOUSTIC TEST SET-UP
(0.4D TIP CLEARANCE)

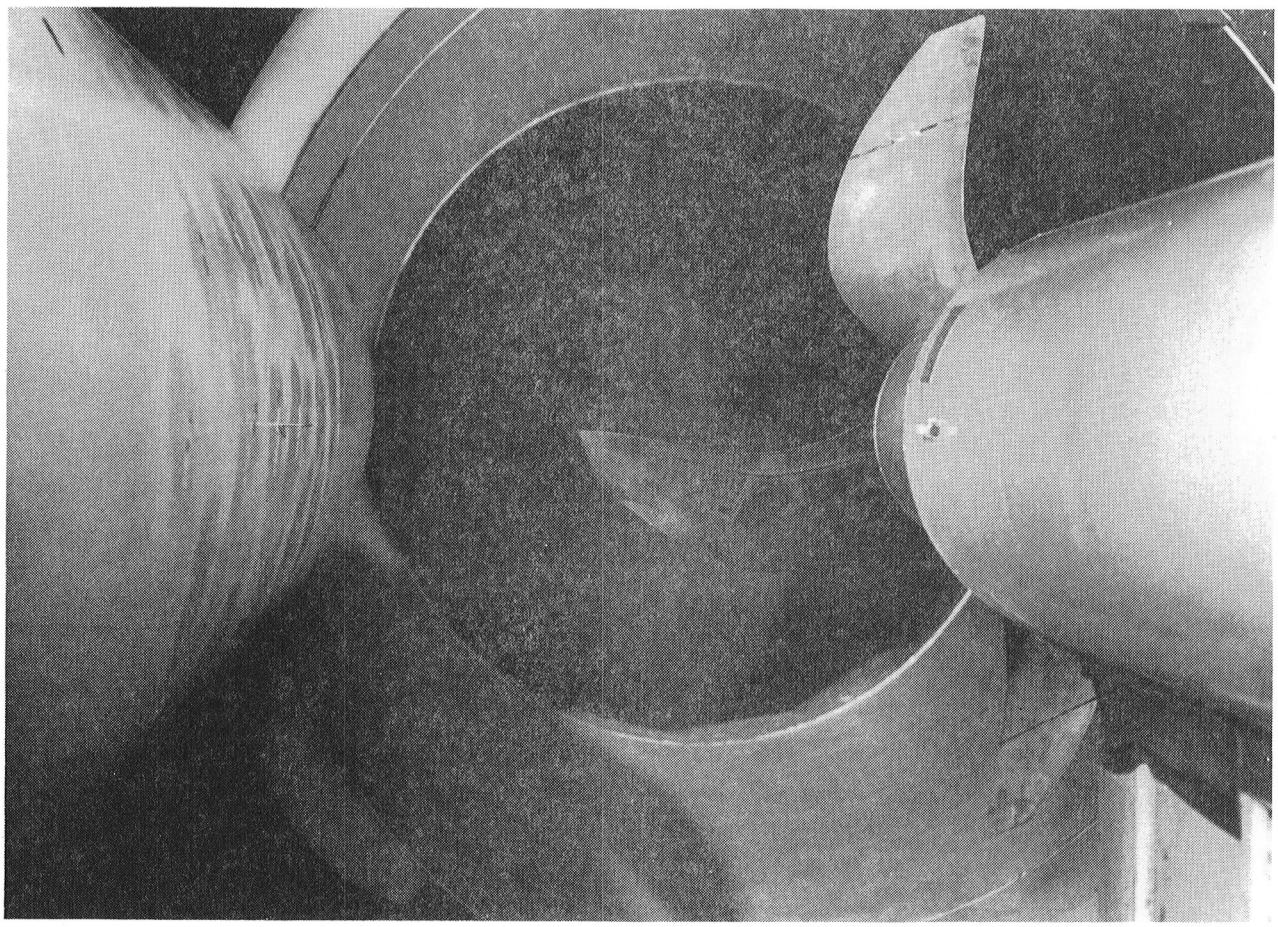

FIGURE 4. SIMULATED FUSELAGE ACOUSTIC TEST SET-UP (0.4D TIP CLEARANCE) VIEWING UPSTREAM

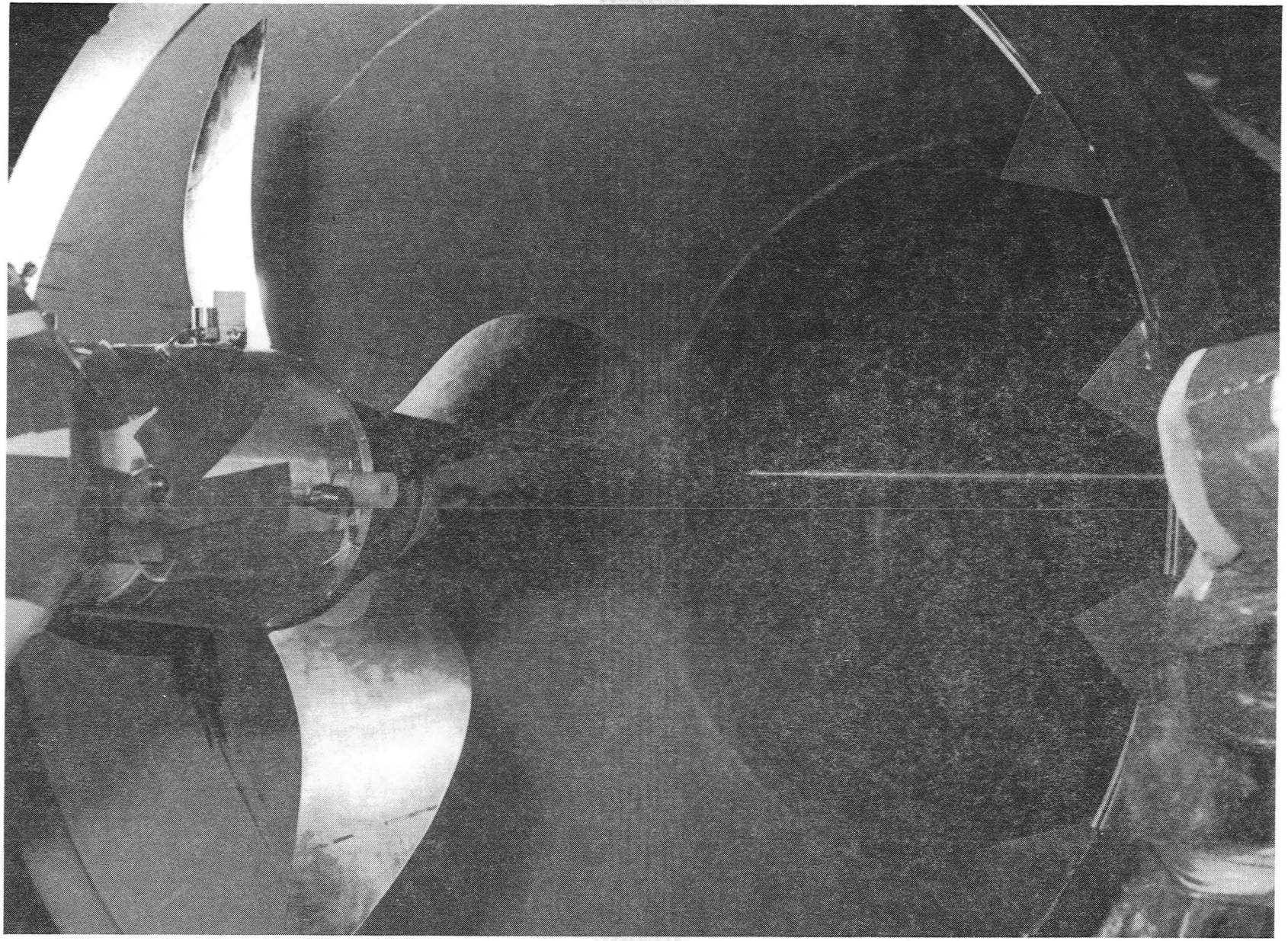

FIGURE 5. HOT WIRE ANEMOMETRY FLOW SURVEY SET-UP

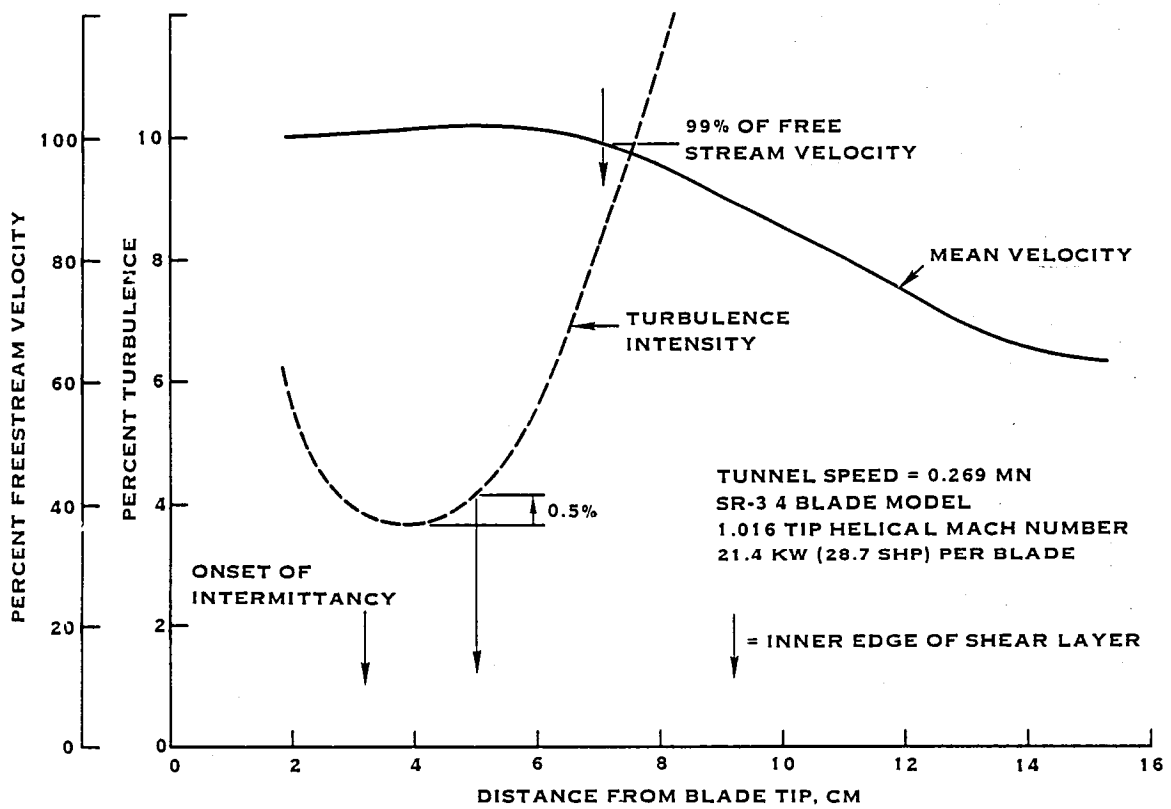


FIGURE 6. RESULTS OF HOT WIRE ANEMOMETRY FLOW SURVEY

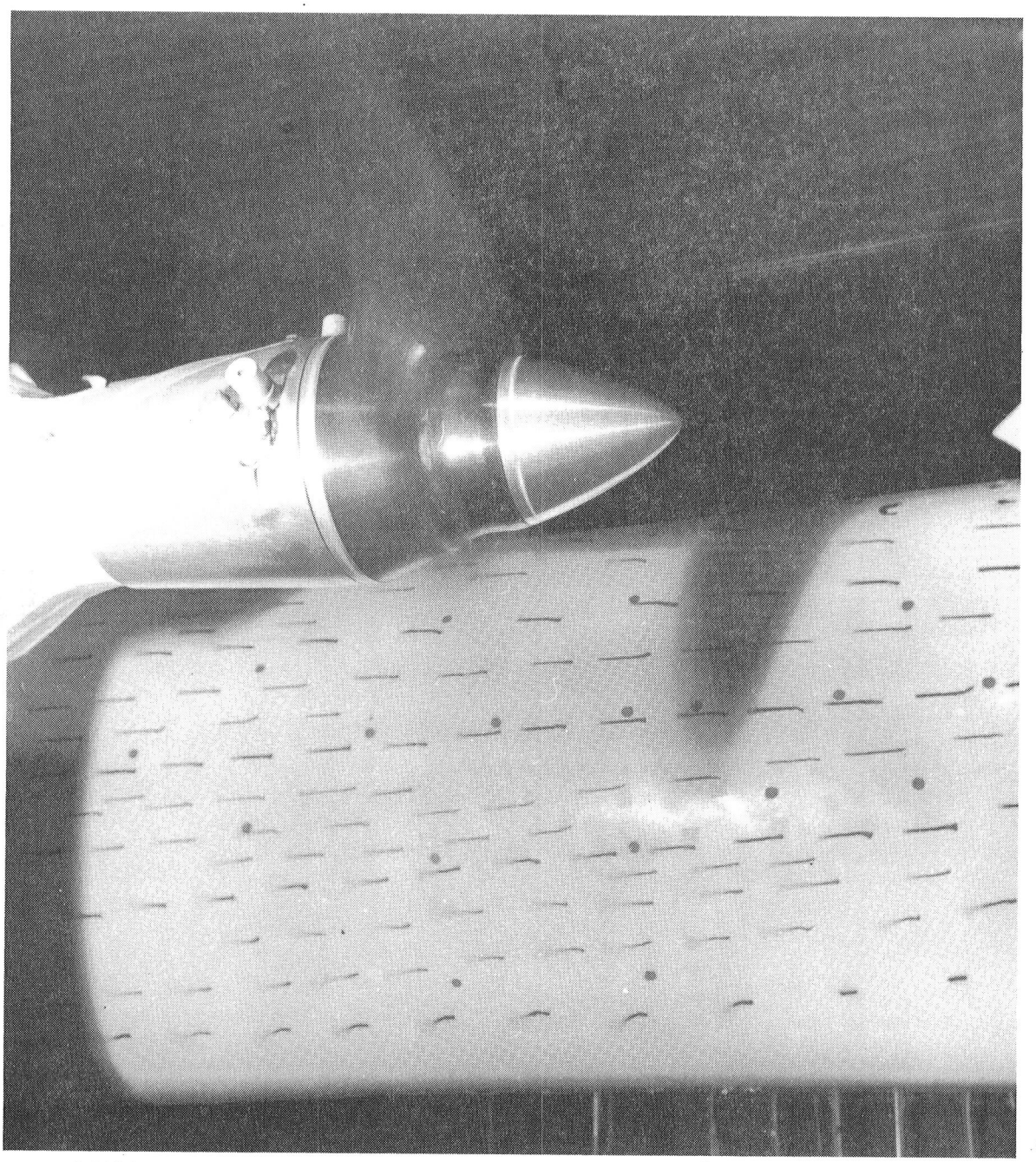

0.267 TUNNEL MN
SR-3 FOUR-BLADE MODEL
1.115 TIP HELICAL MN
25.4 KW PER BLADE

FIGURE 7. SIMULATED FUSELAGE FLOW VISUALIZATION TUFT TEST

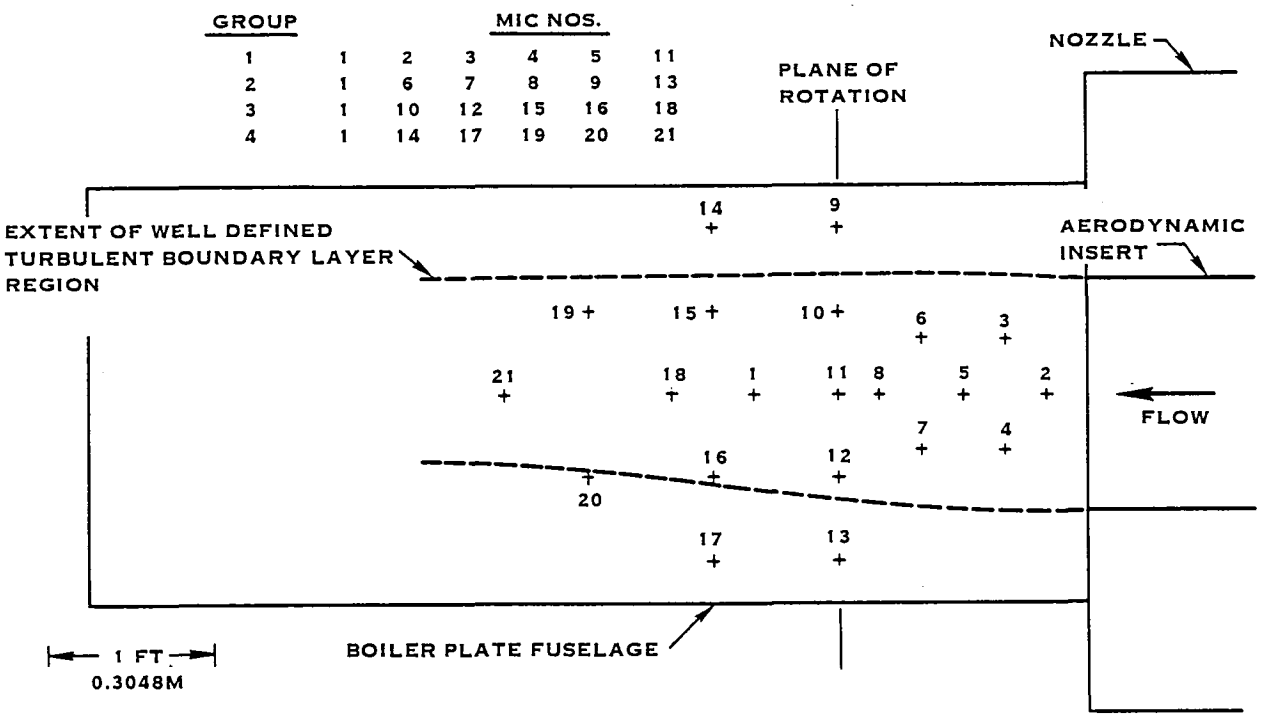


FIGURE 8. BOILER PLATE FUSELAGE MICROPHONE IDENTIFICATION AND LOCATIONS

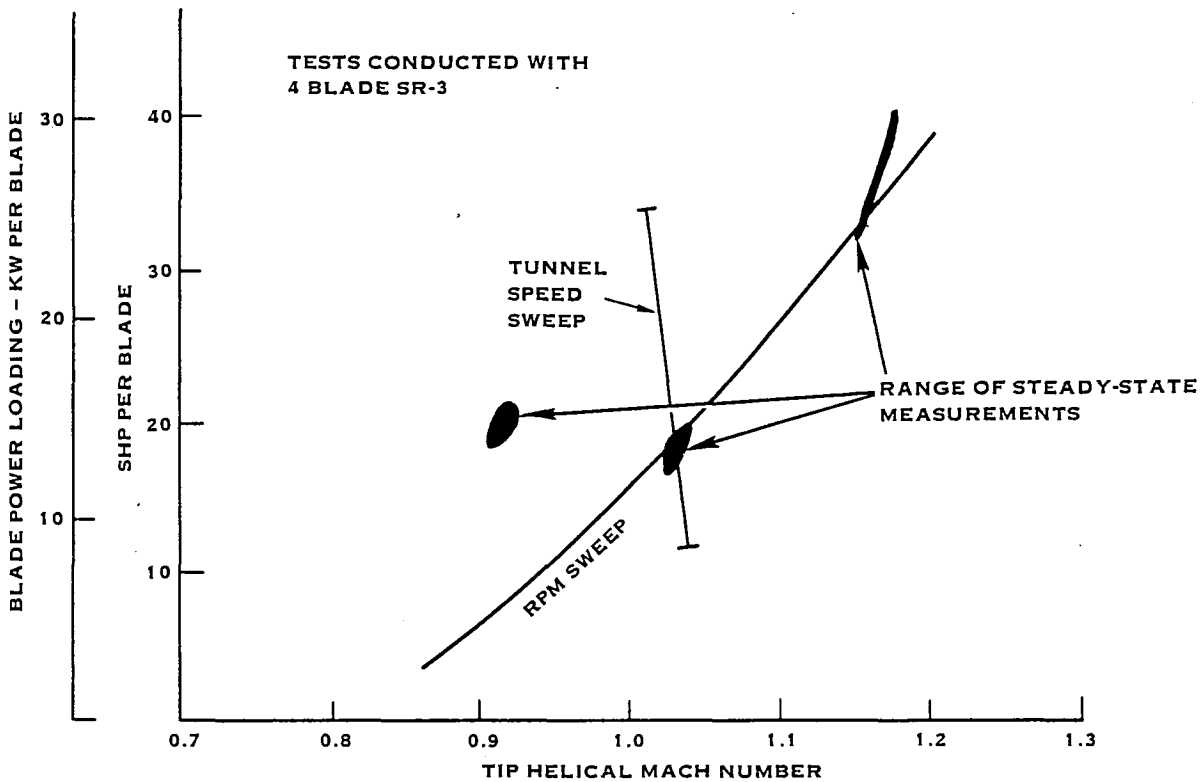


FIGURE 9. SIMULATED FUSELAGE ACOUSTIC TEST OPERATING CONDITIONS

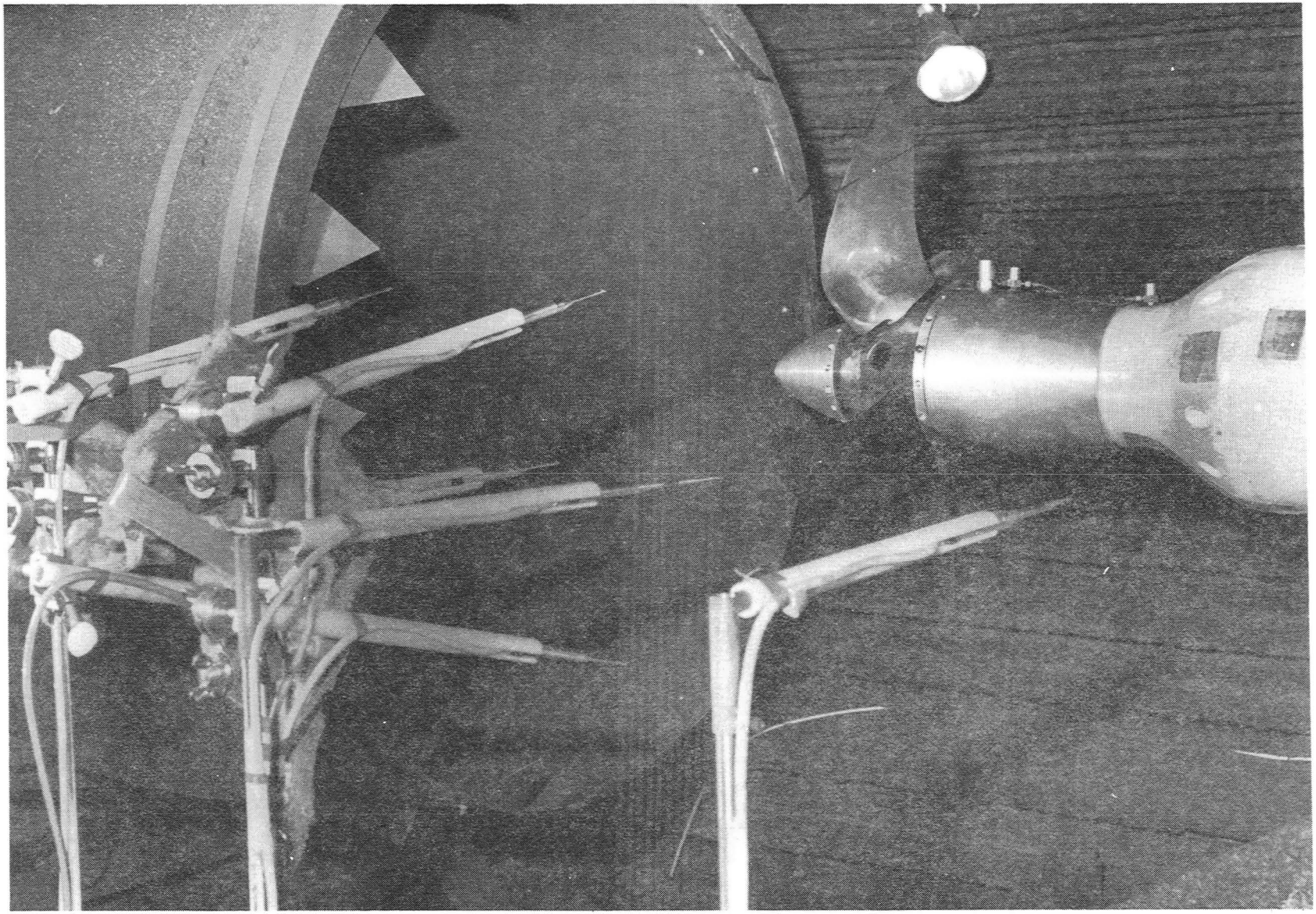

FIGURE 10. MICROPHONE ARRAY FOR LOCATIONS CORRESPONDING TO LOCATIONS ON SIMULATED FUSELAGE AT 0.8D TIP CLEARANCE

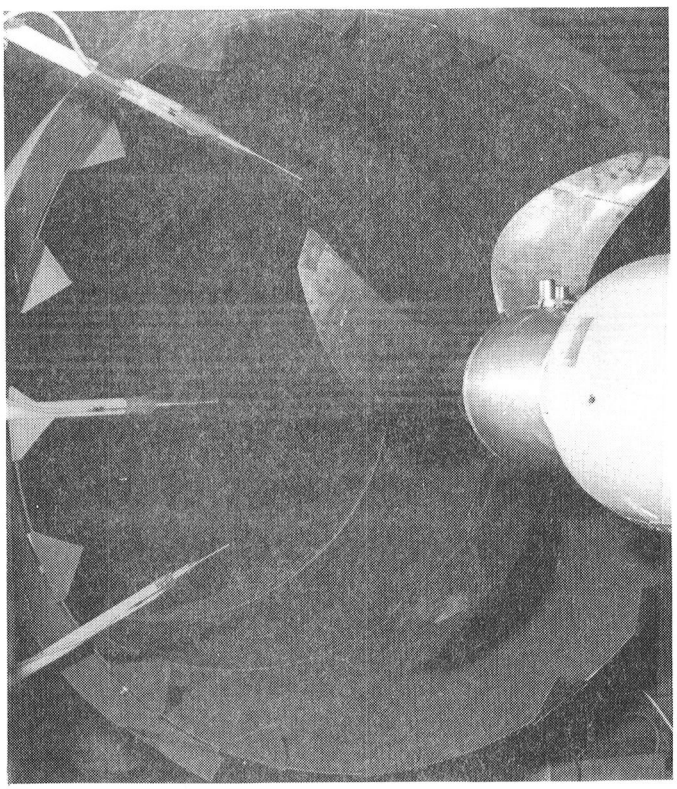

FIGURE 11. NEAR FIELD (INSIDE POTENTIAL CORE) MICROPHONE TEST SET-UP

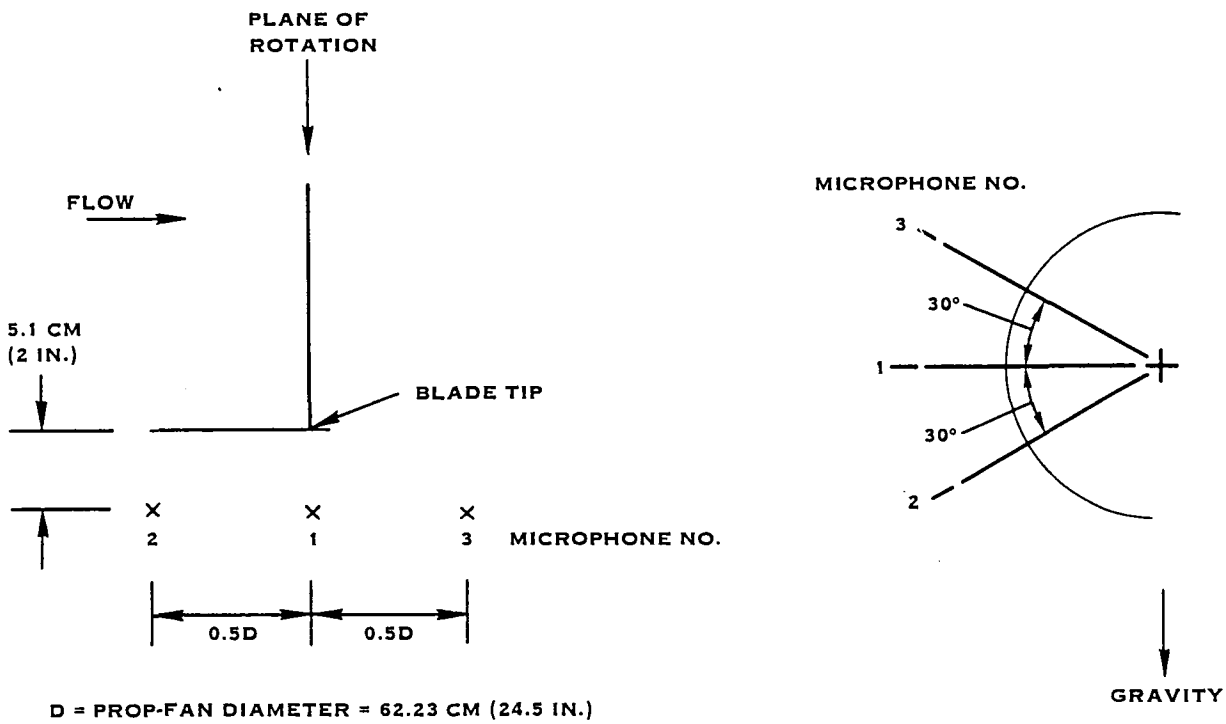


FIGURE 12. NEAR FIELD MICROPHONE LOCATIONS (INSIDE POTENTIAL CORE)

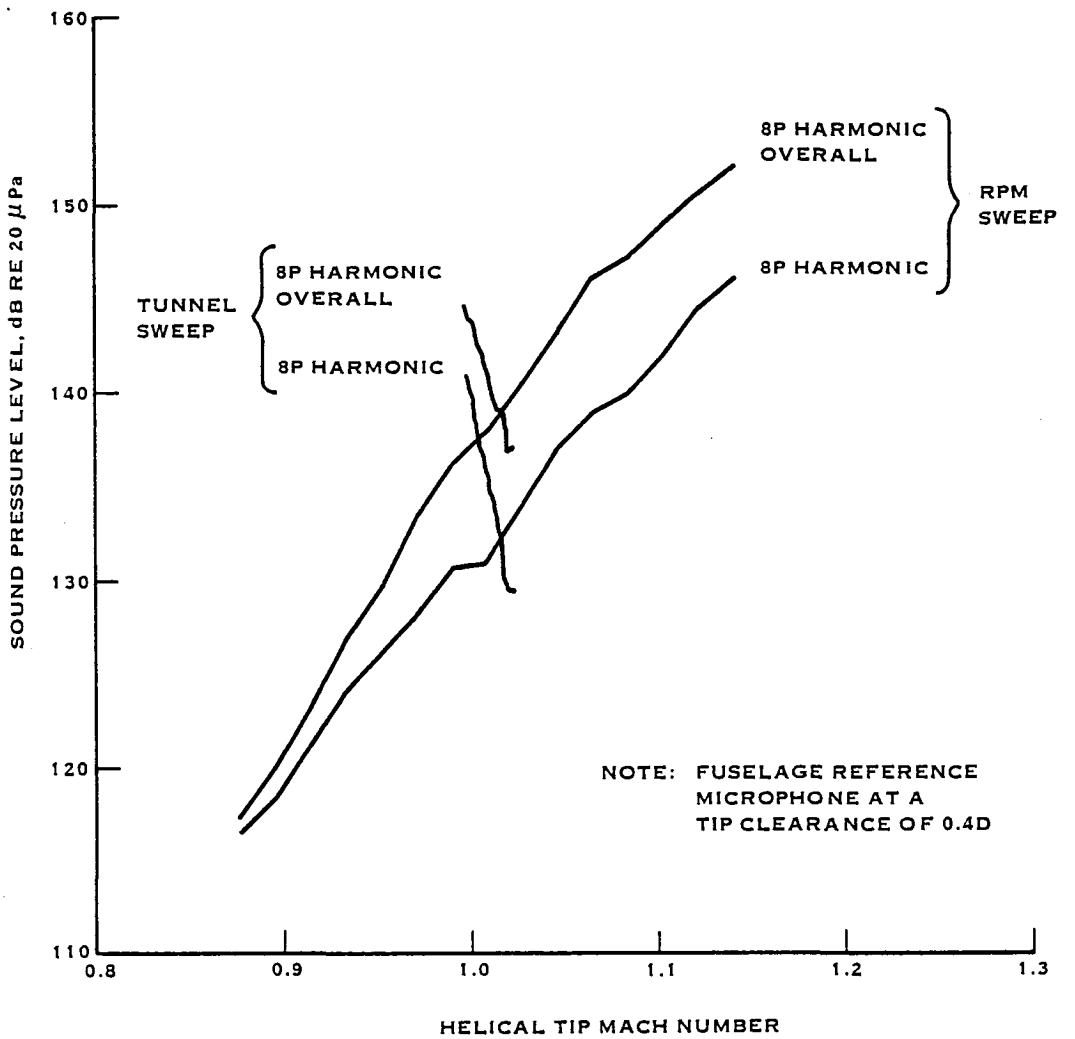


FIGURE 13. VARIATION OF PROP-FAN NOISE LEVEL WITH TIP MACH NUMBER

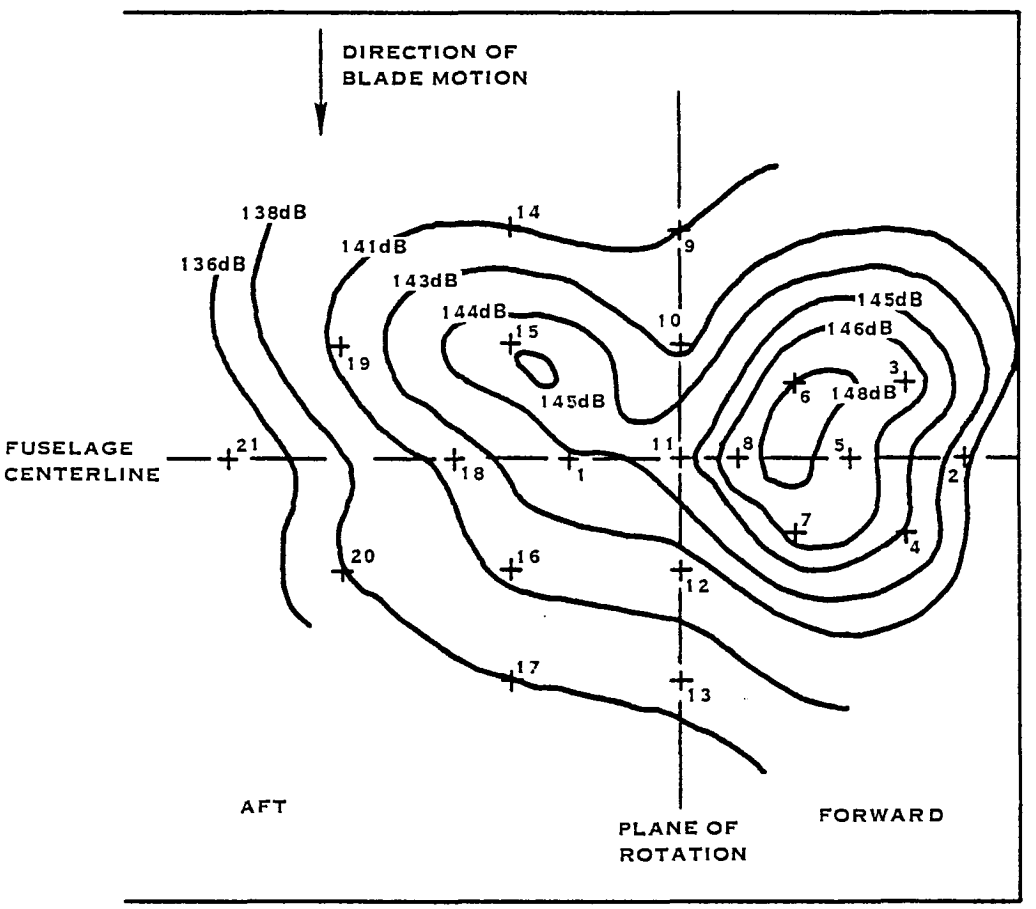


FIGURE 14. MEASURED SOUND PRESSURE AMPLITUDE CONTOURS AT 11300 RPM FOR THE 4P HARMONIC

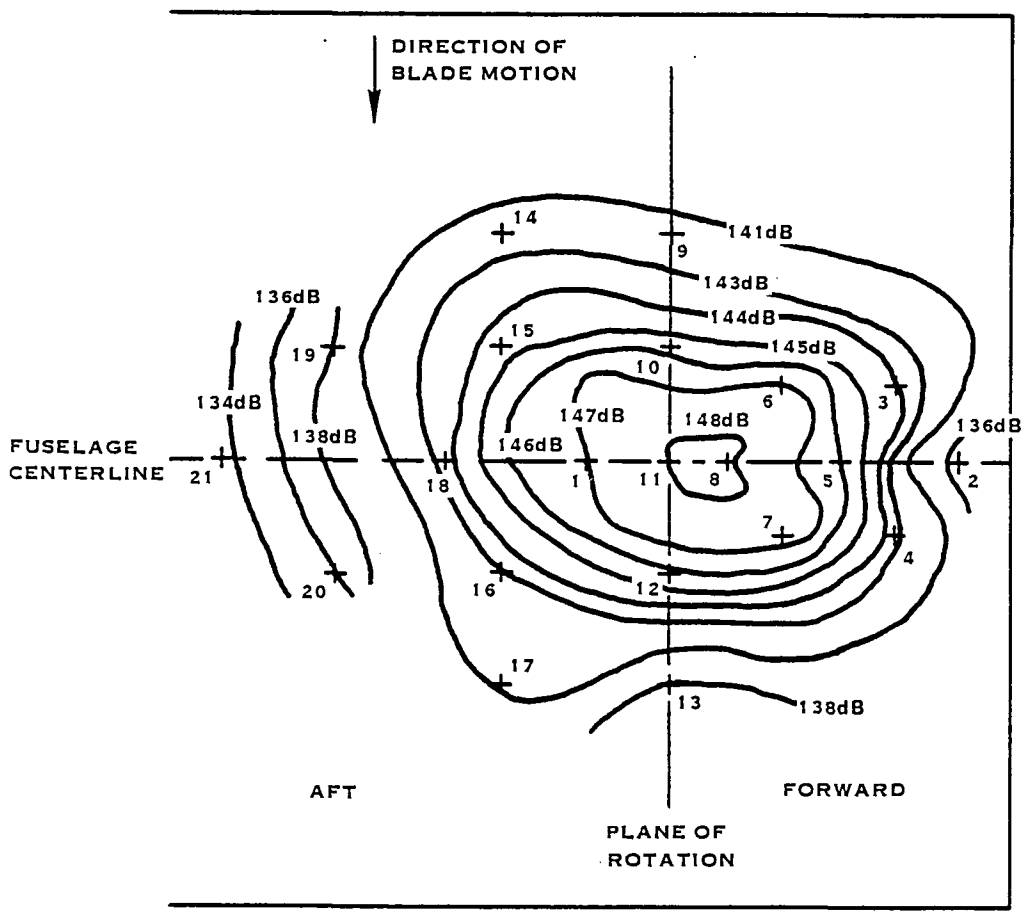


FIGURE 15. MEASURED SOUND PRESSURE AMPLITUDE CONTOURS AT 11300 RPM FOR THE 8P HARMONIC

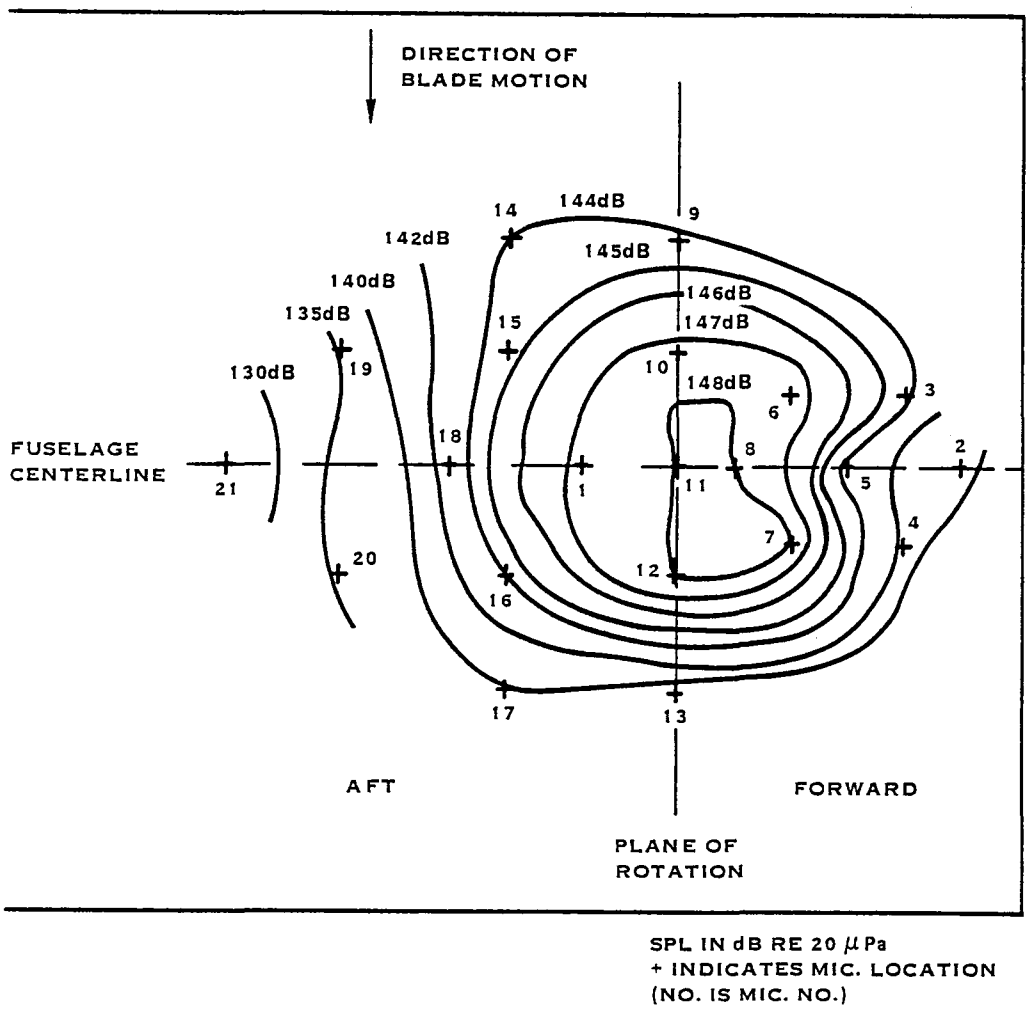


FIGURE 16. MEASURED SOUND PRESSURE AMPLITUDE CONTOURS AT 113000 RPM FOR THE 12P HARMONIC

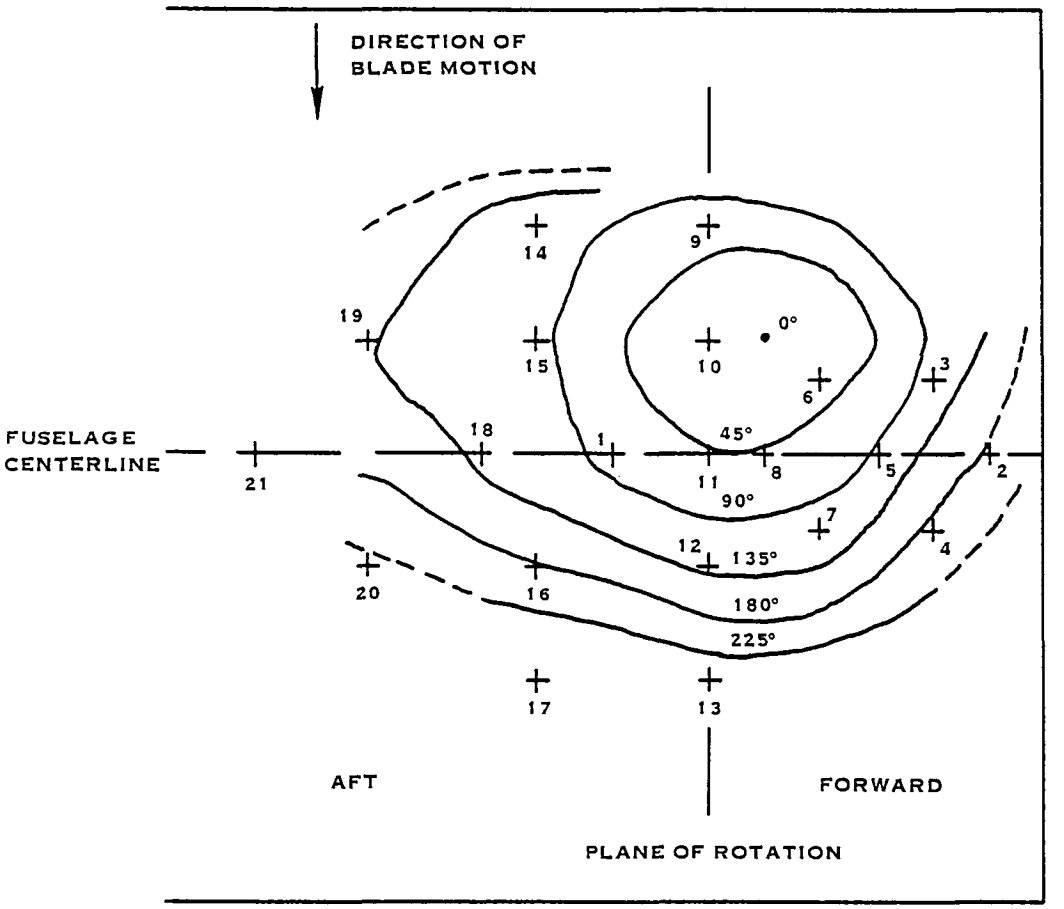


+ INDICATES MIC. LOCATION
(NO. IS MIC. NO.)

FIGURE 17. MEASURED SOUND PRESSURE PHASE ANGLE CONTOURS AT 11300 RPM FOR THE 4P HARMONIC

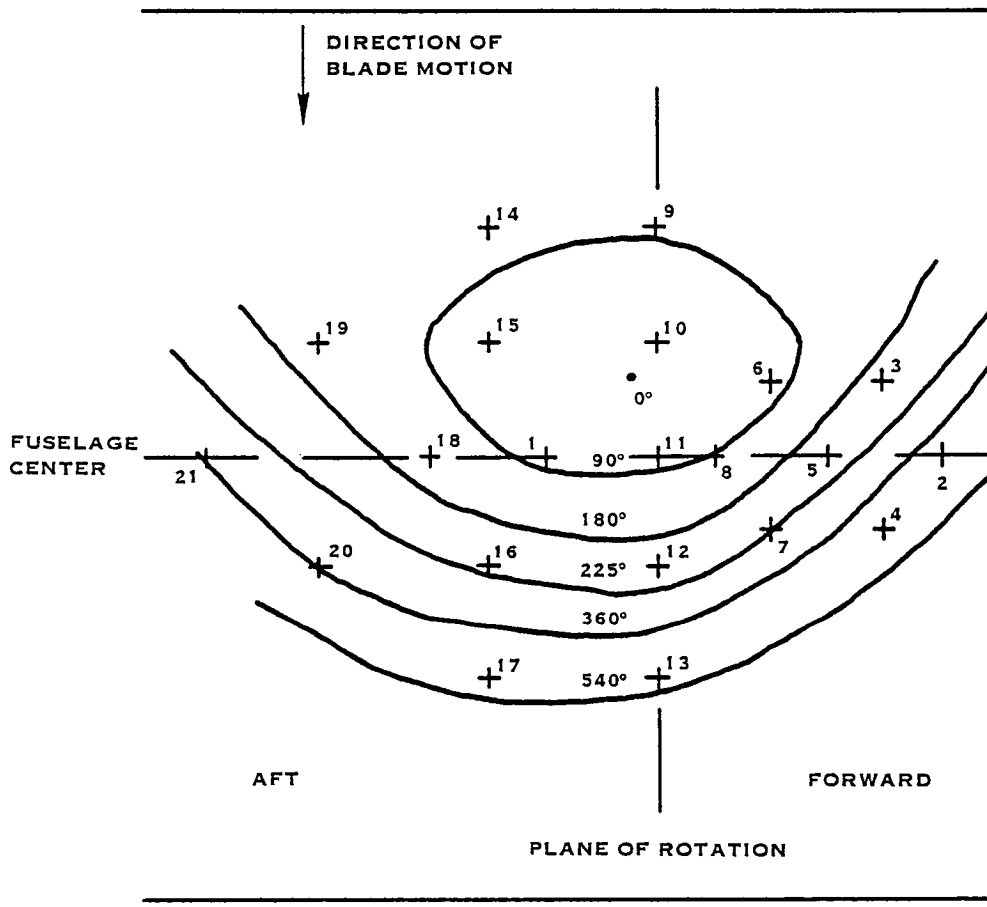


+ INDICATES MIC. LOCATION
(NO. IS MIC. NO.)

FIGURE 18. MEASURED SOUND PRESSURE PHASE ANGLE CONTOURS AT 11300 RPM FOR THE 8P HARMONIC

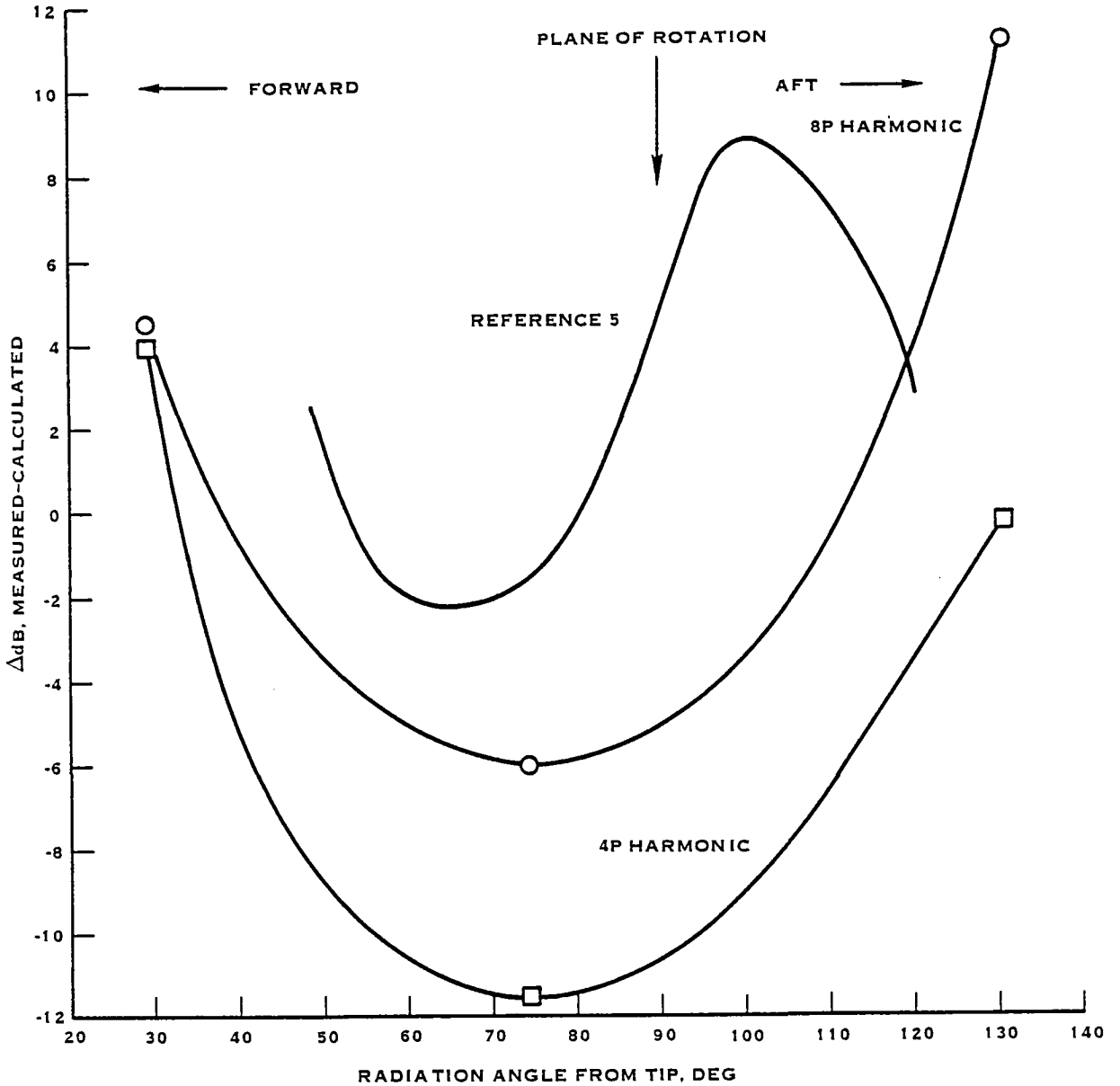


FIGURE 19. EMPIRICAL ADJUSTMENT FACTORS FOR CALCULATED PROP-FAN NOISE LEVELS

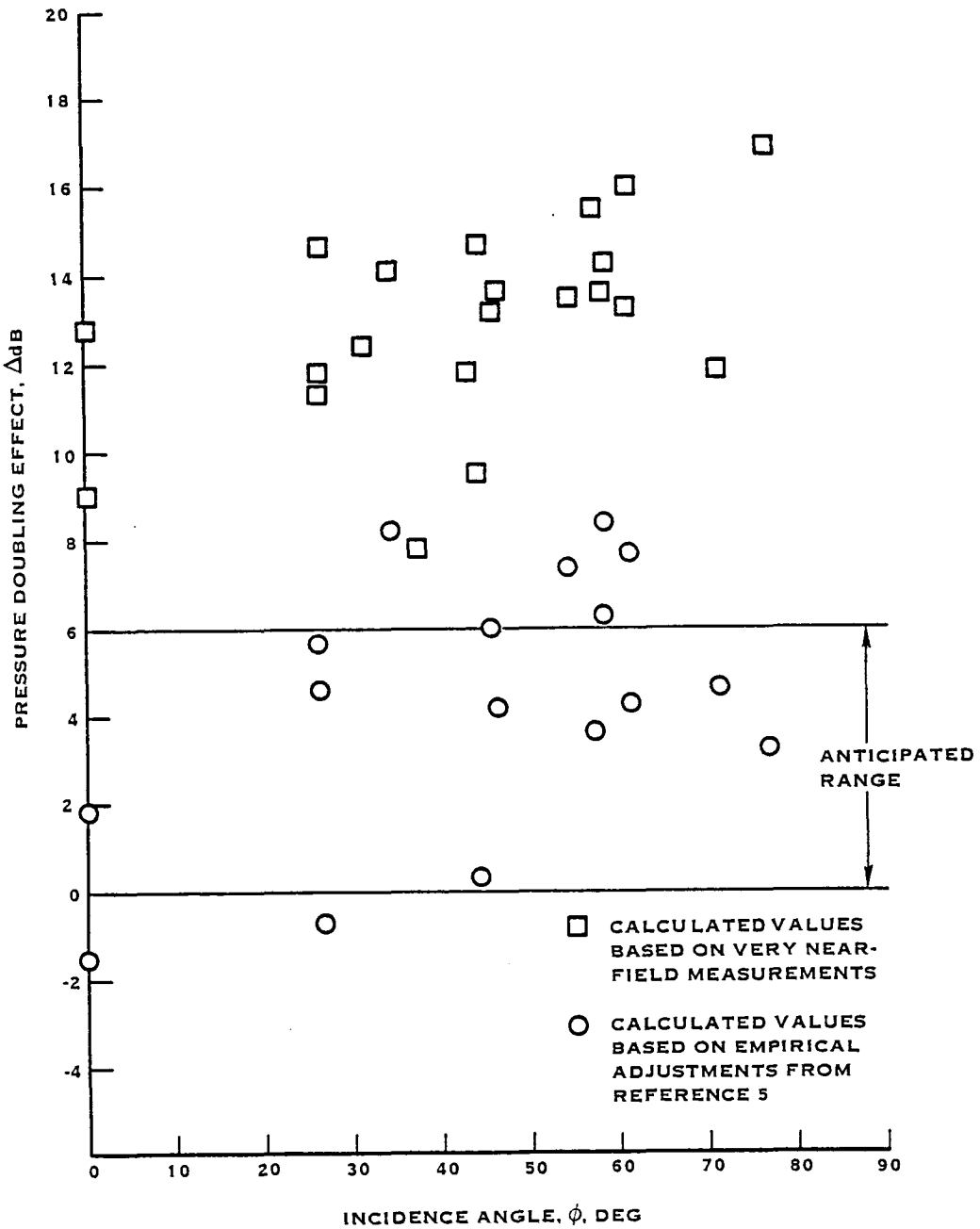


FIGURE 20. PRESSURE DOUBLING EFFECT BASED ON LEVELS MEASURED ON THE FUSELAGE VS. CALCULATED FREE-FIELD LEVELS

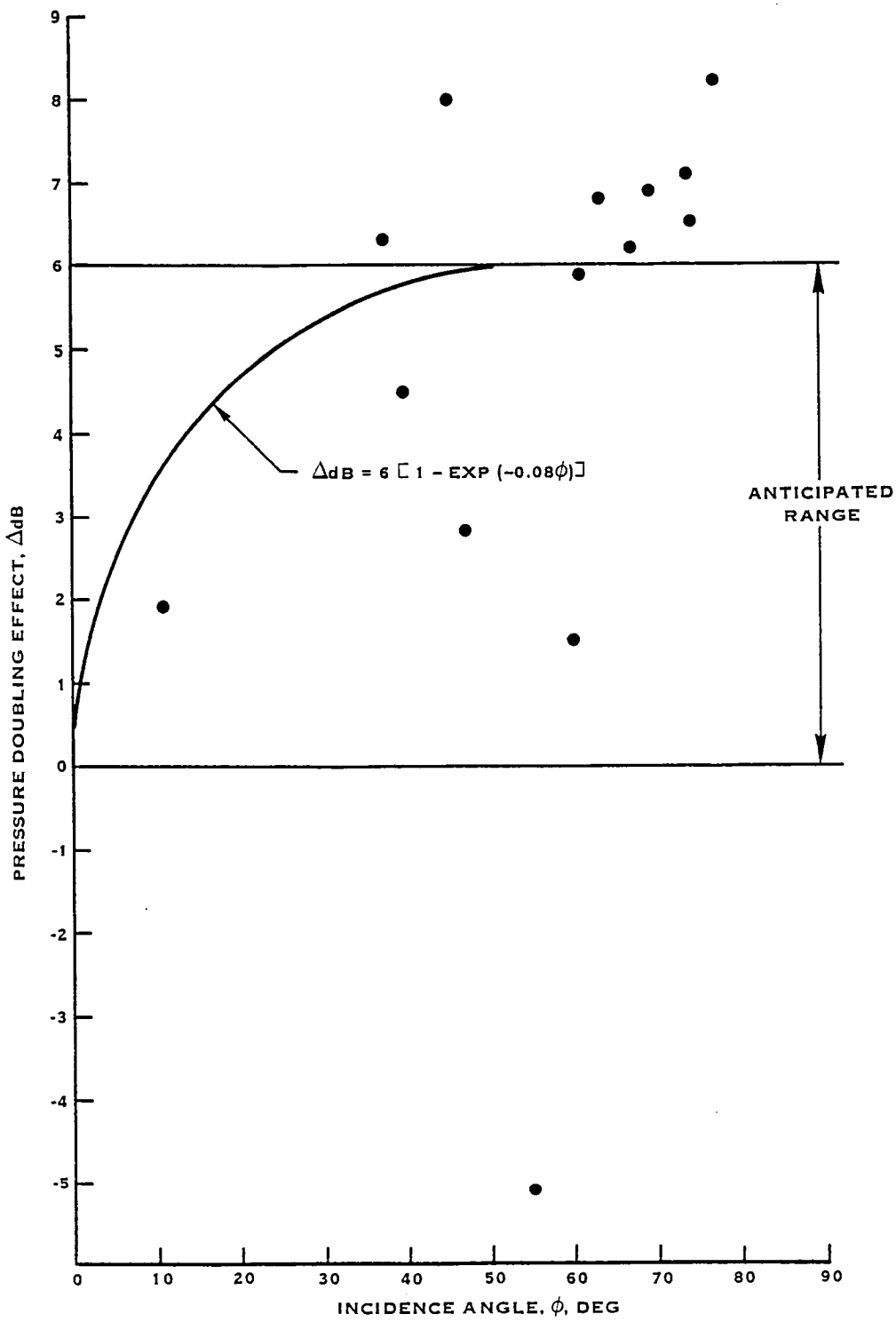


FIGURE 21. DEPENDENCE OF THE PRESSURE DOUBLING EFFECT ON INCIDENCE ANGLE

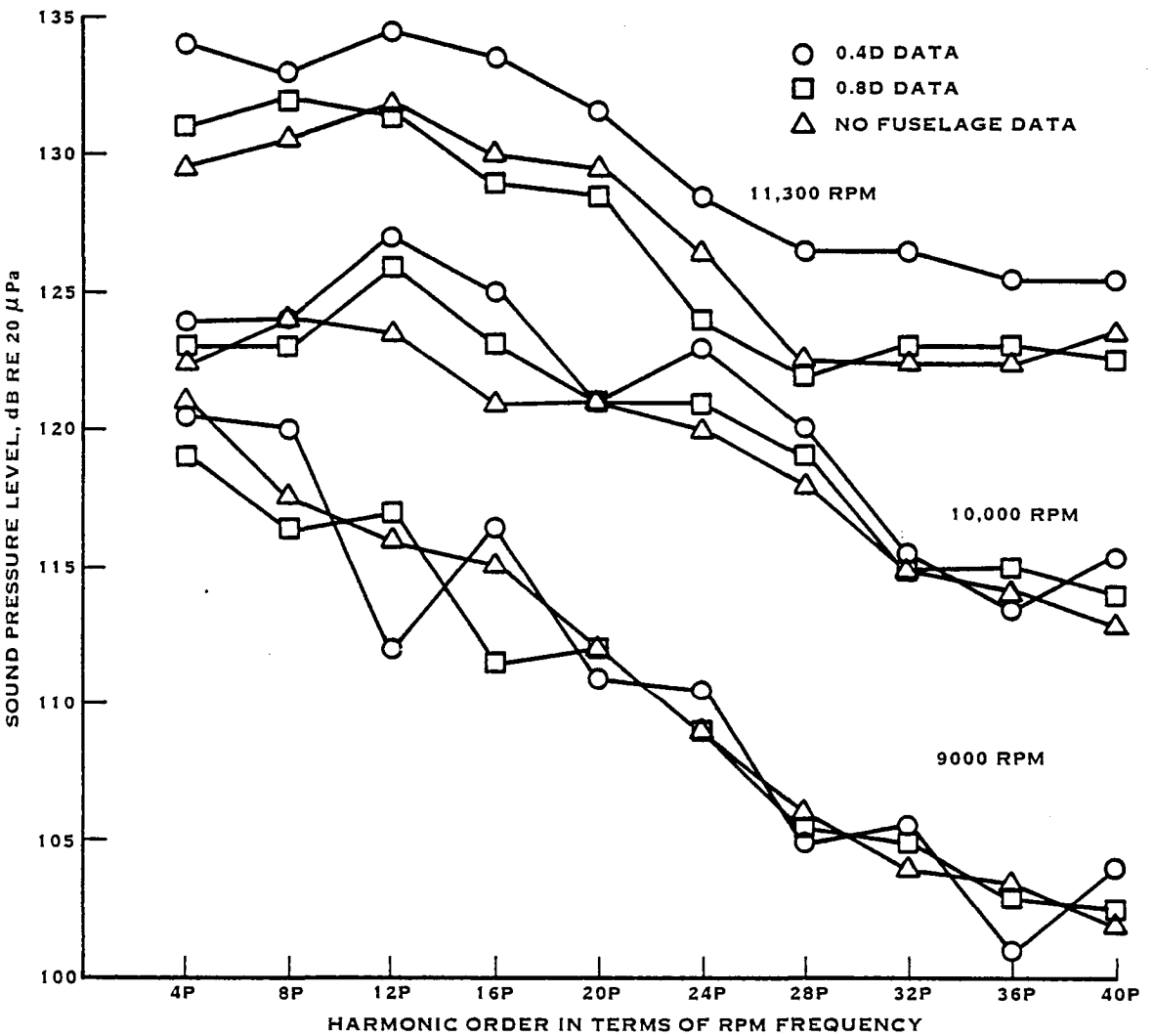


FIGURE 22. EFFECT OF FUSELAGE ON PROP-FAN SOURCE NOISE LEVEL

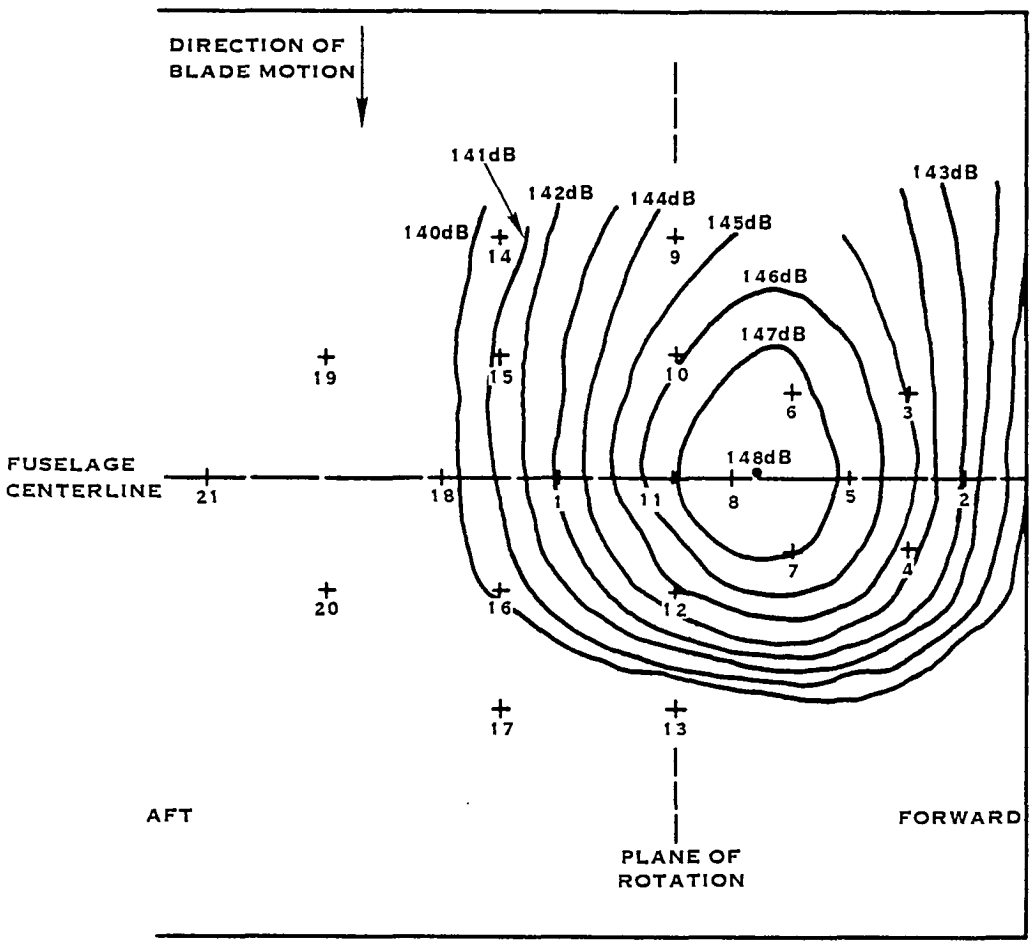


SPL IN dB RE 20 $\mu$ Pa
+ INDICATES MIC. LOCATION
(NO. IS MIC. NO.)

FIGURE 23. CALCULATED SOUND PRESSURE AMPLITUDE CONTOURS AT 11300 RPM FOR THE 4P HARMONIC

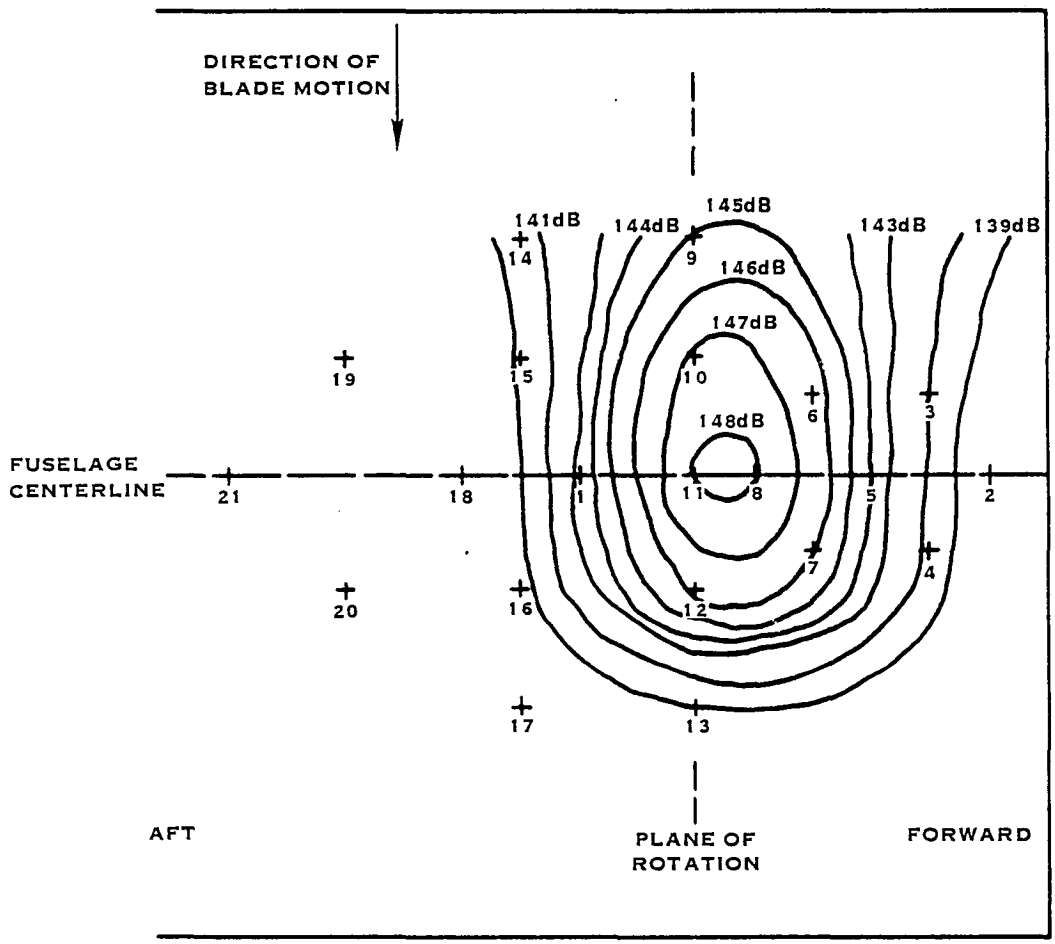


SPL IN dB RE 20 μPa
+ INDICATES MIC. LOCATION
(NO. IS MIC. NO.)

FIGURE 24. CALCULATED SOUND PRESSURE AMPLITUDE CONTOURS AT 11300 RPM FOR THE 8P HARMONIC

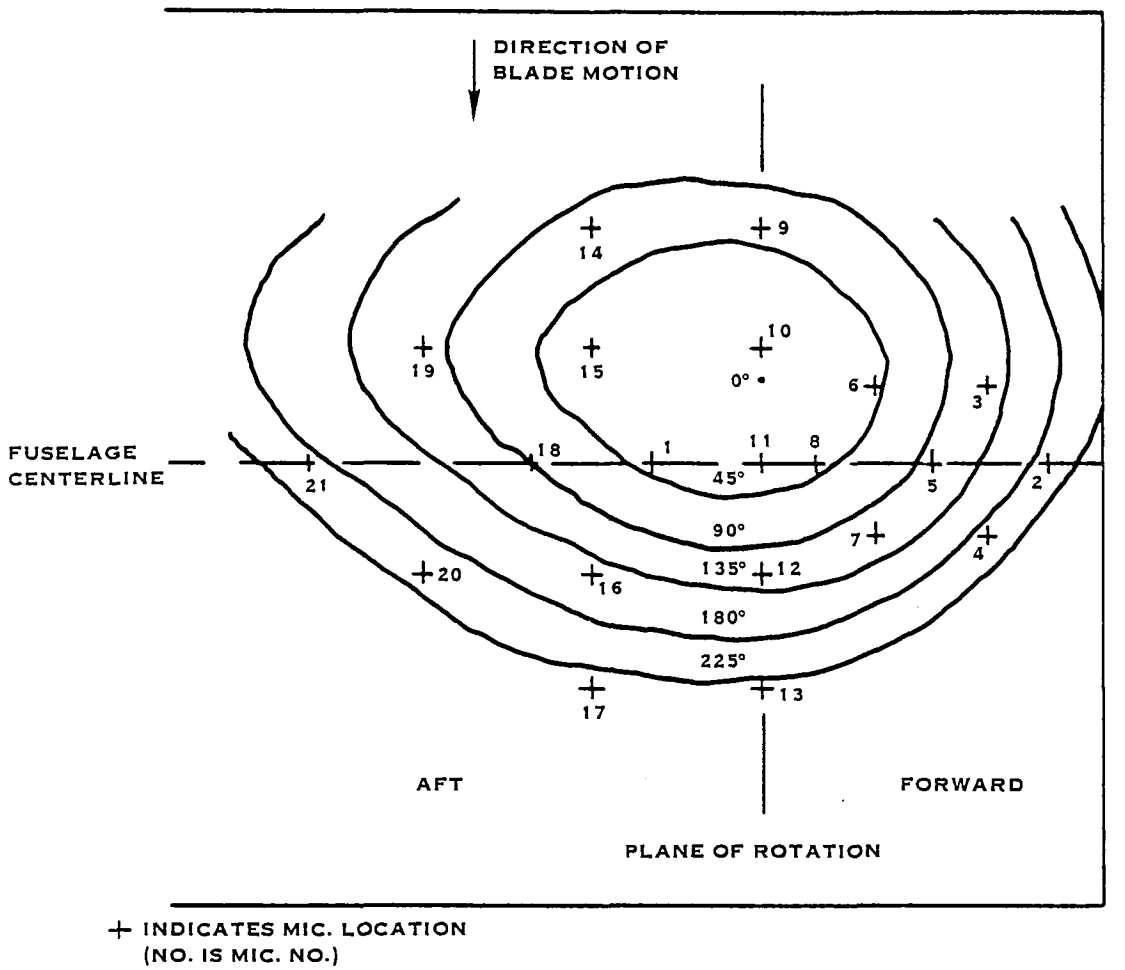


FIGURE 25. CALCULATED SOUND PRESSURE PHASE ANGLE CONTOURS AT 11300 RPM FOR THE 4P HARMONIC

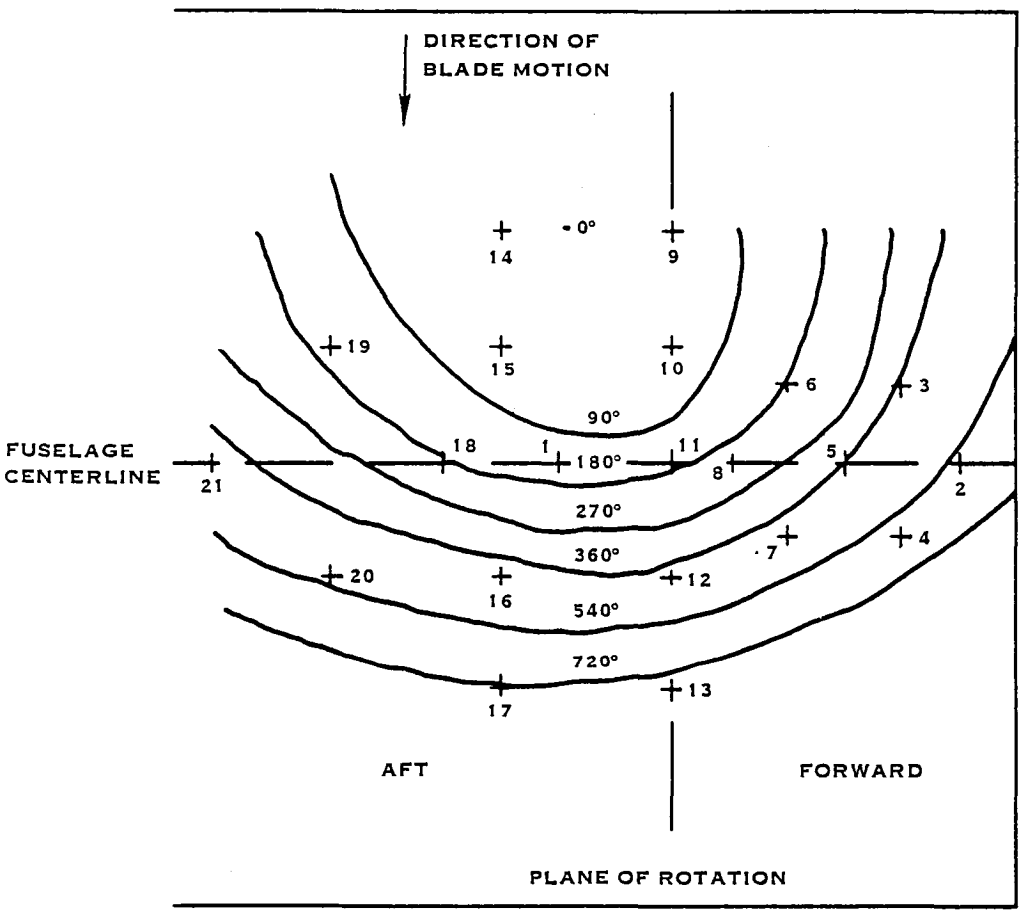


FIGURE 26. CALCULATED SOUND PRESSURE PHASE ANGLE CONTOURS AT 11300 RPM FOR THE 8P HARMONIC

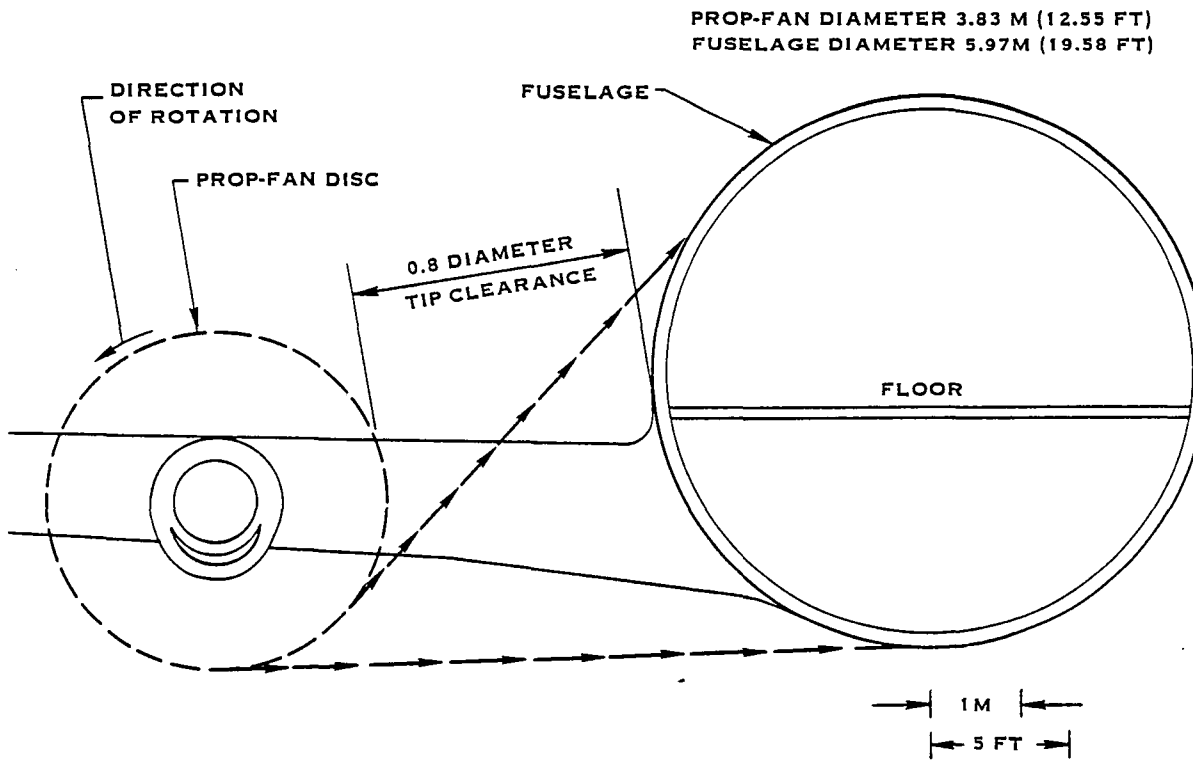


FIGURE 27. FULL SCALE FRONT VIEW OF AIRCRAFT CONFIGURATION USED FOR FUSELAGE SURFACE PRESSURE PREDICTIONS

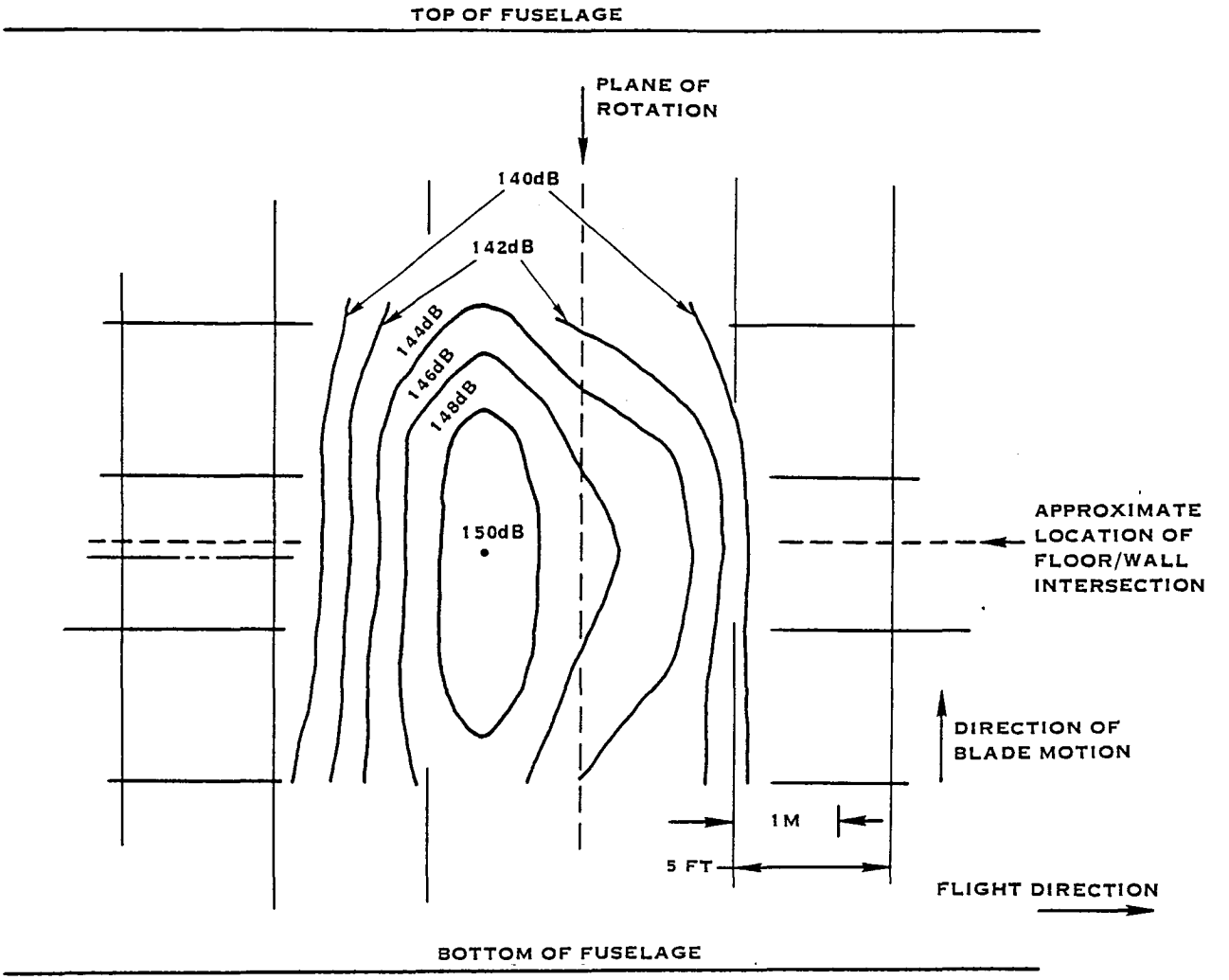


FIGURE 28. UNWRAPPED VIEW OF SOUND PRESSURE AMPLITUDE CONTOURS AT BLADE PASSAGE FREQUENCY PREDICTED FOR FULL SCALE PROP-FAN AIRPLANE

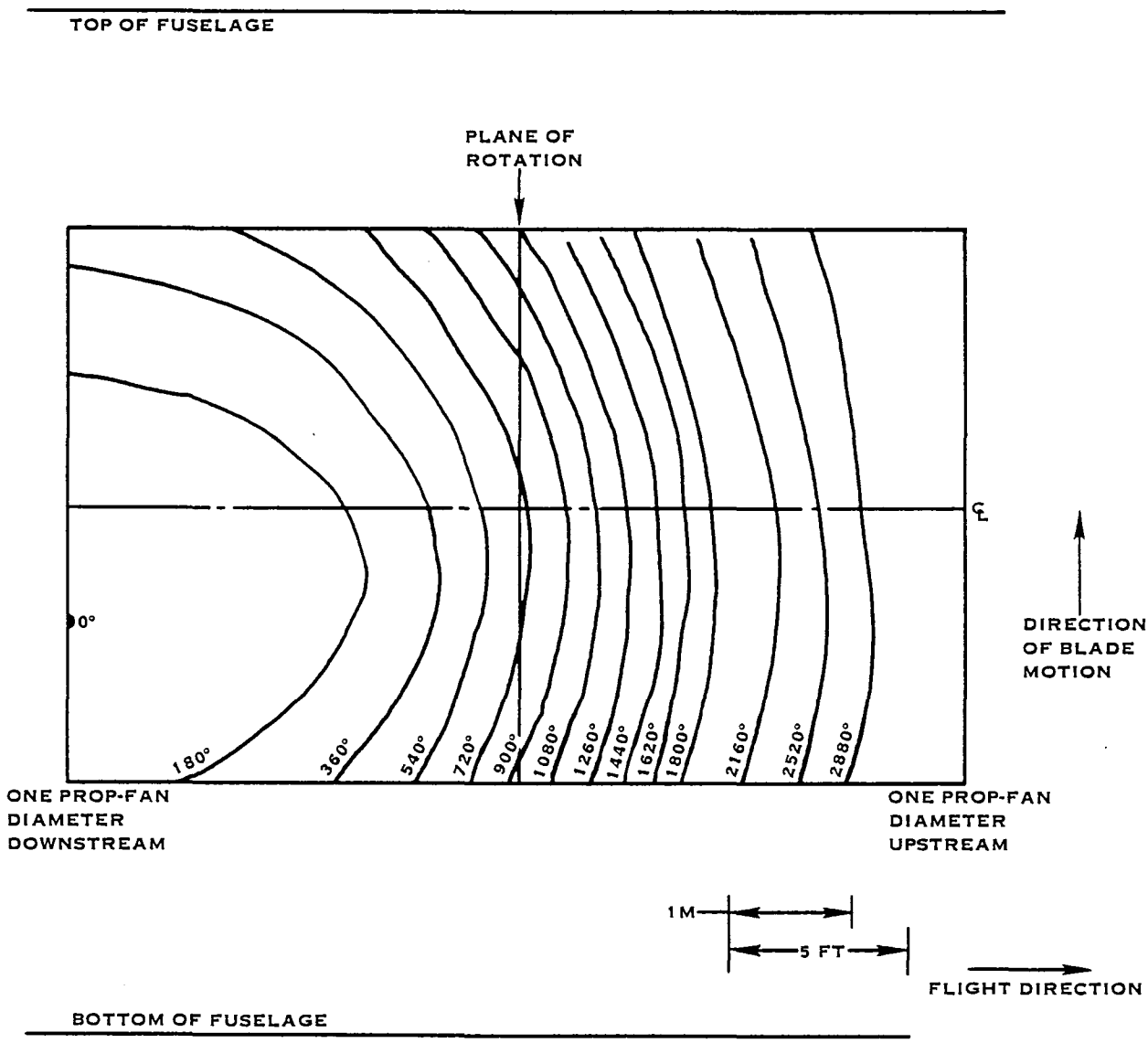


FIGURE 29. UNWRAPPED VIEW OF SOUND PRESSURE PHASE ANGLE CONTOURS AT BLADE PASSAGE FREQUENCY PREDICTED FOR FULL SCALE PROP-FAN AIRPLANE

## APPENDIX A-TABULATED DATA

This appendix contains tabulated amplitude and phase information derived from the test program. The information is presented as functions of microphone number and harmonic of rotational frequency, i.e. 4P is 4 x RPM/60, 8P is 8 x RPM/60, etc. The microphone numbers refer to those at the corresponding locations identified in the test description section of the report. The microphone labeled FF is the free-field reference microphone, which was located at 1.6 diameters from the prop-fan blade tips in the plane of rotation.

Table A-I presents the harmonic levels measured at the fuselage reference microphone at discrete intervals of the prop-fan and tunnel sweep runs. Table A-Ia presents the sound pressure levels of the first six harmonics for an 8-bladed prop-fan and the sum of the six harmonics at 200 RPM intervals from 8500 to 11 300 RPM. The calculated relative (helical) tip Mach numbers are also tabulated. For this sequence, the tunnel Mach number was constant at 0.267. A dynamic prop-fan diameter of 64.77 cm (25.5 in) and ambient total temperature of 300°K (540° R) was used for the relative tip speed calculation. Table A-Ib presents the corresponding data for the tunnel sweep at 10 000 prop-fan RPM.

Table A-II presents the harmonic levels for the 9000 RPM condition. The sequence for the tabulations is as follows: a) with the simulated fuselage located at a clearance of 0.4 diamters, b) with the simulated fuselage located at a clearance of 0.8 diameters, c) at equivalent free-field locations (with simulated fuselage removed) at a clearance of 0.8 diameters, d) the derived pressure doubling effects (the levels from Table b minus those from Table c). Note that all data has been adjusted to the operating condition identified.

Table A-III presents the same information as described for Table A-II except that this data is for the 10 000 RPM condition.

Table A-IV presents the same information as described for Table A-II except that this data is for the 11 300 RPM condition.

Table A-V presents the measured relative phase angles for 9000 RPM condition. These have been corrected for the recording/playback system phase response. Also, the sign has been reversed to be consistent with the convention used in the noise prediction methodology. The order is the same as that presented for the amplitude data, i.e. first the data with the simulated fuselage at 0.4 diameter clearance, then that with the simulated fuselage at 0.8 diameter clearance, finally the data at 0.8 diameter clearance equivalent free-field location.

Table A-VI presents the phase data for the 10 000 RPM condition in the same format as that described for Table A-V.

Table A-VII presents the phase data for the 11 300 RPM condition in the same format as that described for Table A-V.

TABLE A-Ia TABULATED HARMONIC SOUND PRESSURE LEVELS FOR THE RPM SWEEP AT CONSTANT TUNNEL MACH NUMBER

| RPM | 8P | 16P | 24P | 32P | 40P | 48P | Sum | Helical Tip Mach No. |
|---|---|---|---|---|---|---|---|---|
| 8 500 | 116.5 | 106.5 | 106.0 | - | - | - | 117.3 | 0.878 |
| 8 700 | 118.5 | 114.0 | 108.5 | 105.5 | - | - | 120.3 | 0.896 |
| 8 900 | 121.5 | 118.0 | 109.5 | 105.5 | - | - | 123.4 | 0.915 |
| 9 100 | 124.0 | 123.0 | 114.0 | 112.0 | - | - | 126.9 | 0.934 |
| 9 300 | 126.0 | 124.5 | 122.0 | 117.0 | 115.0 | 110.0 | 129.7 | 0.953 |
| 9 500 | 128.0 | 127.0 | 129.0 | 122.0 | 117.5 | 118.0 | 133.4 | 0.972 |
| 9 700 | 130.5 | 130.5 | 129.5 | 127.0 | 125.0 | 120.5 | 136.1 | 0.991 |
| 9 900 | 131.0 | 134.0 | 131.0 | 128.5 | 126.5 | 125.0 | 138.1 | 1.010 |
| 10 100 | 134.0 | 136.5 | 133.0 | 130.0 | 128.5 | 126.5 | 140.5 | 1.029 |
| 10 300 | 137.0 | 138.0 | 137.0 | 134.0 | 131.5 | 130.5 | 143.3 | 1.048 |
| 10 500 | 139.0 | 141.0 | 139.5 | 137.5 | 135.0 | 133.5 | 146.1 | 1.067 |
| 10 700 | 140.0 | 141.5 | 141.0 | 139.5 | 137.5 | 134.0 | 147.3 | 1.086 |
| 10 900 | 142.0 | 144.0 | 143.0 | 139.5 | 137.5 | 137.0 | 149.1 | 1.105 |
| 11 100 | 144.5 | 145.5 | 144.0 | 140.0 | 141.0 | 137.0 | 150.7 | 1.124 |
| 11 300 | 146.0 | 148.0 | 144.5 | 142.5 | 139.5 | 137.5 | 152.1 | 1.143 |

TABLE A-Ib TABULATED HARMONIC SOUND PRESSURE LEVELS FOR THE TUNNEL MACH NUMBER SWEEP AT CONSTANT RPM

| Tunnel Mach No. | 8P | 16P | 24P | 32P | 40P | 48P | Sum | Helical Tip Mach No. |
|---|---|---|---|---|---|---|---|---|
| 0.188 | 141.0 | 140.0 | 135.5 | 131.0 | 132.0 | 128.5 | 144.7 | 0.999 |
| 0.196 | 140.0 | 139.5 | 135.0 | 130.5 | 131.0 | 128.0 | 144.0 | 1.000 |
| 0.204 | 139.5 | 139.5 | 134.5 | 130.5 | 131.0 | 128.0 | 143.7 | 1.002 |
| 0.212 | 138.0 | 139.0 | 134.0 | 130.0 | 129.0 | 127.5 | 142.8 | 1.004 |
| 0.220 | 137.5 | 138.5 | 133.5 | 130.5 | 128.5 | 128.0 | 142.4 | 1.005 |
| 0.227 | 137.0 | 138.0 | 133.0 | 130.0 | 128.0 | 127.5 | 141.9 | 1.007 |
| 0.234 | 136.5 | 137.5 | 132.5 | 129.5 | 127.0 | 127.0 | 141.4 | 1.009 |
| 0.241 | 135.5 | 137.0 | 132.0 | 129.0 | 126.5 | 127.0 | 140.8 | 1.010 |
| 0.248 | 134.5 | 136.5 | 131.5 | 129.0 | 126.0 | 126.5 | 140.1 | 1.012 |
| 0.255 | 134.0 | 136.0 | 131.0 | 128.0 | 125.5 | 125.5 | 139.6 | 1.014 |
| 0.261 | 133.0 | 135.5 | 131.0 | 128.0 | 125.5 | 125.0 | 139.1 | 1.015 |
| 0.268 | 132.0 | 135.5 | 131.5 | 128.5 | 126.5 | 125.5 | 139.1 | 1.017 |
| 0.274 | 130.0 | 134.5 | 130.5 | 127.5 | 126.0 | 124.0 | 137.9 | 1.019 |
| 0.280 | 129.5 | 133.0 | 129.5 | 126.5 | 126.0 | 123.5 | 136.9 | 1.020 |
| 0.286 | 129.5 | 133.5 | 129.5 | 126.5 | 126.0 | 124.0 | 137.1 | 1.022 |

TABLE A-II TABULATED HARMONIC SOUND PRESSURE LEVELS AT 9000 RPM

a. Fuselage at 0.4 D Clearance (adjusted to run 265)

Harmonic Sound Pressure Levels, dB re 20μPa

| Mic No. | 4P | 8P | 12P | 16P | 20P | 24P | 28P | 32P | 36P | 40P |
|---|---|---|---|---|---|---|---|---|---|---|
| 1 | 133.5 | 131.5 | 128.5 | 125 | 120 | 118 | 113 | 109 | 106.5 | 103 |
| 2 | 131 | 120 | 114.5 | 103 | 102.5 | 99 | 98 | 97.5 | - | - |
| 3 | 132.5 | 125 | 119 | 115 | 109.5 | 105.5 | - | - | - | - |
| 4 | 132 | 125.5 | 118.5 | 114.5 | 102.5 | 104 | 98 | - | - | - |
| 5 | 134 | 127 | 123 | 114 | 108.5 | 105 | 101 | 100.5 | 97 | 94.5 |
| 6 | 135 | 131.5 | 126.5 | 124.5 | 121.5 | 116 | 112 | 109 | 107 | 103.5 |
| 7 | 134.5 | 130 | 127.5 | 123.5 | 121 | 114.5 | 112 | 108.5 | 106 | 103.5 |
| 8 | 135 | 132.5 | 130 | 126.5 | 124.5 | 121.5 | 117.5 | 114.5 | 112 | 110 |
| 9 | 130 | 128 | 126.5 | 125 | 122.5 | 120.5 | 118 | 115 | 112.5 | 111.5 |
| 10 | 133.5 | 130.5 | 128.5 | 127 | 124 | 122 | 118 | 115.5 | 113.5 | 111 |
| 11 | 133 | 132 | 130 | 127 | 126 | 122.5 | 120 | 117.5 | 114.5 | 112 |
| 12 | 132 | 130 | 127 | 126.5 | 124 | 122.5 | 119 | 115.5 | 112.5 | 113.5 |
| 13 | 128 | 124.5 | 122 | 119.5 | 119 | 116 | 112.5 | 109.5 | 108.5 | 105.5 |
| 14 | 131.5 | 128 | 124 | 121.5 | 118 | 117 | 112 | 108.5 | 105.5 | 102.5 |
| 15 | 133.5 | 128 | 125 | 122.5 | 115.5 | 114 | 110 | 105.5 | 101.5 | 102 |
| 16 | 132.5 | 128.5 | 123.5 | 119.5 | 115.5 | 111 | 107.5 | 105.5 | 100 | 99.5 |
| 17 | 129 | 125 | 121.5 | 116 | 112.5 | 109.5 | 102.5 | 97.5 | 96 | 97 |
| 18 | 132 | 127 | 118.5 | 115.5 | 105 | 102 | 99.5 | 101.5 | 97.5 | 96 |
| 19 | 127.5 | 120.5 | 108.5 | 111 | 106 | 102 | 102 | 100 | - | - |
| 20 | 129 | 116 | 114.5 | 107.5 | 107 | 103.5 | 98.5 | - | 98.5 | 97.5 |
| 21 | 126.5 | 107 | 107 | 104 | 103 | 103.5 | 99 | 98 | 97 | - |
| FF | 120.5 | 120 | 112 | 116.5 | 111 | 110.5 | 105 | 105.5 | 101 | 104 |

TABLE A-II TABULATED HARMONIC SOUND PRESSURE LEVELS AT 9000 RPM (Cont.)

b. Fuselage at 0.8 D Clearance (adjusted to run 293)

Harmonic Sound Pressure Levels, dB re 20μPa

| Mic No. | 4P | 8P | 12P | 16P | 20P | 24P | 28P | 32P | 36P | 40P |
|---|---|---|---|---|---|---|---|---|---|---|
| 1 | 132.5 | 129 | 126.5 | 124 | 121 | 117.5 | 114 | 112 | 109 | 108 |
| 2 | 128.5 | 133 | 123.5 | 118 | 113.5 | 111 | 110 | 105 | 102 | 97.5 |
| 3 | 135.5 | 124 | 120.5 | 120 | 117.5 | 115.5 | 111 | 110 | 108 | 106 |
| 4 | 128 | 124 | 122 | 120.5 | 118 | 114 | 110 | 106 | 104.5 | 104 |
| 5 | 124 | 117.5 | 114.5 | 112.5 | 110.5 | 108 | 104.5 | 101.5 | 99.5 | 97 |
| 6 | (158) | 130 | 123 | 124 | 121.5 | 119 | 114 | 114 | 114 | 110 |
| 7 | 135 | 128 | 127 | 125 | 121 | 120 | 116 | 113.5 | 112 | 110.5 |
| 8 | 130.5 | 127.5 | 126 | 124 | 123.5 | 120.5 | 117.5 | 114.5 | 113.5 | 113 |
| 9 | 129 | 126.5 | 125 | 122 | 120 | 116.5 | 114 | 112.5 | 110 | 110 |
| 10 | 130.5 | 128.5 | 129.5 | 124.5 | 122.5 | 120.5 | 117 | 113.5 | 112.5 | 111 |
| 11 | 129 | 127.5 | 125 | 122.5 | 120 | 116.5 | 113.5 | 112.5 | 112 | 114 |
| 12 | 129.5 | 128 | 127.5 | 124.5 | 122.5 | 118.5 | 115 | 113 | 111 | 109 |
| 13 | 128.5 | 123 | 123.5 | 120 | 118.5 | 118 | 112 | 111 | 110 | 109 |
| 14 | 131.5 | 127 | 123 | 120 | 116 | 113.5 | 110 | 105.5 | 102.5 | 101 |
| 15 | 131.5 | 129 | 124.5 | 120 | 117 | 111.5 | 106.5 | 104 | 99.5 | 101 |
| 16 | 131.5 | 126.5 | 123 | 119 | 117.5 | 112.5 | 106.5 | 103.5 | 100 | 97.5 |
| 17 | 133 | 124.5 | 126 | 122 | 115 | 110 | 101 | 103 | 100.5 | 98 |
| 18 | 132.5 | 127 | 123 | 119 | 115 | 107 | 104 | 101.5 | 97 | 92.5 |
| 19 | 131 | 121 | 116.5 | 109 | 95 | 99 | 93.5 | 93 | 86.5 | 90 |
| 20 | 131 | 120 | 115.5 | 108.5 | 107 | 106 | 97.5 | 92 | 91 | 89 |
| 21 | 129 | 119 | 100 | 99 | 87.5 | 94 | 86 | 83 | 87 | 81.5 |
| FF | 119 | 116.5 | 117 | 111.5 | 112 | 109 | 105.5 | 105 | 103 | 102.5 |

TABLE A-II TABULATED HARMONIC SOUND PRESSURE LEVELS AT 9000 RPM (Cont.)

c. Equivalent free-field locations (adjusted to run 296)

Harmonic Sound Pressure Level, dB re 20μPa

| Mic No. | 4P | 8P | 12P | 16P | 20P | 24P | 28P | 32P | 36P | 40P |
|---|---|---|---|---|---|---|---|---|---|---|
| 1 | 128 | 124.5 | 122.5 | 117.5 | 115.5 | 113.5 | 108 | 107.5 | 105.5 | 102.5 |
| 2 | 125 | 121.5 | 120 | 116 | 115.5 | 114.5 | 115 | 119 | 108.5 | 105 |
| 3 | | | | | | | | | | |
| 4 | | | | | | | | | | |
| 5 | 128.5 | 123.5 | 118.5 | 118.5 | 112.5 | 114.5 | 109 | 107.5 | 105.5 | 105.5 |
| 6 | | | | | | | | | | |
| 7 | | | | | | | | | | |
| 8 | 126.5 | 123.5 | 121 | 120.5 | 117.5 | 113.5 | 110 | 108 | 106.5 | 105.5 |
| 9 | 123.5 | 119 | 117.5 | 113.5 | 107 | 109 | 101.5 | 101 | 98 | 95.5 |
| 10 | 126 | 122 | 118.5 | 119 | 118.5 | 123 | 117.5 | 115 | 106.5 | 103.5 |
| 11 | 125.5 | 122.5 | 119.5 | 115.5 | 111.5 | 109.5 | 107.5 | 104 | 102 | 102 |
| 12 | 124.5 | 123.5 | 122 | 118 | 117.5 | 113.5 | 110.5 | 106 | 104.5 | 102.5 |
| 13 | 127.5 | 125 | 122.5 | 120 | 117 | 114 | 112 | 109 | 108.5 | 107.5 |
| 14 | | | | | | | | | | |
| 15 | 127 | 121 | 116.5 | 116 | 109 | 107 | 100 | 95.5 | 97.5 | 94 |
| 16 | 127 | 123 | 119 | 116 | 110 | 107 | 102 | 101.5 | 93.5 | 90 |
| 17 | | | | | | | | | | |
| 18 | 127.5 | 123 | 114.5 | 113.5 | 107.5 | 99 | 91.5 | 87 | 94 | 79 |
| 19 | | | | | | | | | | |
| 20 | | | | | | | | | | |
| 21 | 124 | 114 | 108.5 | 97.5 | 95 | 95.5 | 95.5 | 88.5 | 87 | 86 |
| FF | 121 | 117.5 | 116 | 115 | 112 | 109 | 106 | 104 | 103.5 | 102 |

TABLE A-II TABULATED HARMONIC SOUND PRESSURE LEVELS AT 9000 RPM (Concluded)

d. Derived pressure doubling effects

Harmonic Sound Pressure Level Difference, ΔdB

| Mic No. | 4P | 8P | 12P | 16P | 20P | 24P | 28P | 32P | 36P | 40P |
|---|---|---|---|---|---|---|---|---|---|---|
| 1 | 4.5 | 4.5 | 6 | 6.5 | 5.5 | 4 | 6 | 4.5 | 3.5 | 5.5 |
| 2 | 3.5 | 11.5 | 3.5 | 2 | -2 | -3.5 | -5 | -14 | -6.5 | -7.5 |
| 3 | | | | | | | | | | |
| 4 | | | | | | | | | | |
| 5 | -4.5 | -6 | -4 | -6 | -2 | -6 | -4.5 | -6 | -6 | -8.5 |
| 6 | | | | | | | | | | |
| 7 | | | | | | | | | | |
| 8 | 4 | 4 | 5 | 3.5 | 6 | 7 | 7.5 | 6.5 | 7 | 7.5 |
| 9 | 5.5 | 7.5 | 7.5 | 8.5 | 13 | 7.5 | 12.5 | 11.5 | 12 | 14.5 |
| 10 | 4.5 | 6.5 | 11 | 5.5 | 4 | -2.5 | -.5 | -1.5 | 6 | 7.5 |
| 11 | 3.5 | 5 | 5.5 | 7 | 8.5 | 7 | 6 | 8.5 | 10 | 12 |
| 12 | 5 | 4.5 | 5.5 | 6.5 | 5 | 5 | 4.5 | 7 | 6.5 | 6.5 |
| 13 | 1 | -2 | 1 | 0 | 1.5 | 4 | 0 | 2 | 1.5 | 1.5 |
| 14 | | | | | | | | | | |
| 15 | 4.5 | 8 | 8 | 4 | 1 | 4.5 | 6.5 | 8.5 | 2 | 7 |
| 16 | 4.5 | 3.5 | 4 | 3 | 7.5 | 5.5 | 4.5 | 2 | 6.5 | 7.5 |
| 17 | | | | | | | | | | |
| 18 | 5 | 4 | 8.5 | 5.5 | 7.5 | 8 | 12.5 | 14.5 | 3 | 13.5 |
| 19 | | | | | | | | | | |
| 20 | | | | | | | | | | |
| 21 | 5 | 1.5 | -8.5 | 1.5 | -7.5 | -1.5 | -9.5 | -5.5 | 0 | -4.5 |

TABLE A-III TABULATED HARMONIC SOUND PRESSURE LEVELS AT 10 000 RPM

a. Fuselage at 0.4 D Clearance (adjusted to run 267)

Harmonic Sound Pressure Levels, dB re 20μPa

| Mic No. | 4P | 8P | 12P | 16P | 20P | 24P | 28P | 32P | 36P | 40P |
|---|---|---|---|---|---|---|---|---|---|---|
| 1 | 133.5 | 134 | 136 | 134.5 | 134 | 131.5 | 128 | 127.5 | 126 | 123 |
| 2 | 135.5 | 126.5 | 129.5 | 117 | 115 | 117 | 109 | 106.5 | 103 | 104.5 |
| 3 | 140 | 135.5 | 132 | 126 | 124 | 119.5 | 115.5 | 113 | 108 | 107.5 |
| 4 | 137.5 | 135 | 130 | 127 | 124 | 113 | 118 | 110 | 107.5 | 101 |
| 5 | 139 | 136.5 | 131 | 132 | 131 | 126 | 122.5 | 118 | 110 | 105 |
| 6 | 141.5 | 142 | 140 | 137.5 | 136.5 | 134.5 | 132 | 129 | 125.5 | 121.5 |
| 7 | 141 | 139 | 138.5 | 138 | 137 | 134 | 132 | 130 | 126 | 119.5 |
| 8 | 140 | 141 | 141 | 139 | 138 | 137 | 134.5 | 131.5 | 127.5 | 124 |
| 9 | 135 | 136.5 | 135 | 135 | 135.5 | 133.5 | 131.5 | 129 | 136 | 124 |
| 10 | 139 | 139.5 | 140 | 139 | 137.5 | 136.5 | 134 | 131.5 | 129 | 127.5 |
| 11 | 137 | 139 | 139 | 139 | 138.5 | 137 | 135 | 132.5 | 129 | 127.5 |
| 12 | 138.5 | 138 | 139 | 139 | 138 | 136 | 134 | 131 | 129 | 128 |
| 13 | 132 | 132 | 132 | 132 | 130 | 129 | 125.5 | 123 | 120 | 117.5 |
| 14 | 133.5 | 133.5 | 132.5 | 129 | 129.5 | 127.5 | 125.5 | 122.5 | 120.5 | 121 |
| 15 | 135 | 134.5 | 133 | 131.5 | 132 | 127.5 | 122.5 | 120 | 117.5 | 118 |
| 16 | 131.5 | 133.5 | 133 | 131 | 131 | 126.5 | 123.5 | 122.5 | 120 | 120.5 |
| 17 | 132 | 132 | 130 | 126 | 128.5 | 122.5 | 121 | 121.5 | 121.5 | 117 |
| 18 | 134 | 133.5 | 131.5 | 125 | 120 | 123.5 | 118.5 | 108 | 105.5 | 114 |
| 19 | 129 | 125 | 123.5 | 122.5 | 114 | 108.5 | 112.5 | 110 | 108.5 | 104.5 |
| 20 | 130.5 | 128.5 | 118.5 | 110 | 120.5 | 117 | 114 | 110.5 | 106.5 | 111 |
| 21 | 125.5 | 123 | 114 | 115.5 | 115 | 106 | 113 | 106.5 | 103 | 103.5 |
| FF | 124 | 124 | 127 | 125 | 121 | 123 | 120 | 115.5 | 113.5 | 115.5 |

TABLE A-III TABULATED HARMONIC SOUND PRESSURE LEVELS AT 10 000 RPM (Cont.)

b. Fuselage at 0.8 D clearance (adjusted to run 286)

Harmonic Sound Pressure Levels, dB re 20μPa

| Mic No. | 4P | 8P | 12P | 16P | 20P | 24P | 28P | 32P | 36P | 40P |
|---|---|---|---|---|---|---|---|---|---|---|
| 1 | 134 | 134.5 | 133 | 132.5 | 130.5 | 129.5 | 126.5 | 124 | 122.5 | 122 |
| 2 | 134.5 | 142.5 | 136 | 131.5 | 129.5 | 127 | 124 | 121.5 | 116.5 | 114 |
| 3 | 133.5 | 133 | 133.5 | 129.5 | 132.5 | 130 | 128.5 | 127.5 | 125.5 | 121 |
| 4 | 134 | 131.5 | 132 | 131 | 132.5 | 132 | 129.5 | 125 | 122.5 | 118 |
| 5 | 127.5 | 127 | 126 | 124 | 123.5 | 123 | 119 | 115.5 | 112 | 108 |
| 6 | 142 | 140.5 | 128 | 136 | 135 | 132.5 | 132 | 129 | 125 | 124 |
| 7 | 138 | 134 | 135 | 133.5 | 135 | 132.5 | 131.5 | 127.5 | 124.5 | 121 |
| 8 | 135 | 135.5 | 133.5 | 134 | 134 | 132 | 129 | 127 | 124.5 | 123.5 |
| 9 | 133.5 | 133.5 | 132 | 132 | 130.5 | 127.5 | 125.5 | 123.5 | 121 | 120.5 |
| 10 | 135 | 134 | 137 | 134 | 135 | 133 | 131 | 128.5 | 126 | 125.5 |
| 11 | 135 | 134.5 | 132.5 | 132.5 | 132 | 128.5 | 126 | 124 | 123.5 | 124 |
| 12 | 132.5 | 136 | 135 | 135.5 | 134.5 | 132 | 130 | 127 | 125 | 122 |
| 13 | 130 | 130 | 129 | 130 | 128.5 | 127.5 | 126 | 123.5 | 121.5 | 121.5 |
| 14 | 135 | 133.5 | 133 | 129.5 | 126.5 | 124 | 124.5 | 123.5 | 117.5 | 114.5 |
| 15 | 135.5 | 135 | 131 | 132 | 131 | 128 | 125.5 | 121.5 | 117.5 | 116 |
| 16 | 132.5 | 133.5 | 132 | 130.5 | 129.5 | 127.5 | 123.5 | 118.5 | 117.5 | 113.5 |
| 17 | 134 | 131.5 | 132.5 | 127.5 | 130.5 | 126.5 | 123 | 122 | 120 | 117 |
| 18 | 134 | 132 | 132 | 130 | 125 | 119 | 118 | 116 | 112 | 113 |
| 19 | 133.5 | 130.5 | 126.5 | 124 | 120.5 | 115 | 103.5 | 110.5 | 100 | 100 |
| 20 | 132.5 | 131.5 | 123.5 | 123.5 | 115 | 116.5 | 112.5 | 110.5 | 105.5 | 98 |
| 21 | 130.5 | 120.5 | 115.5 | 103 | 105.5 | 100 | 99.5 | 97 | 103 | 98 |
| FF | 123 | 123 | 126 | 123 | 121 | 121 | 119 | 115 | 115 | 114 |

TABLE A-III TABULATED HARMONIC SOUND PRESSURE LEVELS AT 10 000 RPM (Cont.)

c. Equivalent free-field locations (adjusted to run 295)

Harmonic Sound Pressure Levels, dB re 20μPa

| Mic No. | 4P | 8P | 12P | 16P | 20P | 24P | 28P | 32P | 36P | 40P |
|---|---|---|---|---|---|---|---|---|---|---|
| 1 | 127.5 | 126 | 126.5 | 123.5 | 122 | 122.5 | 119 | 117.5 | 114.5 | 113.5 |
| 2 | 126 | 127.5 | 125 | 121.5 | 127.5 | 112 | 121 | 121.5 | 116 | 113 |
| 3 | | | | | | | | | | |
| 4 | | | | | | | | | | |
| 5 | 129 | 125.5 | 124 | 126 | 125.5 | 123 | 122 | 118 | 116.5 | 117 |
| 6 | | | | | | | | | | |
| 7 | | | | | | | | | | |
| 8 | 127 | 127 | 127 | 123.5 | 125 | 123.5 | 119.5 | 118.5 | 115 | 114 |
| 9 | 127.5 | 127.5 | 127 | 125 | 122.5 | 121.5 | 118 | 117 | 110 | 104 |
| 10 | 127.5 | 124.5 | 127 | 123.5 | 126 | 125.5 | 129 | 121 | 119 | 116 |
| 11 | 128 | 128.5 | 128.5 | 126.5 | 125 | 124.5 | 120 | 118 | 113 | 111.5 |
| 12 | 126 | 129.5 | 128 | 126 | 126 | 124.5 | 122.5 | 118 | 115.5 | 115 |
| 13 | 130 | 128.5 | 129.5 | 128 | 126 | 125 | 123.5 | 119.5 | 116.5 | 117 |
| 14 | | | | | | | | | | |
| 15 | 127 | 127 | 124.5 | 123 | 121 | 119.5 | 112.5 | 113 | 114 | 108.5 |
| 16 | 128.5 | 127 | 127 | 122.5 | 123.5 | 120 | 115 | 114.5 | 112 | 110.5 |
| 17 | | | | | | | | | | |
| 18 | 127.5 | 125 | 123.5 | 118.5 | 121 | 118 | 112 | 110 | 109 | 106.5 |
| 19 | | | | | | | | | | |
| 20 | | | | | | | | | | |
| 21 | 125 | 116 | 107.5 | 102.5 | 107 | 108 | 101.5 | 92 | 101 | 89.5 |
| FF | 122.5 | 124 | 123.5 | 121 | 121 | 120 | 117 | 115 | 114 | 113 |

TABLE A-III TABULATED HARMONIC SOUND PRESSURE LEVELS AT 10 000 RPM (Concluded)

d. Derived pressure doubling effects

Harmonic Sound Pressure Level Differences, ΔdB

| Mic No. | 4P | 8P | 12P | 16P | 20P | 24P | 28P | 32P | 36P | 40P |
|---|---|---|---|---|---|---|---|---|---|---|
| 1 | 6.5 | 8.5 | 6.5 | 9 | 8.5 | 7 | 7.5 | 6.5 | 8 | 8.5 |
| 2 | 8.5 | 15 | 11 | 10 | 2 | 15 | 3 | 0 | .5 | 1 |
| 3 | | | | | | | | | | |
| 4 | | | | | | | | | | |
| 5 | -1.5 | 1.5 | 2 | -2 | -2 | 0 | -3 | -2.5 | -4.5 | -9 |
| 6 | | | | | | | | | | |
| 7 | | | | | | | | | | |
| 8 | 8 | 8.5 | 6.5 | 10.5 | 9 | 8.5 | 9.5 | 8.5 | 8.5 | 9.5 |
| 9 | 6 | 9 | 5 | 7 | 8 | 6 | 7.5 | 6.5 | 11 | 16.5 |
| 10 | 7.5 | 9.5 | 10 | 10.5 | 9 | 7.5 | 2 | 7.5 | 7 | 9.5 |
| 11 | 7 | 6 | 4 | 6 | 7 | 4 | 6 | 6 | 10.5 | 12.5 |
| 12 | 6.5 | 6.5 | 7 | 9.5 | 8.5 | 7.5 | 7.5 | 9 | 9.5 | 7 |
| 13 | 0 | 1.5 | -.5 | 2 | 2.5 | 2.5 | 2.5 | 4 | 5 | 4.5 |
| 14 | | | | | | | | | | |
| 15 | 8.5 | 8 | 6.5 | 9 | 8 | 8.5 | 13.5 | 8.5 | 3.5 | 7.5 |
| 16 | 4 | 6.5 | 5 | 8 | 6 | 7.5 | 8.5 | 4 | 5.5 | 3 |
| 17 | | | | | | | | | | |
| 18 | 6.5 | 7 | 8.5 | 11.5 | 4 | 1 | 6 | 6 | 3 | 6.5 |
| 19 | | | | | | | | | | |
| 20 | | | | | | | | | | |
| 21 | 5.5 | 4.5 | 8 | .5 | -1.5 | -8 | -2 | 5 | 2 | 8.5 |

TABLE A-IV TABULATED HARMONIC SOUND PRESSURE LEVELS AT 11 300 RPM

a. Fuselage at 0.4 D Clearance (adjusted to run 266)

Harmonic Sound Pressure Levels, dB re 20μPa

| Mic No. | 4P | 8P | 12P | 16P | 20P | 24P | 28P | 32P | 36P | 40P |
|---|---|---|---|---|---|---|---|---|---|---|
| 1 | 144 | 146 | 147 | 148 | 146.5 | 144 | 143 | 142 | 137 | 135 |
| 2 | 143.5 | 134.5 | 141.5 | 136.5 | 128.5 | 126.5 | 121 | 120.5 | 116.5 | 114.5 |
| 3 | 147 | 144 | 144.5 | 142.5 | 139.5 | 135.5 | 134 | 130.5 | 133 | 126.5 |
| 4 | 145 | 143.5 | 141.5 | 140.5 | 137.5 | 135.5 | 133.5 | 130 | 129 | 124.5 |
| 5 | 146.5 | 146 | 143.5 | 144 | 142.5 | 141.5 | 138 | 136 | 133.5 | 131 |
| 6 | 148 | 147 | 147.5 | 146.5 | 144.5 | 143 | 141.5 | 139 | 137.5 | 137.5 |
| 7 | 147 | 147.5 | 148 | 146 | 145.5 | 143 | 142 | 140 | 137 | 137.5 |
| 8 | 147 | 147.5 | 148 | 147 | 146 | 144 | 141 | 139 | 139 | 140 |
| 9 | 141 | 142 | 144 | 143 | 142 | 139 | 137 | 135.5 | 135.5 | 137.5 |
| 10 | 142.5 | 145.5 | 147.5 | 146 | 145 | 142.5 | 139 | 140 | 140 | 140 |
| 11 | 144.5 | 148 | 148 | 148.5 | 146.5 | 144.5 | 141.5 | 139.5 | 140.5 | 141.5 |
| 12 | 142.5 | 145.5 | 148 | 146 | 144.5 | 142.5 | 140.5 | 138.5 | 140.5 | 140.5 |
| 13 | 139.5 | 138 | 139 | 139 | 139.5 | 135 | 131 | 132.5 | 134 | 135 |
| 14 | 141 | 142 | 144 | 142 | 141 | 138.5 | 137 | 135.5 | 134.5 | 135 |
| 15 | 144.5 | 144.5 | 144.5 | 144.5 | 143 | 141.5 | 138.5 | 136 | 133.5 | 137 |
| 16 | 141.5 | 143 | 144 | 143.5 | 141.5 | 142.5 | 139.5 | 138 | 137 | 137 |
| 17 | 138 | 141.5 | 140.5 | 140.5 | 138.5 | 138 | 133 | 131 | 132 | 133.5 |
| 18 | 142 | 143.5 | 143 | 140.5 | 138 | 134.5 | 131.5 | 129.5 | 130 | 125.5 |
| 19 | 140 | 138 | 135 | 131 | 128.5 | 136 | 135.5 | 132 | 126.5 | 131 |
| 20 | 138 | 136 | 135.5 | 129 | 128 | 114.5 | 122.5 | 122.5 | 117 | 116 |
| 21 | 134 | 133 | 125 | 130 | 120 | 117 | 124 | 118 | 117 | 106.5 |
| FF | 134 | 133 | 134.5 | 133.5 | 131.5 | 128.5 | 126.5 | 126.5 | 125.5 | 125.5 |

TABLE A-IV TABULATED HARMONIC SOUND PRESSURE LEVELS AT 11 300 RPM (Cont.)

b. Fuselage at 0.8 D Clearance (adjusted to run 288)

Harmonic Sound Pressure Levels, dB re 20μPa

| Mic No. | 4P | 8P | 12P | 16P | 20P | 24P | 28P | 32P | 36P | 40P |
|---|---|---|---|---|---|---|---|---|---|---|
| 1 | 142 | 141.5 | 142 | 141.5 | 139 | 137 | 132.5 | 131.5 | 129 | 130 |
| 2 | 136.5 | 141 | 141.5 | 138 | 137.5 | 132 | 129.5 | 130 | 123.5 | 124 |
| 3 | 141 | 139.5 | 138.5 | 137 | 135.5 | 132 | 131 | 131 | 130.5 | 132.5 |
| 4 | 139 | 138.5 | 140 | 138.5 | 137 | 135.5 | 132 | 131.5 | 131.5 | 132.5 |
| 5 | 146 | 126 | 125.5 | 124.5 | 120.5 | 119.5 | 115.5 | 114 | 115 | 114.5 |
| 6 | (154.5) | 148 | 140.5 | 141 | 138 | 134.5 | 133 | 132 | 133 | 135 |
| 7 | 138.5 | 142 | 140.5 | 140.5 | 140 | 137.5 | 134 | 134.5 | 134.5 | 134 |
| 8 | 141 | 141 | 141 | 140 | 137 | 135.5 | 133 | 132.5 | 132 | 134 |
| 9 | 139 | 141.5 | 141 | 139.5 | 137.5 | 133 | 130 | 130 | 130.5 | 130 |
| 10 | 141 | 137 | 143.5 | 143 | 141 | 139 | 136.5 | 135 | 136 | 136.5 |
| 11 | 141 | 140 | 141.5 | 140 | 133 | 130.5 | 131 | 132 | 130 | 131 |
| 12 | 141 | 142 | 143 | 141 | 140.5 | 136.5 | 133.5 | 135 | 133 | 134 |
| 13 | 135.5 | 135.5 | 140 | 138 | 135.5 | 133.5 | 132 | 131 | 131 | 130.5 |
| 14 | 143 | 142 | 141.5 | 138 | 136 | 133.5 | 131 | 130 | 127.5 | 126 |
| 15 | 143.5 | 142.5 | 144 | 143.5 | 141 | 138 | 136 | 134 | 133 | 132 |
| 16 | 142.5 | 141.5 | 142.5 | 141.5 | 136 | 135.5 | 130.5 | 128 | 127.5 | 125 |
| 17 | 139 | 141 | 141 | 141.5 | 138 | 137 | 134 | 133 | 132 | 133 |
| 18 | 141.5 | 142 | 141.5 | 140 | 136 | 135.5 | 131.5 | 130 | 129.5 | 129 |
| 19 | 142 | 141 | 137.5 | 136 | 134 | 130 | 125.5 | 123 | 118.5 | 118.5 |
| 20 | 139.5 | 138.5 | 138.5 | 133.5 | 133 | 127.5 | 122 | 119 | 114.5 | 111 |
| 21 | 135.5 | 132.5 | 127 | 130.5 | 125 | 110 | 120 | 119 | 110 | 114 |
| FF | 131 | 132 | 131.5 | 129 | 128.5 | 124 | 122 | 123 | 123 | 122.5 |

TABLE A-IV TABULATED HARMONIC SOUND PRESSURE LEVELS AT 11 300 RPM (Cont.)

c. Equivalent free-field locations (adjusted to run 297)

Harmonic Sound Pressure Levels, dB re 20μPa

| Mic No. | 4P | 8P | 12P | 16P | 20P | 24P | 28P | 32P | 36P | 40P |
|---|---|---|---|---|---|---|---|---|---|---|
| 1 | 138 | 138 | 135.5 | 133.5 | 134 | 133 | 130 | 127 | 125 | 125 |
| 2 | 134 | 136 | 134 | 130 | 133.5 | 130.5 | 128 | 125 | 123.5 | 124 |
| 3 | | | | | | | | | | |
| 4 | | | | | | | | | | |
| 5 | 131 | 135 | 136.5 | 133 | 134 | 132.5 | 126.5 | 127.5 | 128 | 129 |
| 6 | | | | | | | | | | |
| 7 | | | | | | | | | | |
| 8 | 135 | 134.5 | 134.5 | 133.5 | 133 | 130.5 | 127 | 125 | 127.5 | 126.5 |
| 9 | 134 | 135 | 137 | 137 | 133 | 129.5 | 127 | 121.5 | 118.5 | 120.5 |
| 10 | 134 | 136 | 137 | 136 | 134 | 119 | 130.5 | 129 | 130 | 129 |
| 11 | 134.5 | 136 | 135.5 | 134.5 | 133 | 130 | 128.5 | 123 | 125 | 125 |
| 12 | 134 | 136 | 137.5 | 136.5 | 135.5 | 131.5 | 128 | 128 | 128 | 130 |
| 13 | 136.5 | 136.5 | 137 | 136.5 | 132 | 130.5 | 128 | 128.5 | 128 | 128 |
| 14 | | | | | | | | | | |
| 15 | 136 | 136 | 137 | 135 | 131.5 | 128.5 | 129 | 126 | 126 | 124 |
| 16 | 136 | 136 | 138.5 | 134.5 | 135 | 132 | 130 | 128 | 127 | 126.5 |
| 17 | | | | | | | | | | |
| 18 | 137 | 136.5 | 135.5 | 131 | 130 | 128 | 122.5 | 126 | 122.5 | 123.5 |
| 19 | | | | | | | | | | |
| 20 | | | | | | | | | | |
| 21 | 134 | 130.5 | 127 | 122.5 | 113 | 105 | 113.5 | 114.5 | 109 | 104 |
| FF | 129.5 | 130.5 | 132 | 130 | 129.5 | 126.5 | 122.5 | 122.5 | 122.5 | 123.5 |

TABLE A-IV TABULATED HARMONIC SOUND PRESSURE LEVELS AT 11 300 RPM (Concluded)

d. Derived pressure doubling effects

Harmonic Sound Pressure Level Differences, ΔdB

| Mic No. | 4P | 8P | 12P | 16P | 20P | 24P | 28P | 32P | 36P | 40P |
|---|---|---|---|---|---|---|---|---|---|---|
| 1 | 4 | 3.5 | 6.5 | 8 | 5.5 | 6 | 3.5 | 5.5 | 3 | 4.5 |
| 2 | 2.5 | 5 | 7.5 | 8 | 4 | 1.5 | 1.5 | 5 | 0 | 0 |
| 3 | | | | | | | | | | |
| 4 | | | | | | | | | | |
| 5 | 15 | -9 | -11 | -8.5 | -13.5 | -13 | -11 | -13.5 | -13 | -14.5 |
| 6 | | | | | | | | | | |
| 7 | | | | | | | | | | |
| 8 | 6 | 6.5 | 6.5 | 6.5 | 4 | 5 | 6 | 7.5 | 4.5 | 7.5 |
| 9 | 5 | 6.5 | 4 | 2.5 | 4.5 | 3.5 | 3 | 8.5 | 12 | 9.5 |
| 10 | 7 | 1 | 6.5 | 7 | 7 | 20 | 6 | 6 | 6 | 7.5 |
| 11 | 6.5 | 4 | 6 | 5.5 | 0 | .5 | 2.5 | 9 | 5 | 6 |
| 12 | 7 | 6 | 5.5 | 4.5 | 5 | 5 | 5.5 | 7 | 5 | 4 |
| 13 | -1 | -1 | 3 | 1.5 | 3.5 | 3 | 4 | 2.5 | 3 | 2.5 |
| 14 | | | | | | | | | | |
| 15 | 7.5 | 6.5 | 7 | 8.5 | 9.5 | 9.5 | 7 | 8 | 7 | 8 |
| 16 | 6.5 | 5.5 | 4 | 7 | 1 | 3.5 | .5 | 0 | .5 | -1.5 |
| 17 | | | | | | | | | | |
| 18 | 4.5 | 5.5 | 6 | 9 | 6 | 7.5 | 9 | 4 | 7 | 5.5 |
| 19 | | | | | | | | | | |
| 20 | | | | | | | | | | |
| 21 | 1.5 | 2 | 0 | 8 | 12 | 5 | 6.5 | 4.5 | 1 | 10 |

TABLE A-V TABULATED HARMONIC SOUND PRESSURE PHASE ANGLES AT 9000 RPM

a. Fuselage at 0.4 D Clearance

Harmonic Phase Angle, Deg.

| Mic No. | 4P | 8P | 12P |
|---|---|---|---|
| 2 | 34.5 | 166.0 | -58.9 |
| 3 | 20.2 | 85.6 | -145.6 |
| 4 | 47.7 | -154.4 | 30.9 |
| 5 | -28.6 | 52.7 | 136.3 |
| 6 | -81.8 | -59.3 | -40.1 |
| 7 | 7.7 | 134.9 | -133.6 |
| 8 | -51.3 | -17.8 | 17 |
| 9 | -55.0 | -45.7 | -33.2 |
| 10 | -87.6 | -107.1 | -124.4 |
| 11 | -55.2 | -35.7 | -4.6 |
| 12 | 58.5 | 151.2 | -129 |
| 13 | 155.4 | -26.8 | 172.8 |
| 14 | -18.4 | -18.6 | -20.7 |
| 15 | -23.4 | -44.3 | -72.6 |
| 16 | 90 | 175.6 | -68.3 |
| 17 | 169 | 28.9 | -159 |
| 18 | 38.3 | 54.1 | 89.0 |
| 19 | 42.2 | 43.2 | 114.9 |
| 20 | 107.4 | -147.5 | -38.3 |
| 21 | 112.5 | -131.5 | -9.9 |

b. Fuselage at 0.8 D Clearance

Harmonic Phase Angle, Deg.

| 4P | 8P | 12P |
|---|---|---|
| -26.1 | 53.1 | -172.8 |
| -8.2 | 20.1 | 61.2 |
| 2.4 | 128.4 | -133.6 |
| -7.8 | 37.0 | 89.1 |
| -52.2 | -64.8 | -69.0 |
| 16.4 | 73.0 | 138.0 |
| -26.8 | -12.6 | 7.2 |
| -5.9 | 34.1 | 58.6 |
| -42.9 | -44.2 | -51 |
| -15.3 | -10 | 10.9 |
| 38.7 | 117.1 | 180.3 |
| 148.8 | -67 | 108.8 |
| 23.2 | 27.9 | 91.6 |
| .2 | -2.9 | -12.4 |
| 70.3 | 147.5 | -135 |
| -178.3 | -29.6 | 122.1 |
| 36.3 | 59.1 | 77.5 |
| 57.9 | 78.3 | 139.8 |
| 98.3 | -160.5 | -103.1 |
| 117.9 | -160.9 | -76.3 |

c. Equivalent free-field locations

Harmonic Phase Angle, Deg.

| Mic No. | 4P | 8P | 12P |
|---|---|---|---|
| 2 | 9.7 | 30.6 | 57.1 |
| 5 | 146.2 | -31 | 146.6 |
| 8 | -13.9 | -5.6 | 8.2 |
| 9 | .1 | 123.9 | -146.2 |
| 10 | -25 | -42.9 | -44.7 |
| 11 | -16.1 | 33.8 | 103.5 |
| 12 | -134.3 | 108.9 | 181.2 |
| 13 | -19.2 | 3.4 | 21.1 |
| 15 | 89 | 146.1 | -108.7 |
| 16 | 5.8 | 3.6 | 2.5 |
| 18 | 40.9 | 48.1 | 71.9 |
| 21 | 120.8 | -169.9 | -58.6 |

TABLE A-VI TABULATED HARMONIC SOUND PRESSURE PHASE ANGLES AT 10 000 RPM

a. Fuselage at 0.4 D Clearance

Harmonic Phase Angle, Deg.

| Mic No. | 4P | 8P | 12P |
|---|---|---|---|
| 2 | 79.8 | -60 | 134.3 |
| 3 | 12.8 | 141.5 | 113.3 |
| 4 | 109.1 | -49.5 | 170.8 |
| 5 | 10.8 | 121 | -107.3 |
| 6 | -56.3 | -.4 | 38 |
| 7 | 42.8 | 169.2 | -63 |
| 8 | -34.5 | 13.9 | 55.5 |
| 9 | -42.9 | 4.8 | 31.8 |
| 10 | -84.2 | -93.3 | -99.4 |
| 11 | -53.1 | 5.4 | 46.1 |
| 12 | 31.6 | 150 | -94.3 |
| 13 | -48.2 | -26.8 | 8.8 |
| 14 | -4.9 | 5.2 | 24.5 |
| 15 | -17.2 | -47.2 | -65.4 |
| 16 | 104.9 | -160.7 | -71.1 |
| 17 | 150.1 | 40.2 | -121 |
| 18 | 52.9 | -73.8 | 99.3 |
| 19 | 52.3 | 86.5 | 87.5 |
| 20 | 155.5 | -150.4 | 24.2 |
| 21 | 175.7 | -126.7 | 33.6 |

b. Fuselage at 0.8 D Clearance

Harmonic Phase Angle, Deg.

| 4P | 8P | 12P |
|---|---|---|
| 19.8 | 97.8 | -81.5 |
| 6.1 | 70.2 | 154.1 |
| 58.2 | 183.6 | -52.2 |
| 25 | 61.6 | 137.3 |
| 93.3 | -2 | -15.1 |
| 24 | 108.1 | 181.9 |
| -15.8 | -3.4 | 25.7 |
| 22.7 | 75 | 131.4 |
| -32.3 | -30.1 | -34 |
| -12.3 | -1.4 | 21.7 |
| 55.2 | 123.3 | -163.2 |
| 153.1 | -24.7 | 179.7 |
| 43.2 | 93.8 | 128 |
| 14.8 | 9.1 | 4.2 |
| 98 | 165.1 | -132.1 |
| 179 | 1.5 | 155.1 |
| 48.4 | 66.6 | 81.4 |
| 81 | 121.3 | 118.1 |
| 120.6 | -154.9 | -81.3 |
| 138.8 | -149.5 | -82.8 |

c. Equivalent free-field locations

Harmonic Phase Angle, Deg.

| Mic No. | 4P | 8P | 12P |
|---|---|---|---|
| 2 | -5.4 | 66 | 115.4 |
| 5 | 180.9 | -3.8 | 166.9 |
| 8 | -12.7 | -1.5 | 19.8 |
| 9 | 33 | 166.3 | -71.3 |
| 10 | -27.6 | -16.4 | -6 |
| 11 | 2 | 70.5 | 145.1 |
| 12 | -3.4 | 123.5 | -144.3 |
| 13 | -11.8 | 15.9 | 59.8 |
| 15 | 102.1 | 169.5 | -92.6 |
| 16 | 5.9 | 16.4 | 29.4 |
| 18 | 44.3 | 66.6 | 100.8 |
| 21 | 142.2 | -169.7 | -29.3 |

TABLE A-VII TABULATED HARMONIC SOUND PRESSURE PHASE ANGLES AT 11 300 RPM

a. Fuselage at 0.4 D Clearance

Harmonic Phase Angle, Deg.

| Mic. No. | 4P | 8P | 12P |
|---|---|---|---|
| 2 | 111 | -30.4 | -124.4 |
| 3 | 24.5 | 173.4 | -33.4 |
| 4 | 115.7 | -.9 | -136.7 |
| 5 | 18.9 | 159.8 | -62.2 |
| 6 | -48.5 | 1.4 | 75.8 |
| 7 | 43.9 | 180.9 | -20.8 |
| 8 | -32 | 15.2 | 74.9 |
| 9 | -10.1 | 33.8 | 102.2 |
| 10 | -63.5 | -78.1 | -74.2 |
| 11 | -58.9 | -15.3 | 27 |
| 12 | 48.9 | 159.7 | -72.4 |
| 13 | -172.3 | 50.6 | -58.7 |
| 14 | 32 | 34.1 | 75 |
| 15 | 116 | -27 | -44.2 |
| 16 | 103.6 | -159 | -56.8 |
| 17 | -147.8 | 57.1 | -60.7 |
| 18 | 43.8 | 58.3 | 89.3 |
| 19 | 44 | 76.9 | 123 |
| 20 | 125.1 | -81.6 | 5.9 |
| 21 | 144.7 | -82.2 | -147 |

b. Fuselage at 0.8 D Clearance

Harmonic Phase Angle, Deg.

| 4P | 8P | 12P |
|---|---|---|
| 19.8 | 175.2 | -11.1 |
| 20.7 | 86.6 | -144.5 |
| 55.2 | -144.9 | 12.6 |
| 22.2 | 96.4 | 188.7 |
| 93.9 | 31 | 66.3 |
| 8.2 | 135.9 | -132.5 |
| -25.8 | 18.6 | 61.3 |
| 32.3 | 119.4 | -161.4 |
| -30.7 | .7 | -2.7 |
| -19.1 | 2.6 | 31.2 |
| 59 | 152.2 | -127.9 |
| 166.7 | 25.3 | -127.9 |
| 62 | 118.6 | 170.3 |
| 13.9 | 17.1 | 26.9 |
| 87.7 | 179.6 | -105.2 |
| -168.5 | 29.9 | -157.9 |
| 42.7 | 73.4 | 103.4 |
| 68 | 111.6 | 147.9 |
| 116.9 | -151.5 | -58.1 |
| 124.5 | -127.5 | -59.2 |

c. Equivalent free-field locations

Harmonic Phase Angle, Deg.

| Mic No. | 4P | 8P | 12P |
|---|---|---|---|
| 2 | 11.4 | 110.8 | 175.4 |
| 5 | 151.1 | 43.9 | -115.1 |
| 8 | -30.7 | 21.6 | 48 |
| 9 | 26.4 | -150.8 | 17.6 |
| 10 | -21.7 | -12.8 | -1.9 |
| 11 | -14.9 | 128.7 | -151.3 |
| 12 | 50.6 | 139.6 | -144.9 |
| 13 | -31.8 | 39.7 | 88.9 |
| 15 | 86.3 | 172 | -104 |
| 16 | 8.5 | -3.7 | 7.4 |
| 18 | 43.9 | 46 | 70.1 |
| 21 | 117.7 | -146 | -32.6 |

## APPENDIX B
## CALCULATION OF SOUND INCIDENCE ANGLE

The sound incidence angle was calculated from the definition of 2 angles using the geometry defined in Figure B-1. The first angle, $\gamma$, is the angle in the prop-fan plane of rotation. The second angle, $\psi$, is the angle based on the fore and aft location of the microphone. It should be noted that inherent in this derivation are the assumptions of 1) the source location is at an effective radius of 85 to 90% and 2) the noise is "beamed" along a line perpendicular to the blade pitch-change axis. These assumptions are based on the prop-fan noise prediction methodology. Also, the angle of incidence is defined to be 90 degrees when normal and 0 degrees when grazing. Thus this angle is always within the limits 0 to 90 degrees.

From Figure B-1, the law of cosines gives:

$$a^2 = R^2 + (R+d+r)^2 - 2R(R+d+r)\cos\theta \tag{1}$$

where the angle $\theta$ is equal to (distance on the fuselage x 180 degrees)/$\pi$ x fuselage radius).

From the law of sines,

$$(R+d+r)/\sin\alpha = a/\sin\theta \tag{2}$$

from which we have

$$\alpha = \sin^{-1}[(R+d+r)\sin\theta/a] \tag{3}$$

Since $\alpha$ is generally an obtuse angle, to avoid ambiguity we will redefine $\alpha$ to be

$$\alpha = \pi - \sin^{-1}[(R+d+r)\sin\theta/a] \tag{4}$$

so that the proper value of 180 degrees is obtained when $\theta = 0$.

Finally, it is obvious that

$$\beta = \sin^{-1}\frac{r_e}{a} \tag{5}$$

$$\gamma = \beta+\alpha - 90° \tag{6}$$

$$b^2 = a^2 - r_e^2 \tag{7}$$

$$\psi = \tan^{-1}\frac{b}{x} \tag{8}$$

It should be noted that at this point, the angle $\psi$ does not yet include convection and shear layer refraction effects. These will be discussed later.

Referring to Figure B2, the incidence angle, $\phi$, is related to the angles $\gamma$ and $\psi$ from the following derivation:

$$\phi = \cos^{-1} \rho'/\rho \tag{9}$$

$$\rho = (x^2+y^2+z^2)^{\frac{1}{2}} \tag{10}$$

$$\rho' = (x^2+y^2)^{\frac{1}{2}} \tag{11}$$

$$z = y \tan \gamma \tag{12}$$

$$z = x \tan \psi \tag{13}$$

From equations 12 and 13

$$x = y \tan \gamma/\tan \psi \tag{14}$$

Substituting equations 12 and 14 into equation 10 gives

$$\rho = \left[y^2 \left(\frac{\tan\gamma}{\tan\psi}\right)^2 + y^2 + y^2 \tan^2\gamma\right]^{\frac{1}{2}} \tag{15}$$

Substituting equation 14 into equation 11 gives

$$\rho' = \left[y^2 \left(\frac{\tan\gamma}{\tan\psi}\right)^2 + y^2\right]^{\frac{1}{2}} \tag{16}$$

Finally, substituting equations 15 and 16 into Equation 9 gives

$$\phi = \cos^{-1} \left[\frac{1 + \frac{\tan^2\gamma}{\tan^2\psi}}{1 + \tan^2\gamma + \frac{\tan^2\gamma}{\tan^2\psi}}\right]^{\frac{1}{2}}$$

$$= \cos^{-1} \left[\frac{\tan^2\gamma + \tan^2\psi}{\tan^2\gamma + \tan^2\psi + \tan^2\gamma \tan^2\psi}\right]^{\frac{1}{2}} \tag{17}$$

When flight is present, the apparent source location when the sound arrives at the observer and the location of the source when the sound was emitted are not equal. This results in a change in the angle of incidence. Figure B3 shows the relationship between S, the source location when the sound is emitted, and S', the

apparent source location when the sound arrives at the observer, 0. In this figure, $\psi$ is the geometric angle of incidence, while $\psi'$ is the desired actual angle of incidence.

From Figure B3, the following relations are apparent:

$$\psi' = \tan^{-1} \frac{b}{(x+x')} \tag{18}$$

$$h'^2 = (x+x')^2 + b^2 \tag{19}$$

Now, during the time the sound propagates from S' to 0, the apparent source location has moved from S to S'. Thus:

$$\frac{h'}{C} = \frac{x'}{M_x C} \longrightarrow h' = x'/M_x \tag{20}$$

where C is the local speed of sound.

Substituting equation 20 into equation 19 results in the quadratic in x'

$$x'^2 (1-M_x^2) - 2M_x^2 x x' - M_x^2 (x^2+b^2) = 0 \tag{21}$$

which has for solutions:

$$x' = \frac{M_x^2 x \pm M_x [x^2 + b^2(1-M_x^2)]^{\frac{1}{2}}}{1 - M_x^2} \tag{22}$$

The positive square root is the one which gives the physically meaningful value for x'.

Once x' has been determined, $\psi'$ can be calculated from equation 18. Using $\psi'$ and $\gamma$ in equation 17 then gives the incidence angle $\phi'$ including convection effects.

This procedure was used to calculate the sound incidence angle for the test configuration with the simulated fuselage at 0.4D clearance and for the full scale prop-fan airplane configuration.

The angle of incidence at each of the 21 microphone locations was calculated for the model test. These calculations are summarized in Table B-I. For these, the following values were used:

R = 38.10 cm (15.00 in.) $r_e$ = 27.53 cm (10.84 in.)

d = 24.89 cm (9.80 in.) $M_x$ = 0.267

r = 32.39 cm (12.75 in.)

In Table B-I, the unprimed quantities are those without convection effects. The primed quantities are those with convection effects. As may be seen by comparing $\phi'$ with $\phi$, the convection effects can have a substantial effect on the incidence angle, even at a relatively low flight Mach number.

For the full scale configuration, the incidence angles were also computed. For these calculations, the following values were used:

R = 2.98 m (9.79 ft) $r_e$ = 1.72 m (5.65 ft)

d = 1.53 m (5.02 ft) $M_x$ = 0.800

r = 1.91 m (6.28 ft)

Table B-II summarizes the calculation of the angle of incidence including convection effects, $\phi'$, and the values of pressure doubling effects at each of the 40 microphone locations used for the full scale prop-fan analysis.

When the sound wave propagates through a shear-layer, the angle $\psi$ is further modified by refraction effects. Figure B4 shows the situation when a shear layer is present between the source and the observer. In this sketch, it is assumed that the source has emitted a ray at an angle $\theta$ from the axis. This ray will be propagated such that it reaches the observer at 0. It will appear to have originated at S' (due to convection effects) and have been refracted at $X_s$.

When an acoustic wave propagates across an interface between two fluids in relative motion, the trace velocity along the boundary must be the same in both media. Thus:

$$\frac{C_1}{\cos\beta} + V_1 = \frac{C_2}{\cos(180-\theta)} + V_2 \qquad (23)$$

where $C_1$ and $C_2$ are the speeds-of-sound and $V_1$ and $V_2$ are the speeds of the media in the two regions. In this case $V_1 = 0$ (i.e., region 1 is outside the shear-layer) and assume that $C_1 = C_2$. Equation 23 can then be rewritten as:

$$\beta = \cos^{-1}\left[\left(M_x - \frac{1}{\cos\theta}\right)^{-1}\right] \qquad (24)$$

where $M_x = V_2/C_2$ = tunnel Mach number.

In the time, t, that is takes the ray to reach the shear-layer, the source has convected a distance x'. Thus the following two relationships apply:

$$x' = -CM_x t \quad \text{and} \quad r = ct = Y/\sin\theta$$

From which the convection distance, x', the shear-layer distance from the source, Y, and the radiation angle $\theta$ can be related:

$$x' = -M_x Y/\sin\theta \tag{25}$$

From Figure B4, the geometric relationship between $x_s$, the shear-layer/acoustic-ray intersection location and the apparent (convected) source location can be determined:

$$x_s = x' + Y/\tan\theta = \frac{Y\cos\theta}{\sin\theta} - \frac{M_x Y}{\sin\theta} = \frac{Y}{\sin\theta}(\cos\theta - M_x) \tag{26}$$

where equation 25 was used for x'.

The observer location, x, is then:

$$x = x_s + \frac{Y-b}{\tan\beta} \tag{27}$$

Combining equation 26 and 27 yields:

$$x = \frac{Y}{\sin\theta}(\cos\theta - M_x) + \frac{Y-b}{\tan\beta} \tag{28}$$

From Figure B4, the shear-layer location Y can be determined to be:

$$Y = (r_s^2 - r_e^2)^{\frac{1}{2}} \tag{29}$$

Finally, the incidence angle, $\psi''$, is defined to be equal to $\beta$ for $\beta \leq 90$ degrees or to $180-\beta$ for $\beta > 90$ degrees.

The above system of equations do not allow the incidence angle to be calculated directly, as the radiation angle $\theta$ is not known. The desired solution is determined by iterating on $\theta$ until the desired value of x (microphone location) is found. Then $\psi''$ can be determined from $\beta$. The procedure is as follows: for a given microphone axial location x, an arbitrary starting value for $\theta$ is selected; this value is used in equation 24 to calculate $\beta$; $\theta$ and $\beta$ are then used in equation 28 to calculate x; if the calculated value of x is greater than the desired value, a larger value of $\theta$ is chosen and the procedure repeated. In this way, a value for $\theta$ which gives the desired value for X can quickly be determined. The value for $\beta$ then gives the desired value for $\psi''$.

Once $\psi''$ has been determined, the sound incidence angle $\phi''$ can be calculated using $\psi''$ and $\gamma$ in equation 17.

This procedure was used to calculate the sound incidence angle for the test configurations with the simulated fuselage at 0.8D clearance and with the equivalent free-field microphone locations. These calculations are summarized in Table B-III. The following values were used for these calculations:

R = 38.10 cm (15.00 in.) $r_e$ = 27.53 cm (10.84 in.)

d = 49.78 cm (19.60 in.) $M_x$ = 0.267

r = 32.39 cm (12.75 in.) $r_s$ = 58.42 cm (23.00 in.)

It should be noted that this analysis is simplified, in that refraction effects along b in the cross-section view of Figure B4 are ignored. A computer program for calculating shear-layer effects based on a more rigorous analysis is described in reference 5. This computer program was used to perform the analysis described in the main text of this report. However, comparison of the values of incidence angle calculated using the propagation angles determined using the computer program and those from the simplified analysis described in this appendix show relatively small differences, as can be seen by comparing Table V and Table BIII.

TABLE B-I
CALCULATION OF INCIDENCE ANGLE FOR MODEL TEST
FUSELAGE AT 0.4 DIAMETERS

| MIC No. | $\theta$, Deg | $\gamma$, Deg | b, cm | x, cm | $\psi$, Deg | $\phi$, Deg | x', cm | $\psi'$, Deg | $\phi'$, Deg |
|---|---|---|---|---|---|---|---|---|---|
| 1 | 0 | 61.27 | 50.22 | -15.24 | 73.12 | 57.93 | 13.41 | 87.91 | 61.22 |
| 2 | 0 | 61.27 | 50.22 | 38.10 | 52.81 | 46.89 | 20.62 | 40.53 | 37.75 |
| 3 | 15.28 | 87.42 | 52.73 | 30.48 | 59.97 | 59.89 | 19.38 | 46.60 | 46.57 |
| 4 | -15.28 | 37.44 | 52.73 | 30.48 | 59.97 | 35.00 | 19.38 | 46.60 | 31.81 |
| 5 | 0 | 61.27 | 50.22 | 22.86 | 65.52 | 54.53 | 17.15 | 51.46 | 45.96 |
| 6 | 15.28 | 87.42 | 52.73 | 15.24 | 73.88 | 73.70 | 16.43 | 59.01 | 58.94 |
| 7 | -15.28 | 37.44 | 52.73 | 15.24 | 73.88 | 36.78 | 16.43 | 59.01 | 34.82 |
| 8 | 0 | 61.27 | 50.22 | 7.62 | 81.37 | 60.37 | 14.68 | 66.05 | 54.80 |
| 9 | 45.84 | 44.33 | 68.76 | 0 | 90.00 | 44.33 | 19.05 | 74.51 | 43.32 |
| 10 | 22.92 | 79.58 | 55.63 | 0 | 90.00 | 79.58 | 15.42 | 74.51 | 71.60 |
| 11 | 0 | 61.27 | 50.22 | 0 | 90.00 | 61.27 | 13.92 | 74.51 | 58.44 |
| 12 | -22.92 | 26.92 | 55.63 | 0 | 90.00 | 26.92 | 15.42 | 74.51 | 26.69 |
| 13 | -45.84 | 0.69 | 68.76 | 0 | 90.00 | 0.69 | 19.05 | 74.51 | 0.69 |
| 14 | 45.84 | 44.33 | 68.76 | -22.86 | 71.61 | 42.90 | 18.39 | 86.28 | 44.27 |
| 15 | 22.92 | 79.58 | 55.63 | -22.86 | 67.66 | 65.76 | 15.01 | 81.97 | 76.95 |
| 16 | -22.92 | 26.92 | 55.63 | -22.86 | 67.66 | 26.43 | 15.01 | 81.97 | 26.86 |
| 17 | -45.84 | 0.69 | 68.76 | -22.86 | 71.61 | 0.69 | 18.39 | 86.28 | 0.69 |
| 18 | 0 | 61.27 | 50.22 | -30.48 | 58.74 | 50.72 | 14.10 | 71.93 | 57.47 |
| 19 | 22.92 | 79.58 | 55.63 | -45.72 | 50.58 | 49.89 | 16.74 | 62.48 | 61.08 |
| 20 | -22.92 | 26.92 | 55.63 | -45.72 | 50.58 | 25.11 | 16.74 | 62.48 | 26.15 |
| 21 | 0 | 61.27 | 50.22 | -60.96 | 39.48 | 36.90 | 17.70 | 49.26 | 44.41 |

TABLE B-II CALCULATION OF INCIDENCE ANGLE AND PRESSURE DOUBLING EFFECTS FOR THE FULL SCALE PROP-FAN

| Mic No. | $\theta$ Deg | $\gamma'$ Deg | b m | x m | x' m | $\psi$ Deg | $\phi'$ Deg | Press Doub Eff, dB |
|---|---|---|---|---|---|---|---|---|
| 1 | 45.0 | 41.24 | 5.974 | -3.825 | 4.849 | 80.27 | 40.92 | 5.9 |
| 2 | 22.5 | 73.97 | 5.038 | -3.825 | 4.036 | 87.61 | 73.81 | 6.0 |
| 3 | 0 | 69.75 | 4.666 | -3.825 | 3.734 | 88.88 | 69.72 | 6.0 |
| 4 | -22.5 | 36.25 | 5.038 | -3.825 | 4.036 | 87.61 | 36.24 | 5.8 |
| 5 | -45.0 | 9.10 | 5.974 | -3.825 | 4.849 | 80.27 | 9.10 | 2.9 |
| 6 | 45.0 | 41.24 | 5.974 | -2.869 | 5.102 | 69.50 | 39.80 | 5.9 |
| 7 | 22.5 | 73.97 | 5.038 | -2.869 | 4.161 | 75.62 | 68.94 | 6.0 |
| 8 | 0 | 69.75 | 4.666 | -2.869 | 3.807 | 78.64 | 67.21 | 6.0 |
| 9 | -22.5 | 36.25 | 5.038 | -2.869 | 4.161 | 75.62 | 35.78 | 5.8 |
| 10 | -45.0 | 9.10 | 5.974 | -2.869 | 5.102 | 69.50 | 9.08 | 2.9 |
| 11 | 45.0 | 41.24 | 5.974 | -1.913 | 5.630 | 58.11 | 37.58 | 5.8 |
| 12 | 22.5 | 73.97 | 5.038 | -1.913 | 4.551 | 62.36 | 59.15 | 6.0 |
| 13 | 0 | 69.75 | 4.666 | -1.913 | 4.136 | 64.52 | 58.92 | 6.0 |
| 14 | -22.5 | 36.25 | 5.038 | -1.913 | 4.551 | 62.36 | 34.39 | 5.7 |
| 15 | -45.0 | 9.10 | 5.974 | -1.913 | 5.630 | 58.11 | 9.06 | 2.9 |
| 16 | 45.0 | 41.24 | 5.974 | -0.956 | 6.544 | 46.91 | 34.13 | 5.7 |
| 17 | 22.5 | 73.97 | 5.038 | -0.956 | 5.346 | 48.94 | 47.47 | 6.0 |
| 18 | 0 | 69.75 | 4.666 | -0.956 | 4.877 | 49.97 | 47.47 | 6.0 |
| 19 | -22.5 | 36.25 | 5.038 | -0.956 | 5.346 | 48.94 | 31.71 | 5.6 |
| 20 | -45.0 | 9.10 | 5.974 | -0.956 | 6.544 | 46.91 | 9.00 | 2.9 |
| 21 | 45.0 | 41.24 | 5.974 | 0 | 7.964 | 36.87 | 29.68 | 5.4 |
| 22 | 22.5 | 73.97 | 5.038 | 0 | 6.718 | 36.87 | 36.25 | 5.7 |
| 23 | 0 | 69.75 | 4.666 | 0 | 6.221 | 36.87 | 35.86 | 5.7 |
| 24 | -22.5 | 36.25 | 5.038 | 0 | 6.718 | 36.87 | 27.67 | 5.3 |
| 25 | -45.0 | 9.10 | 5.974 | 0 | 7.964 | 36.87 | 8.90 | 2.8 |
| 26 | 45.0 | 41.24 | 5.974 | 0.956 | 9.946 | 28.72 | 24.92 | 5.1 |
| 27 | 22.5 | 73.97 | 5.038 | 0.956 | 8.748 | 27.44 | 27.18 | 5.2 |
| 28 | 0 | 69.75 | 4.666 | 0.956 | 8.275 | 26.82 | 26.43 | 5.2 |
| 29 | -22.5 | 36.25 | 5.038 | 0.956 | 8.748 | 27.44 | 22.96 | 4.9 |
| 30 | -45.0 | 9.10 | 5.974 | 0.956 | 9.946 | 28.72 | 8.74 | 2.8 |
| 31 | 45.0 | 41.24 | 5.974 | 1.913 | 12.430 | 22.61 | 20.62 | 4.7 |
| 32 | 22.5 | 73.97 | 5.038 | 1.913 | 11.351 | 20.80 | 20.69 | 4.7 |
| 33 | 0 | 69.75 | 4.666 | 1.913 | 10.936 | 19.96 | 19.80 | 4.6 |
| 34 | -22.5 | 36.25 | 5.038 | 1.913 | 11.351 | 20.80 | 18.64 | 4.3 |
| 35 | -45.0 | 9.10 | 5.974 | 1.913 | 12.430 | 22.61 | 8.50 | 2.7 |
| 36 | 45.0 | 41.24 | 5.974 | 2.869 | 15.304 | 18.20 | 17.11 | 4.3 |
| 37 | 22.5 | 73.97 | 5.038 | 2.869 | 14.362 | 16.30 | 16.25 | 4.2 |
| 38 | 0 | 69.75 | 4.666 | 2.869 | 14.009 | 15.46 | 15.38 | 4.1 |
| 39 | -225 | 36.75 | 5.038 | 2.869 | 14.362 | 16.30 | 15.20 | 4.1 |
| 40 | -45.0 | 9.10 | 5.974 | 2.869 | 15.304 | 18.20 | 8.19 | 2.6 |

TABLE B-III. CALCULATION OF INCIDENCE ANGLE FOR MODEL TEST INCLUDING CONVECTION AND SHEAR-LAYER EFFECTS

| Mic No. | $\theta$ Deg | $\beta$ Deg | x' cm | $x_s$ cm | b cm | Y cm | $\psi''$ Deg | $\gamma$ Deg | $\phi''$ Deg |
|---|---|---|---|---|---|---|---|---|---|
| 1 | 91.1 | 88.9 | -13.77 | -14.81 | 77.42 | 51.54 | 88.9 | 70.4 | 70.4 |
| 2 | 57.1 | 129.4 | -16.38 | 16.97 | 77.42 | | 50.6 | 70.4 | 48.1 |
| 3 | 61.5 | 123.2 | -15.65 | 12.32 | 79.50 | | 56.8 | 87.0 | 56.8 |
| 4 | 61.5 | 123.2 | -15.65 | 12.32 | 79.50 | | 56.8 | 48.8 | 42.5 |
| 5 | 65.0 | 118.4 | -15.19 | 8.84 | 77.42 | | 61.6 | 70.4 | 57.1 |
| 6 | 70.2 | 111.9 | -14.63 | 3.94 | 79.50 | | 68.1 | 87.0 | 68.0 |
| 7 | 70.2 | 111.9 | -14.63 | 3.94 | 79.50 | | 68.1 | 48.8 | 46.1 |
| 8 | 74.6 | 106.6 | -14.27 | -0.08 | 77.42 | | 73.4 | 70.4 | 65.1 |
| 9 | 81.7 | 98.6 | -13.89 | -6.38 | 93.68 | | 81.4 | 44.3 | 44.0 |
| 10 | 80.5 | 99.9 | -13.94 | -5.33 | 81.97 | | 80.1 | 75.8 | 72.9 |
| 11 | 79.9 | 100.6 | -13.97 | -4.80 | 77.42 | | 79.4 | 70.4 | 68.1 |
| 12 | 80.5 | 99.9 | -13.94 | -5.33 | 81.97 | | 80.1 | 38.6 | 38.4 |
| 13 | 81.7 | 100.6 | -13.89 | -6.38 | 93.68 | | 79.4 | 11.5 | 11.5 |
| 14 | 95.6 | 84.5 | -13.82 | -18.87 | 93.68 | | 84.5 | 44.3 | 44.2 |
| 15 | 96.4 | 83.8 | -13.84 | -19.63 | 81.97 | | 83.8 | 75.8 | 74.6 |
| 16 | 96.4 | 83.8 | -13.84 | -19.63 | 81.97 | | 83.8 | 38.6 | 38.5 |
| 17 | 95.6 | 84.5 | -13.82 | -18.87 | 93.68 | | 84.5 | 11.5 | 11.5 |
| 18 | 102.2 | 78.5 | -14.07 | -25.22 | 77.42 | | 78.5 | 70.4 | 67.7 |
| 19 | 111.4 | 70.6 | -14.78 | -34.98 | 81.97 | | 70.6 | 75.8 | 66.5 |
| 20 | 111.4 | 70.6 | -14.78 | -34.98 | 81.97 | | 70.6 | 38.6 | 37.6 |
| 21 | 121.4 | 62.8 | -16.13 | -47.57 | 77.42 | | 62.8 | 70.4 | 58.0 |

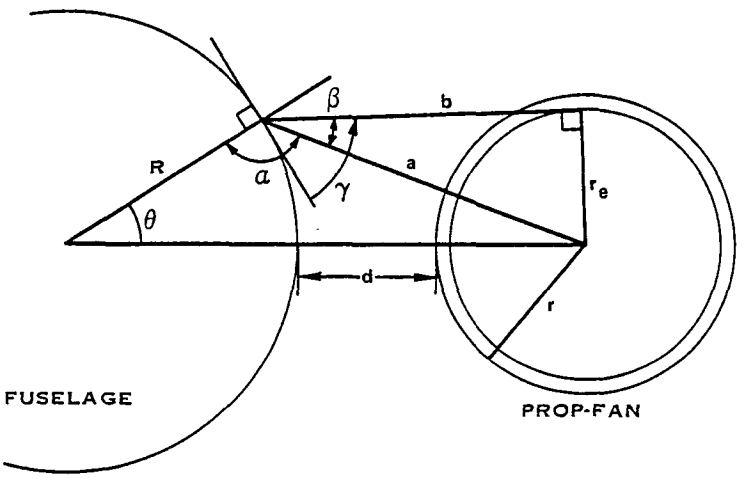


a. VIEW IN PLANE OF ROTATION

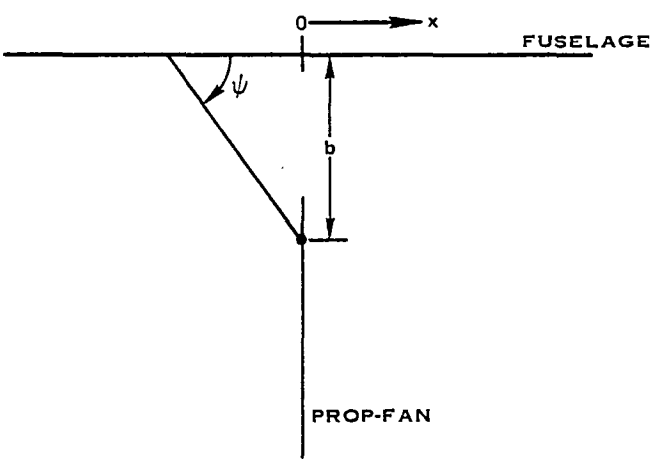


b. PLAN VIEW

FIGURE B1. FUSELAGE - PROP-FAN GEOMETRY

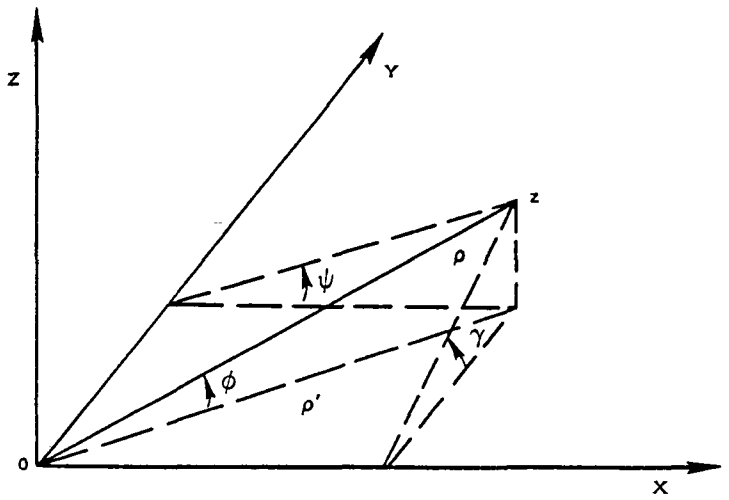


FIGURE B2. RELATION AMONG INCIDENCE ANGLE $\phi$ AND DERIVED ANGLES $\gamma$ AND $\psi$

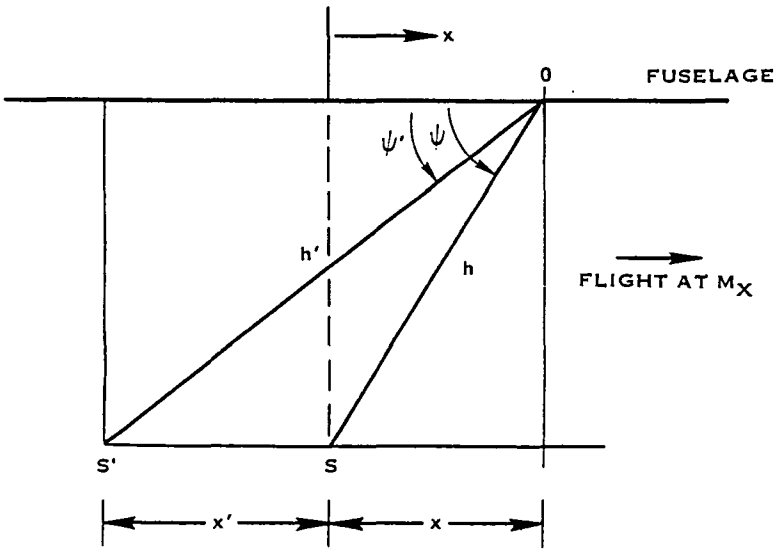


FIGURE B3. RELATION BETWEEN VISUAL SOURCE LOCATION AND RETARDED SOURCE LOCATION

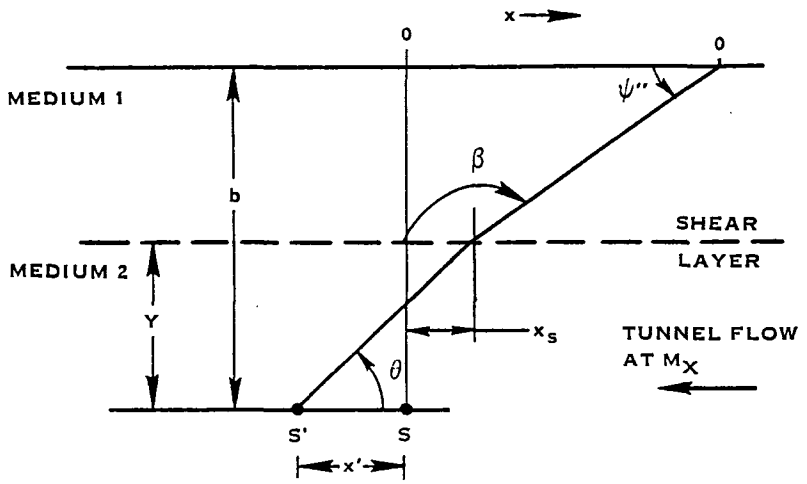


a. PLAN VIEW (IN THE PLANE PARALLEL TO THE TUNNEL AXIS CONTAINING b)

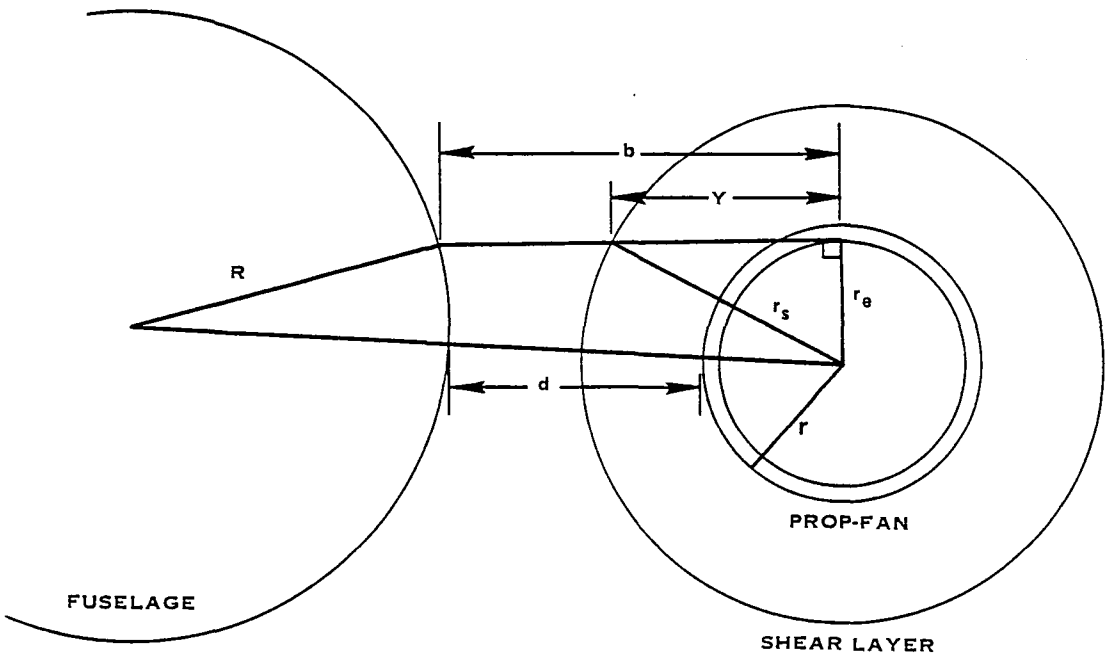


b. CROSS-SECTION VIEW (IN PLANE OF ROTATION)

FIGURE B4. RELATION AMONG VARIOUS QUANTITIES FOR THE CASE OF PROPAGATION THROUGH A SHEAR LAYER.